NASA TECHNICAL NOTE

NASA TN D-7559

NASA TN D-7559

GUST ALLEVIATION FOR A STOL TRANSPORT BY USING ELEVATOR, SPOILERS, AND FLAPS

by Frederick J. Lallman

Langley Research Center
Hampton, Va. 23665

NATIONAL AERONAUTICS AND SPACE ADMINISTRATION • WASHINGTON, D. C. • OCTOBER 1974

GUST ALLEVIATION FOR A STOL TRANSPORT BY USING ELEVATOR, SPOILERS, AND FLAPS

By Frederick J. Lallman
Langley Research Center

SUMMARY

Control laws were developed to investigate methods of alleviating the response of a STOL transport to gusty air. The aircraft was simulated in a low-speed approach configuration. The elevator, spoilers and trailing edge flap element were used as control devices. Two accelerometers, one mounted vertically and one mounted longitudinally with respect to the airframe, pitch angle and pitch rate gyros, and an airspeed sensor were used to generate feedback control commands. A conjugate gradient optimization procedure was used to select the feedback gain matrix which minimized the average of a quadratic functional involving normal acceleration (at both the C.G. and tail of the aircraft), longitudinal acceleration, pitch angle and rate, inertial speed, and glide path angle variations. The optimization was performed for a selected gust field consisting of vertical and horizontal gusts in the form of series of constant amplitude pulses with various durations.

Feedback matrices for various combinations of elevator, flap, and spoilers were obtained. The root-mean-square (rms) magnitude of several variables appearing in the performance index are presented for each control configuration. The closed-loop pole locations and magnitude versus frequency plots of the aircraft transfer functions relative to horizontal and vertical gust inputs were obtained and compared.

Feedback matrices were also obtained for a number of sensor configurations utilizing pitch angle and rate and one or more of the following variables: normal acceleration, axial acceleration, relative airspeed at the center of gravity or at the nose of the airframe, and angle of attack at the nose of the airframe. The closed loop system characteristics for these sensor configurations are compared with the case utilizing only pitch angle and rate feedback.

The study was performed on the EAI 690 hybrid computer facility at the Langley Research Center. The linearized equations for the longitudinal dynamics of the aircraft and the control system were simulated on an analog computer, and the optimization algorithm was programmed on a digital computer. The modal and frequency response computations were performed on a large general purpose digital computer.

INTRODUCTION

The reduced wing loading required for STOL capability increases the aircraft's sensitivity to atmospheric gust disturbances. This, in turn, increases the motions and accelerations imposed upon the passenger compartment and adds to the level of pilot work load in gusty weather. In addition, the low speed of operation results in a reduced aerodynamic control surface effectiveness. In view of these factors, a study was made of the longitudinal control of a STOL aircraft. The object of this study was to determine the benefits to be realized by utilizing aerodynamic control surfaces on the wing and tail to improve the stability and ride quality. This study considered the reduction of aircraft motions relative to a steady flight condition and did not address the problem of flight control by the pilot.

The geometric characteristics of the high-wing STOL aircraft examined in this study are presented in figure 1. The aircraft has triple-slotted, externally-blown jet flaps and a large T-tail. A detail of the wing showing the configuration of the engines, spoiler, and flap assembly is presented in figure 2. The three control devices considered in this study were the spoiler, the trailing-edge element of the flaps (hereafter referred to as the flaps), and the elevator. The spoiler provided, primarily, lift modulation. The flap element provided substantial modulation of both lift and drag. The elevator acted as a conventional rotation controller. The engines were fixed at the trim thrust level.

Aircraft simulation and control system configuration studies were performed on the EAI 690 hybrid computing facility at Langley Research Center. The linearized longitudinal dynamics of the transport, equipped with fast acting elevator, spoilers, and flaps, were programmed on the analog portion of the hybrid computer (EAI 680). The aircraft was configured for landing approach. First order lags were used to represent actuator dynamics. A feedback control matrix operated on a number of sensor signals to produce control command signals. Sensor variables, selected flight variables, and control command variables were tabulated at regular intervals by the digital portion of the hybrid computer (EAI 640). Two series of rectangular test wave forms for horizontal and vertical gust inputs were generated according to stored tables in the digital computer. A quadratic performance index and its gradient were evaluated, off-line, by the digital computer. A conjugate gradient optimization procedure (ref. 1) was used to generate feedback gain matrices minimizing the performance index.

Feedback gain matrices were computed for the cases of elevator, spoilers, and flaps each operating alone, in combinations of two, and all three together. The magnitude of each of the variables contributing to the performance index for each combination of control devices is presented. Closed loop pole locations and magnitude versus frequency plots of the aircraft transfer function relative to sinusoidal horizontal and vertical

gusts are examined for each feedback gain matrix obtained above. These items are compared to determine the relative effectiveness of each control configuration in modifying the gust response of the aircraft.

Feedback gain matrices were then computed for elevator, spoiler, and flap controls and several sensor configurations. The case utilizing pitch angle and rate variables as feedback quantities was used as a baseline for comparison. Signals from normal and axial accelerometers, airspeed sensors at the nose of the airframe and at the center of gravity, and an angle of attack sensor at the nose of the airframe were added individually to the basic sensor configuration. In addition, both the airspeed sensor at the nose and the normal accelerometer and then the airspeed sensor at the nose and the angle of attack sensor were added to the basic configuration. These cases were compared to determine the effects of each sensor addition upon the stability of the system and the system response to gust inputs.

SYMBOLS

a_B normal acceleration at rear passenger station, g units

a_n normal acceleration at the C.G., g units

a_X axial deceleration, g units

$\bar{c}$ mean aerodynamic chord, meters (feet)

C_D drag coefficient, $\frac{D}{\bar{q}S}$

C_L lift coefficient, $\frac{L}{\bar{q}S}$

C_m pitching moment coefficient, $\frac{M}{\bar{q}\bar{c}S}$

$C_{m_{\dot{\theta}}} = \frac{\partial C_m}{\partial \dot{\theta}}$, example of aerodynamic derivative

C_μ engine thrust coefficient

C.G. center of gravity

D drag force, newtons (pounds)

g gravitational acceleration, m/s^2 (ft/sec^2)

g_i	gradient vector for ith approximation of the solution set of gains
G	feedback gain matrix
G_{ij}	element of the gain matrix identified by two indices
$G^{(i)}$	ith approximation of the solution set of gains
h_t	vertical distance from C.G. to the horizontal tail divided by $\bar{c}$
i_t	incidence of tail, degrees
J	performance index
k	index denoting sample time of variable
k_y	radius of gyration divided by $\bar{c}$
L	lift force perpendicular to velocity vector, newtons (pounds)
l_n	distance from the nose of the aircraft to the C.G. divided by $\bar{c}$
l_p	distance from C.G. to rear passenger station divided by $\bar{c}$
l_t	longitudinal distance from C.G. to aerodynamic center of tail divided by $\bar{c}$
M	pitching moment, N-m (lb-ft)
m	mass, kg (slugs)
n	number of samples used in evaluation of performance index
$\bar{q}$	dynamic pressure, N/m^2 (lb/ft^2)
Q	symmetric weighting matrix on control commands
rms	root mean square value
S	symmetric weighting matrix on measured variables

s_i	ith search direction in optimization algorithm
S_t	area of the tail, meters^2 (ft^2)
S_w	area of the wing, meters^2 (ft^2)
t	time
t_e	time constant of elevator actuator, seconds
t_f	time constant of flap actuator, seconds
t_s	time constant of spoiler actuator, seconds
u	nondimensional speed variation, $\Delta V/V_o$
u_A	nondimensional airspeed measured at C.G., V_A/V_o
u_F	nondimensional airspeed measured at nose of aircraft, V_F/V_o
u_t	stream velocity variation at tail due to gusts, m/sec (ft/sec)
u_H	nondimensional horizontal gust component, V_H/V_o
u_V	nondimensional vertical gust component, V_V/V_o
$\underline{u}$	vector of control commands
V	inertial velocity, m/sec (ft/sec)
V_A	airspeed measured at C.G.
V_F	airspeed measured at nose of aircraft
V_H	horizontal gust component
V_V	vertical gust component
v	inertial velocity variation, m/sec (ft/sec)

$\underline{y}$	vector of performance variables
$\underline{y}^d$	vector of desired performance variables
$\underline{z}$	vector of sensor signals
A	angle of attack, radians
A_I	portion of angle of attack due to aircraft motion, radians
α	angle of attack variation, radians
α_I	portion of angle of attack variation due to aircraft motion, radians
α_F	sensed angle of attack at nose of airframe, radians
Γ	flight path angle, radians
γ	flight path angle variation, radians
δe	elevator variation, radians
δf	flap variation, radians
δs	spoiler variation, radians
ϵ	downwash angle, radians
η	weighting on gain matrix elements in performance index
Θ	pitch angle, radians
Θ	pitch angle variation, radians
ρ	air density, kg/m^3 ($slugs/ft^3$)
σ	one-dimensional search parameter
τ	defined as $l_t \bar{c}/V_o$

Subscripts:

c	control command signals
i,j,l,m	indices used in identifying gain matrix elements
o	nominal flight variables
t	tail parameters
w	wing (tail-off) parameters

Superscripts:

d	desired flight variables
o	nominal parameters and variables in optimization algorithm
T	transpose of a vector or matrix
' (prime)	vector evaluated for a perturbed set of gains

A dot over a variable denotes the first derivative with respect to time.

Two dots over a variable denotes the second derivative with respect to time.

SIMULATION EQUATIONS

Aircraft Model

The mathematical model of the aircraft used in this study is developed in appendix A. The longitudinal dynamics are linearized about a steady flight condition and are referenced to the wind axis coordinate system (see fig. 3). The flow variations in the vicinity of the tail (downwash and stream velocity) are considered to be delayed by the time required for a change occurring at the wing takes to have an effect at the tail. These delays are modeled at first order lags. The equations of the aircraft model follow.

$$-\dot{\alpha}_I = \frac{g}{V_o}\left[\Theta - \alpha_I\right]\sin\Gamma_o - \dot{\Theta} + \frac{1}{2}\frac{\rho}{m}V_o S\left\{C_{L_{\alpha_w}}\alpha_I + C_{L_{\dot{\Theta}}}\dot{\Theta}\right.$$
$$+ \left[C_{L_{u_w}} + 2C_{L_o}\right]u + C_{L_{uV_w}}u_V + C_{L_{uH_w}}u_H + C_{L_{\delta f_w}}\delta f$$
$$\left. + C_{L_{\delta e}}\delta e + C_{L_{\delta s_w}}\delta s + 2C_{L_t}u_t - C_{L_{\alpha_{t_o}}}\left(\epsilon - \alpha_I\right)\right\}$$

$$\ddot{\Theta} = \frac{1}{2}\frac{\rho V_o^2 S}{m k_y^2 \bar{c}}\left\{C_{m_{\alpha_w}}\alpha_I + C_{m_{\dot{\Theta}}}\dot{\Theta} + C_{m_{u_w}}u + C_{m_{uV_w}}u_V + C_{m_{uH_w}}u_H\right.$$
$$\left. + C_{m_{\delta f_w}}\delta f + C_{m_{\delta e}}\delta e + C_{m_{\delta s_w}}\delta s + 2C_{m_t}u_t - C_{m_{\alpha_t}}\left(\epsilon - \alpha_I\right)\right\}$$

$$\dot{u} = -\frac{1}{2}\frac{\rho}{m}V_o S\left\{C_{D_{\alpha_w}}\alpha_I + C_{D_{\dot{\Theta}}}\dot{\Theta} + \left[C_{D_{u_w}} + 2C_{D_o}\right]u + C_{D_{uV_w}}u_V\right.$$
$$+ C_{D_{uH_w}}u_H + C_{D_{\delta f_w}}\delta f + C_{D_{\delta e}}\delta e + C_{D_{\delta s_w}}\delta s + 2C_{D_t}u_t$$
$$\left. - C_{D_{\alpha_t}}\left(\epsilon - \alpha_I\right)\right\} - \frac{g}{V_o}\cos\Gamma_o\left[\Theta - \alpha_I\right]$$

$$\frac{\bar{c}l_t}{v}\dot{\epsilon} = \left\{\frac{\partial\epsilon}{\partial\alpha}\alpha_I + \frac{\partial\epsilon}{\partial u_V}u_V + \frac{\partial\epsilon}{\partial u_H}u_H + \frac{\partial\epsilon}{\partial u}u + \frac{\partial\epsilon}{\partial\delta s}\delta s + \frac{\partial\epsilon}{\partial\delta f}\delta f\right\} - \epsilon$$

$$\frac{\bar{c}l_t}{v}\dot{u}_t = \left\{\frac{\partial u_t}{\partial u_V}u_V + \frac{\partial u_t}{\partial u_H}u_H\right\} - u_t$$

The actuator dynamics are modeled as first order lags. The dynamic equations for the control surface deflections are

$$\dot{\delta f} = \left(\delta f_c - \delta f\right)/t_f$$

$$\dot{\delta s} = \left(\delta s_c - \delta s\right)/t_s$$

$$\dot{\delta e} = \left(\delta e_c - \delta e\right)/t_e$$

where δf_c, δs_c, and δe_c are the flap, spoiler, and elevator command signals, respectively. These signals are to be generated according to a feedback control law.

Sensor Signals

Pitch angle and pitch rate gyros are assumed to provide measurements of Θ and $\dot{\Theta}$. An accelerometer is mounted vertically with respect to the fuselage at the aircraft's center of gravity. The signal produced is a mixture of acceleration components in the lift and drag directions:

$$a_n = \frac{V_o}{g}\left[(\dot{\Theta} - \dot{\alpha}_I)\cos \alpha_o - \dot{u} \sin \alpha_o\right]$$

where a_n is measured in g units.

A second accelerometer is mounted longitudinally with respect to the fuselage at the aircraft center of gravity. The signal produced by this sensor is:

$$a_X = \frac{V_o}{g}\left[(\dot{\Theta} - \dot{\alpha}_I)\sin \alpha_o + \dot{u} \cos \alpha_o\right]$$

where a_X is measured in g units.

An airspeed sensor is placed at the center of gravity. The sensed signal is the magnitude of the velocity of the air relative to the aircraft:

$$u_A = u + u_H \cos \gamma_o - u_V \sin \gamma_o$$

Relative airspeed and angle of attack sensors were placed on the nose of the aircraft. These sensors provide measurements of gust inputs before they effect the forces on the aircraft. The equations describing the outputs of these sensors are

$$u_F = u + u_H \cos \gamma_o - u_V \sin \gamma_o - \frac{\dot{\Theta} l_n \dot{c}}{V} \sin \alpha_o$$

$$\alpha_F = \alpha_I + u_H \sin \gamma_o + u_V \cos \gamma_o - \frac{\dot{\Theta} l_n \bar{c}}{V} \cos \alpha_o$$

All sensors are assumed to be ideal with infinite bandpass and no lags.

The inertial flight path angle is

$$\Gamma = \Gamma_o + \Theta - \alpha_I$$

The normal acceleration of a point in the fuselage located l_p wing chords behind the center of gravity is

$$a_B = a_n - \frac{l_p \bar{c} \ddot{\Theta}}{g}$$

Control Law

A linear control law is used to generate the actuator signals for each control configuration investigated. The general form of the control law is

$$\underline{u} = G\underline{z}$$

where

$\underline{u}$ vector of actuator command signals
G control gain matrix
$\underline{z}$ vector of sensor variables

The elements of $\underline{u}$ and $\underline{z}$ and the dimensions of G are selected as appropriate for each control configuration.

Performance Index

The quadratic performance index used in this study has the general form

$$J = \frac{1}{n} \sum_{k=1}^{n} \left\{ \frac{1}{2} \left(\underline{y}_k - \underline{y}_k^d \right)^T S \left(\underline{y}_k - \underline{y}_k^d \right) + \frac{1}{2} \underline{u}^T Q \underline{u} \right\} + \frac{\eta}{2} \sum_{i,j} \left(G_{ij} \right)^2$$

where

$\underline{y}_k$ vector of all measured variables at sample instant k
$\underline{y}_k^d$ vector of desired values for the measured variables at sample instant k
$\underline{u}_k$ vector of control commands at sample instant k
G_{ij} ijth element of the feedback gain matrix, G
S, Q symmetric weighting matrices on the state errors and control commands, respectively
η weighting on the gain elements

and

$$\underline{y} = \begin{bmatrix} a_n \\ \dot{\Theta} \\ \Theta \\ u_A \\ a_X \\ \gamma \\ u \\ a_B \end{bmatrix} \qquad \underline{u} = \begin{bmatrix} \delta f_c \\ \delta s_c \\ \delta e_c \end{bmatrix}$$

The performance index is composed of terms weighing the difference between the desired values of the measured variables and their actual values, and the values of the control command signals with a penalty placed on the magnitudes of the gain elements. The penalty restricts the magnitudes of the elements of the gain matrix to acceptable values. In the absence of this term several gain elements have invariably taken on excessive values with little change in the control commands.

Given a small perturbation in the value of the gain element G_{lm} from its normal value G^o_{lm}, the measured variables and the control commands are assumed to attain new values according to

$$\underline{y}_k = \underline{y}^o_k + \delta\underline{y}_k = \underline{y}^o_k + \left[\frac{\partial \underline{y}}{\partial G_{lm}}\right]_k \delta G_{lm}$$

$$\underline{u}_k = \underline{u}^o_k + \delta\underline{u}_k = \underline{u}^o_k + \left[\frac{\partial \underline{u}}{\partial G_{lm}}\right]_k \delta G_{lm}$$

where the superscript o denotes variables evaluated for a nominal gain matrix G^o.

Given this assumption, the first order variation of the performance index due to a perturbation of the gain element, G_{lm}, can be expressed as

$$\delta J^o = \left[\frac{1}{n}\sum_{k=1}^{n}\left\{\left(\underline{y}^o_k - \underline{y}^d_k\right)^T S\left[\frac{\partial \underline{y}}{\partial G_{lm}}\right]_k + \left(\underline{u}^o\right)^T Q\left[\frac{\partial \underline{u}}{\partial G_{lm}}\right]_k\right\} + \eta G^o_{lm}\right]\delta G_{lm}$$

$$= \left[\frac{\partial J^o}{\partial G_{lm}}\right]\delta G_{lm}$$

The term $\left[\frac{\partial J^o}{\partial G_{lm}}\right]$ is the variation of the performance index J with respect to the gain element G_{lm} about $G = G^o$.

The matrix

$$g_o = \begin{bmatrix} \frac{\partial J^o}{\partial G_{11}} & \frac{\partial J^o}{\partial G_{12}} & \cdots \\ \frac{\partial J^o}{\partial G_{21}} & & \\ \vdots & & \\ \vdots & & \end{bmatrix}$$

is defined as the gradient of J with respect to the matrix G evaluated at $G = G^o$. This is analogous to the definition of the gradient with respect to a vector.

The value of an element of g_o is approximated by changing the corresponding element of G by a small amount and computing:

$$\frac{\partial J}{\partial G_{lm}} \approx \frac{1}{n} \frac{\sum_{k=1}^{n} \left\{ \left(\underline{y}_k^o - \underline{y}_k^d \right)^T S \left(\underline{y}_k' - \underline{y}_k^o \right) + \left(\underline{u}_k^o \right)^T Q \left(\underline{u}_k' - \underline{u}_k^o \right) \right\}}{\partial G_{lm}} + \eta G_{lm}$$

where $\underline{y}_k'$ and $\underline{u}_k'$ are the vectors $\underline{y}_k$ and $\underline{u}_k$ evaluated for the gain matrix G^o with the element G_{lm}^o replaced by $G_{lm}^o + \delta G_{lm}$.

Notice that neither the evaluation of the performance index nor its gradient requires explicit knowledge of the plant parameters. This technique could be used in simulations utilizing hardware elements without requiring explicit mathematical models of the elements.

COMPUTATIONAL TECHNIQUE

A conjugate gradient method of minimizing a performance index with respect to the elements of a feedback matrix was used to generate feedback matrices for several control and sensor configurations. This method is attractive since it exhibits second order convergence with the amount of computation comparable to first order methods. The method used in this study was patterned after the method of reference 1. It is a first order algorithm similar to steepest descent in that successive search directions are based on gradient of the performance index at each step.

The simple steepest descent method uses the current gradient as the search direction:

$$s_i = -g_i$$

where g_i is the gradient of the performance index with respect to the gain elements for the ith gain matrix and s_i is the ith search direction.

The conjugate gradient method of reference 1 improves on the steepest descent method by utilizing information contained in the previous search direction in forming a new search direction. The algorithm used in the study computed the search directions according to:

$$s_1 = -g_1$$

$$s_i = -g_i + \frac{(g_i, g_i)}{(g_{i-1}, s_{i-1})} s_{i-1}$$

where (g_i, g_i) denotes the inner product of g_i with itself and (g_{i-1}, s_{i-1}) denotes the inner product of g_{i-1} with s_{i-1}. A single parameter minimization is performed along the search direction at each iteration step. The solution of this search is the nominal set of gain elements for the following step.

The computational logic flow chart for implementing this conjugate gradient algorithm is given in figure 4. This chart includes some reasonableness tests and restart loops that are not discussed here.

AIRCRAFT PARAMETERS

The aircraft parameters were based on references 2 and 3. The configuration has full span, triple slotted flaps with the trailing flap element (hereafter referred to as the flap unless otherwise specified) used as a control device. Spoilers are mounted ahead of the flaps to provide direct lift control. Aerodynamic coefficients were obtained for a nominal flap setting of $25^{\circ}/10^{\circ}/50^{\circ}$ for the three flap elements, engine thrust coefficient $C_{j\mu} = 1.87$, spoiler prop-up (up-rig) of 15°, and angle of attack of 10°. This condition results in a 3.88° glide slope at 35.4 m/sec for a 25 000 kg aircraft. Estimates of downwash angle characteristics and of tail plane and elevator lift and drag were empirically derived from references 2 and 3. A complete list of parameters for the study case is presented in appendix B.

COMPUTER OPERATIONS

The simulation of the aircraft dynamics, actuators, and sensors was performed on an EAI 680 analog computer. This was interfaced with an EAI 640 digital computer through digital-to-analog and analog-to-digital channels and binary control lines. Figure 5 illustrates the configuration of the hybrid computer system for automatic simulation and control law optimization. The aircraft dynamics, sensors, and actuators are simulated in the conventional analog fashion. Gust inputs are generated by the digital computer. Control loops from a number of sensors to the control actuators are implemented by digital-analog multipliers. These devices are used as analog attenuators whose gains are manipulated by the digital computer. Sensor outputs and other variables used in the performance index are routed to the digital computer through analog-to-digital converters.

A setup and static check program was written in the HYTRAN Operations Interpreter Language (HOI). This digital computer program processes the aerodynamic coefficients, derivatives, and kinematic data to determine the potentiometer settings for the analog simulation. The potentiometers are set to these values and series of static checks of the analog setup are made. Test signals are applied to the initial condition terminals of each integrator and to each input to the simulation. The output of each

potentiometer and amplifier and the input to each integrator is checked by the program. This procedure identifies each component whose output is out of tolerance or which is wired incorrectly.

A simulation control and optimization program was written in FORTRAN. Upon satisfaction of the static checks, this program is compiled, loaded, and executed. This program provides outer loop control of the analog simulation, generates the test gust signals, evaluates the performance index and its gradient, and varies the feedback gains according to the conjugate gradient optimization procedure.

The simulation of the aircraft was performed for a flight interval of 20 seconds duration. This is subdivided into 100 subintervals of 0.2 second each. The test gust signals were set before each subinterval. Then, the sensed variables were transferred to the digital computer through analog-to-digital converters. The digital computer commands the analog to resume simulation. Upon completion of the 0.2 second subinterval, the analog goes into the hold mode and sends a signal to the digital computer.

After commanding the analog to simulate, the digital computer stores the sensed variables and computes their contribution to the performance index. Then the digital computer waits for the interval completion signal from the analog before obtaining the next set of sensed variables. After 100 such intervals, the stored performance information is used in the optimization routine. The optimization routine continues until manually terminated.

RESULTS AND DISCUSSION

Effects of Control Configuration

A series of optimization runs were performed for various combinations of flap, spoiler, and elevator to determine the effects of each control combination on the performance of the optimized systems. The performance index used for this series was

$$J = \frac{1}{101}\sum_{k=1}^{101}\frac{1}{2}\left\{200\,a_{n_{(k)}}^2 + 200\,\dot{\Theta}^2_{(k)} + 100\,\Theta^2_{(k)} + 100\,a_{x_{(k)}}^2 + 100\,\gamma^2_{(k)} + 200\left(\frac{V_{(k)}}{V_o}\right)^2 + 100\,a_{B_{(k)}}^2 + 100\,\delta f_{c_{(k)}}^2 + 20\,\delta e_{c_{(k)}}^2 + 20\,\delta s_{c_{(k)}}^2\right\} + 0.002\sum_{i,j}(G_{ij})^2$$

where the (k) refers to the values of the variables at the $(k+1)^{st}$ sample time. This index is comprised of terms relating to ride qualities, a_n, $\dot{\Theta}$, a_X, and a_B; flight parameters, Θ, γ, and V; control command signals, δe_c, δf_c, and δs_c; and the magnitudes of the elements of the gain matrix, G_{ij}.

The simulation of the aircraft was initialized in steady, trimmed flight. Two predetermined rectangular waveforms, figure 6, were used as test gust inputs. These test gusts were chosen because they are easily generated on the hybrid computer, have a wide frequency spectrum, and are repeatable. Also, transport lags between sensor stations can be readily simulated for this form of gust.

The general form of the feedback loops in this series was

$$\begin{bmatrix} \delta f_c \\ \delta s_c \\ \delta e_c \end{bmatrix} = [G] \begin{bmatrix} a_n \\ \dot{\theta} \\ \theta \\ V_A \\ \overline{V}_o \\ a_x \end{bmatrix}$$

The gains for the various control configurations are listed in appendix C.

Figure 7 illustrates the effects of utilizing the different control surfaces upon the magnitudes of the sensed variables. The root mean square of each variable is plotted for each combination of active controls used on the feedback system. The values were obtained for the test gust disturbances with magnitudes of 1.77 m/sec. The points are plotted against the number of active controls with interconnecting lines added to aid visualization of the results.

Since the phugoid period of 16 seconds for the basic airplane is within the 20 second simulation interval, the results include contributions from both long and short period motions. However, since a finite time interval was used in computing the performance information, very long period motions of the closed loop systems, which might appear, would not grow fast enough to be detected. An adjustment of some of the feedback gains might be used to stabilize these modes without increasing the gust response.

Care should be exercised in interpreting the results presented in figure 7. The aircraft with controls locked at the trim positions (free aircraft case) exhibits relatively large magnitudes for all the variables presented. These magnitudes are due to the poorly damped phugoid mode being excited by the gusts. Most of the control configurations investigated show a sizable improvement relative to this case. However, a piloted aircraft would certainly not achieve the magnitudes presented for the free aircraft case.

The normal acceleration magnitudes may also be misleading. In the simulation model, the normal acceleration has a term that is proportional to the gust velocity. Step changes in the gusts produce a step change in the normal acceleration. Since the

control actuators have lag, they cannot react immediately to these transitions. In the simulation several of the normal acceleration measurements are taken immediately after the gust transitions. Therefore, due to the form of the gusts and the method of measurement, the measured RMS magnitude of the normal acceleration (for all control configurations) is higher than the magnitude to be expected for more realistic gust forms. For these reasons, the results presented in figure 7 are complemented by a closed loop pole analysis and a frequency response analysis in later sections of this report.

The spoiler used alone is not as effective as flap and elevator alone cases. The direct lift modulation produced by the spoiler improves the normal acceleration and flight path angle variations with no substantial change in the other measured variables.

The flap only control configuration shows improvement of all measured variables. The magnitudes of the accelerations a_n and a_x are smaller than for the spoiler alone and elevator alone cases. Although the flap is not intended for pitch control, a substantial improvement in the pitching response is apparent.

The elevator only configuration shows improvement of all the variables presented over the controls locked case and exhibits the least pitch angle and rate variation of all the control configurations investigated. This result is expected since the elevator is the obvious pitch control device; however, the lag involved in producing lift and drag changes is evidenced by greater accelerations than obtained by the flap only control configuration. The airspeed and flight path angle variations for the elevator case are similar to the variations for the flap case.

Flight path angle, speed variations, and normal acceleration are each improved by the addition of a second control device. However, these improvements are often accompanied by an increase in the pitch motion.

The control configuration with all three control devices active has less flight pitch angle and speed variations than any other configuration. The normal and axial accelerations and the pitch angle variations are not improved over the values obtained for two controls active. The pitch rate is increased over the cases with either flap or spoiler locked.

Pole Locations for Various Control Configurations

The roots of the characteristic equation (eigenvalues or poles) of the simulation model were examined. Figure 8 illustrates the pole locations in the complex plane for the various controls involving different combinations of control devices. In each case, any mode of the aircraft and control system which is not excited by control activity is deleted from the analysis. The deleted modes include the u_t mode that is excited only

by gusts and those actuator modes for control devices which are locked in place. The mode shapes (eigenvectors) were also examined and the results are discussed.

The pole locations for the aircraft with locked controls is given in figure 8(a). Five poles are shown; one of these is the result of the first order lag representation for the wing to tail transport lag of the downwash. Two poles form a very lightly damped oscillatory mode with period of 16.5 seconds. This corresponds to a phugoid motion but has a large amount of angle of attack variation $\left(\alpha \approx \frac{1}{4}\Theta\right)$. One pole corresponds to an exponentially decaying mode with time constant of 2 seconds. This is principally a plunging (angle of attack variation) mode. The two remaining poles form a well damped oscillatory mode with undamped natural frequency of 2.0 rad/sec and damping ratio 0.96. This is the short period mode with little speed and flight path angle variation.

The control actuator dynamics are also represented on this figure. The elevator and spoiler actuators are first order lags with time constants of 0.2 second each. The flap actuator is a first order lag with 0.5 second time constant.

Figures 8(b) to 8(h) illustrate the closed loop pole locations for the various control configurations. These locations show some similar features among the different cases. With the exception of the spoiler only control case, the poles form similar patterns. One pair, which may be either real or complex, appears near the origin. These poles may represent modes with time constants in the order of 100 seconds. These modes are primarily involved with speed and flight path angle variations as is the conventional phugoid motion. Each case involving the elevator as a controlling device has a relatively large angle of attack variation for these modes whereas the cases of flap only control and flap and spoiler control have relatively large pitch angle variation. This shift between angle of attack and pitch angle variations indicates the elevator's effectiveness in reducing pitch variations.

A second pair of poles appears with undamped natural frequency between 0.7 and 1.0 radian per second and damping ratio between 0.45 and 0.82 for the cases considered. This oscillatory mode involves angle of attack and pitch angle variations of approximately equal magnitudes (and phase). The magnitude of the speed variation is approximately 0.15 m/sec per degree of pitch angle variation. This coupling between pitch angle and speed is a bit larger than would be expected for a short period mode.

Either one or two, real or complex poles appear in the vicinity of the -2 point on the real axis. These modes are characterized by essentially equal pitch angle and angle of attack variations, large pitch rate magnitude, and small speed and flight path angle variations. Flight path angle and speed variations are 0.1° and 0.6 m/sec, respectively, per pitch rate magnitude of one degree per second. These characteristics are typical for conventional short period modes.

The remaining modes are easily identified with actuator dynamics with little involvement of aircraft flight variables.

The spoiler control case, figure 8(c), is the exception to the above general remarks. Two pairs of complex poles result with undamped natural frequency of approximately 0.46 rad/sec each and damping ratios of 0.9 and 0.3. Both of these modes have relative speed variations of 0.36 m/sec per 1^{o} of pitch variation. The closeness of the natural frequencies of the complex modes indicates that this closed loop system has very poor control characteristics and it would be unsuitable for use.

Frequency Response Characteristics

The response of the various closed loop systems to gusts were examined over a broad frequency spectrum. Figures 9(a) to 9(h) are frequency response plots of the amplitudes of normal acceleration of the center of gravity, pitch angle, flight path angle, and speed variation with respect to unit magnitude horizontal and vertical sinusoidal gusts. The plots are given for the cases of locked controls, elevator only control, elevator with flap control, elevator with spoiler control, and elevator with flap and spoiler. Comparison of these plots with different control configurations gives some insight into the effects and benefits of the utilization of the individual control devices.

The controls locked case exhibits a high phugoid resonance peak at 0.45 rad/sec due to poor damping in this mode. However, there is no distinguishable short period mode.

It is evident from the figures that the aircraft with locked controls is much more sensitive to horizontal gusts than to vertical gusts. The large horizontal gust responses are related to the high lift coefficient, C_L, and the positive aerodynamic derivative C_{m_u}. A head-on gust produces a large lift force due to the size of C_L. Also, the head-on gust produces a nose-up moment. The resulting pitch-up increases angle of attack, increasing lift and drag supplementing the values directly attributable to the gust. On the other hand, a vertical, up-gust produces a nose-down moment, since C_{m_α} is negative. The resulting pitch down motion decreases angle of attack and therefore lift and drag are diminished.

It is also known that a positive C_{m_u} has a pronounced destabilizing effect upon the phugoid mode. This effect is evidenced by the high phugoid peak responses due to both horizontal and vertical gusts.

The use of elevator feedback eliminates the strong phugoid response peak. Distinct phugoid and short period peaks appear at approximately 0.15 rad/sec and 1.0 rad/sec, respectively. These peaks are relatively broad; indicating good damping.

Addition of flap or spoiler to the control configuration generally decreases the aircraft response to gusts. However, the pitch angle and speed variations in response to vertical gusts show increases in amplitude with these additions. These increases reflect the tradeoff activity present in the design process.

Figures 9(a) and 9(b) illustrate the pitch angle variation due to horizontal and vertical gusts, respectively. The elevator only control law reduces the peak amplitudes considerable. The pitch response of this closed loop system is most sensitive to horizontal gusts at phugoid frequencies. Addition of flap or spoiler results in diminished phugoid response to either gust input while the short period response to horizontal gust is virtually unchanged. However, the short period response to vertical gusts is more than doubled with the addition of flap or spoiler. This increase is the result of tradeoffs occurring between the angular and the acceleration terms in the performance index. Examination of the pitch response characteristics shows no preference between the flap and the spoiler as active control devices.

Figures 9(c) and 9(d) illustrate the normal acceleration response to horizontal and vertical gusts, respectively. Since the gusts were assumed to act upon a single, unswept lifting-line located at the center of gravity, i.e., at a single point in the longitudinal plane, there is no cancellation of gust due to distribution of the sinusoidal forcing function along the wing chord and length of the fuselage. Also, the effects of varying downwash angle and stream velocity in the vicinity of the tail diminish at high frequency due to the method of modeling the wing-to-tail transport lag. Therefore, the computed transfer functions for normal acceleration approach a constant level at high frequency. In reality, however, the normal acceleration responses trailoff towards zero. The mentioned deficiencies in the simulation model cause the magnitude of the normal acceleration to be overestimated at high frequencies.

The elevator only controller eliminates the large resonant peaks in the normal acceleration transfer functions but increases the response in the short period region. The addition of the flap to the control configuration reduces the responses over all frequencies. However, the spoiler has much more effect at higher frequencies. These results suggest the desirability of utilizing the spoilers in the control system.

Figures 9(e) and 9(f) illustrate the flight path angle response to horizontal and vertical gusts, respectively. The elevator only control reduces the phugoid resonance peak to a smaller broad peak. The addition of the flap or spoiler to the control configuration generally reduces the flight path angle response throughout the frequency range shown, especially at the phugoid frequency. The spoiler has slightly more effect than the flap.

Figures 9(g) and 9(h) illustrate the speed response transfer functions for horizontal and vertical gusts, respectively. The elevator only feedback law results in a broad peak

at the phugoid frequency and greatly reduced response to horizontal gusts at the short period frequency. The addition of the spoiler to the control configuration improves the low frequency responses by a small amount with some increase in the short period region. Including the flap in the control configuration results in a large reduction in response to horizontal gusts, especially at low frequencies. However, this reduction is accompanied by a substantial increase in response to vertical gusts at very low frequencies. This increase is the result of small angle approximations used in developing the linearized model used in this study. The effectiveness of the flap in improving speed response as evidenced by figure 9(g) indicates the desirability of its incorporation into the feedback control system.

In summary, the frequency response to gust plots have demonstrated the effects of feedback control laws in reducing STOL motions in gusty conditions during the landing approach. The elevator provides stability as evidenced by the obvious reduction in resonant peaks. The addition of the spoiler to the control configuration is effective in reducing normal acceleration and flight path angle responses. The utilization of the flap effectively reduces speed variations. This analysis indicates that it would be desirable to include elevator, flap, and spoiler in a feedback control scheme for the STOL aircraft.

Time Histories

Figure 10 gives the time histories of the test gust signals and the corresponding control surface deflections for the case of flap, spoiler, and elevator control. Close examination of the first few seconds of simulation reveals the nature of the control movements in response to the gusts. Vertical gusts are counteracted mainly by a spoiler deflection accompanied by a small retraction of the flap. These motions tend to reduce the wing lift coefficient in regions of updraft. Horizontal gusts are counteracted by simultaneous deflection of spoiler, retraction of the flap, and downward movement of the elevator. In regions of head-on gust, the spoiler and flap motions reduce the lift and drag coefficients of the wing. The elevator motion counteracts the tail download produced by the increase in dynamic pressure at the stabilizer.

Figure 11 compares the time histories of several variables for the cases of locked controls and flap, spoiler, and elevator feedback controller. The test gust signals are used in these simulations. Excitation of the undamped long period mode of the open-loop system is readily apparent in the figure. The transitions evident in the normal acceleration result from the step changes in the horizontal and vertical gust velocities. The feedback control law effectively reduces the pitch angle, flight path angle, and speed variation of the aircraft. The normal acceleration retains its sharp transitions due to the

rectangular nature of the gusts and the limited bandwidth of the actuators. There is, however, a definite reduction in acceleration magnitude immediately after these transitions.

Effects of Sensor Configuration

A series of feedback gain matrices were computed for the control configuration utilizing elevator, flap, and spoiler surfaces and various combinations of sensors. The system obtained for pitch angle and rate feedback was used as a basis for comparison. Normal acceleration, axial acceleration, relative airspeed at the center of gravity, and relative airspeed and angle of attack measured at the nose of the airframe were each added to the pitch angle and rate feedback system and the feedback matrices were computed. In addition, configurations utilizing both airspeed at the nose and normal acceleration at the C.G. and both airspeed at the nose and angle of attack at the nose were used. Appendix D lists the gains for various sensor configurations.

The placement of sensors at the nose of the aircraft necessitated changes in the simulation. Rather than attempt prediction of the nose location sensor signals, the time base for the gust signals was moved from the C.G. to the nose. Then a transport lag was simulated to represent the delay of the gust between the nose and the wing. These changes resulted in a shift in the relative phasing of the performance variable measurement times and the times of the transitions in the wing forces produced by the gusts. The result was solution control laws which had very large spoiler deflections relative to the other controls. In order to reduce the spoiler deflection magnitude to a level approximately equal to that of the previously discussed systems, the weight on the spoiler command signal squared was increased from 20 to 100.

Figure 12 illustrates the effects of utilization of various sensor combinations upon the observed RMS values of several flight variables in response to the test gust signals. The cautions previously given relative to interpreting figure 7 apply also to figure 12. The addition of an airspeed sensor to the basic system results in the best improvement in the response of the pitch angle and inertial speed variations, and a notable improvement in the normal acceleration and flight path angle response. The speed response is better when the airspeed sensor is located at the nose of the airframe, u_F, rather than at the center of gravity, u_A. These improvements are the results of a large airspeed to elevator gain which decreases the download on the tail induced by head-on gusts. This loop compensates for the large $C_{m_{u_H}}$ of the basic aircraft.

The addition of normal acceleration, a_n, to the basic feedback system yields a good improvement in the normal acceleration response, as might be expected, with

small improvements in pitch angle and flight path angle variations. However, with this sensor combination, the speed response is degraded.

The addition of axial acceleration, a_X, feedback to the basic system results in small improvements in the pitch angle and speed responses.

The angle of attack sensor placed at the nose of the airframe, α_F, contributes only a small improvement in the speed response relative to the basic system. Examination of the gains for this case in table III shows that a sensed upgust results in an extension of both the flaps and spoiler and an upward motion of the elevator. The net result of these control motions is an increase in lift and drag and a nose-up moment. These control forces are opposite to those required to cancel the effects of an up-gust. This apparent contradiction in design specification and results is caused by the contamination of the vane signal by the pitch rate of the airframe. A pitch-up motion, which is produced by a horizontal gust, results in a negative angle of attack indication by the angle of attack sensor. The control motions reduce the lift and drag and counter the pitch-up tendency of the airframe. The optimization process has resulted in a feedback system which uses the intended angle of attack sensor as a pitch rate sensor in this case.

Two configurations utilizing four sensed variables were studied. The first had normal acceleration of the center of gravity and airspeed measured at the nose of the airframe in addition to the pitch angle and rate of the basic system; the second substituted the angle of attack at the nose for the normal acceleration. The observed RMS response to the test gust signals for the normal acceleration and flight path angle variations were improved for these two sensor configurations. However, the speed and pitch angle variations were degraded relative to the previous cases utilizing airspeed sensors. The former of these two cases (utilizing normal acceleration) had the best overall responses in normal acceleration and flight path angle. The latter (utilizing angle of attack) had slightly better pitch angle and speed responses. Examination of the feedback gains for this last case shows that the angle of attack sensor is indeed behaving as an angle of attack sensor. That is, the inclusion of airspeed sensing has effectively removed the corrupting pitch rate signal.

Pole Locations for Various Sensor Configurations

Figures 13(a) to 13(d) illustrate the closed loop pole locations for each of the sensor configurations. The baseline case utilizing only pitch angle and rate feedback has an overdamped phugoid mode with 3.64 seconds time to half amplitude and short period damping ratio of 0.55. The addition of sensors generally decreases the undamped natural frequency of the short period but there is little effect on the damping ratio. The addition of either normal acceleration, axial acceleration, or angle of attack sensors at the nose of the airframe generally doubles the phugoid time to half amplitude. Each

sensor configuration utilizing an airspeed sensor has a pole practically on the origin. This condition of marginal stability arises due to conflicting requirements of aircraft insensitivity to airspeed changes caused by horizontal gusts and speed (phugoid motion) stability produced by drag coefficient variation with speed.

Frequency Responses

Figure 14 gives frequency response curves of the magnitudes of pitch angle, normal acceleration, glide path angle, and inertial speed variations for the various sensor configurations. The responses are computed using sinusoidal horizontal and vertical gusts of unit amplitude. These curves generally agree with the responses observed for the test gust disturbances and they include much lower frequencies than could be contained in the 20 second simulation interval.

The addition of normal acceleration to the basic sensor configuration of pitch angle and rate resulted in a significant decrease in the normal acceleration response to both horizontal and vertical gusts. However, this alleviation is accompanied by increased responses of the pitch angle, speed, and flight path angle at the phugoid frequency.

The addition of the angle of attack at the nose of the aircraft to the basic sensor configuration resulted in small improvements in the aircraft responses to horizontal gusts and, in general, degradation of the responses to vertical gusts. The gains in this case were such that a sensed upward gust causes trailing edge upward motion of the elevator. In the event of a head-on gust, the airframe pitches up, inducing a down-gust indication from the angle of attack sensor. The resulting downward motion of the elevator tends to cancel the pitching moment due to the gust. Therefore, this control law has improved response to horizontal gusts. However, updrafts cause an up-gust indication. The resulting upward motion of the elevator tends to pitch the nose up. This increases the aircraft's response to vertical gusts.

The addition of axial acceleration to the basic sensed variables resulted primarily in a decrease of the pitching response to horizontal gusts, increase of the pitching response to vertical gusts, and decreases of speed variations in response to both types of gusts.

The sensor configuration utilizing airspeed at the nose in addition to the basic pitch angle and rate sensors results in improved flight path angle responses, especially in response to horizontal gusts. There is no apparent difference in moving this sensor to the center of gravity. The addition of angle of attack or normal acceleration sensors further improves the flight path angle responses, with the accelerometer being the more effective. However, very low frequency responses deteriorate with these last additions, indicating the approach of neutral stability.

The sensor configurations utilizing airspeed display considerable improvement in speed response to horizontal gust and varying degrees of increase in speed response to vertical gust. The smallest response to either gust type are obtained with the airspeed sensor located at the nose. The addition of the angle of attack sensor or normal acceleration sensor to this configuration results in larger speed responses to either horizontal or vertical gusts. The system acquires large responses to very low frequency vertical gusts with these additions.

The sensor configurations utilizing an airspeed sensor show significant reductions in the pitch angle response to horizontal gusts, accompanied by increases in response to vertical gusts. The least pitch variations of the sensor configurations studied occurred with the airspeed sensor located at the nose in addition to the pitch angle and rate feedback sensors. Moving the airspeed sensor to the center of gravity nearly doubles the height of the response peaks at 1 rad/sec. The pitch angle response is progressively greater for the configurations using the angle of attack at the nose, and normal acceleration in addition to the airspeed at the nose.

The configurations utilizing an airspeed sensor are characterized by improvement of the normal acceleration response to horizontal gusts. Of these configurations, the responses are greatest for the case of airspeed sensor at the center of gravity, and are progressively less for the cases of airspeed sensor at the nose, airspeed and angle of attack at the nose, and airspeed at the nose and normal acceleration sensor.

CONCLUSIONS

1. The aircraft examined in this report which flies at a high lift coefficient and has a large pitching moment change due to changes in airspeed, was found to have large responses to horizontal gusts.

2. Modeling the transport lag of the downwash variation between the wing and the tail with a first order lag makes the aircraft dynamics a fifth order system. For the aircraft studied in this report, modes similar to the conventional phugoid and short period modes can be identified. In addition, there is a first order plunging (angle of attack and speed) mode in the unaugmented aircraft dynamics.

3. Feedback control using the elevator results in decreased aircraft response to gusts. This is largely due to increased stability of the phugoid mode.

4. Inclusion of spoilers in feedback control systems decreases the normal acceleration and flight path angle responses to gusts.

5. The use of the trailing edge element of the flaps in feedback control systems reduces the low frequency pitch angle and speed responses to horizontal gusts.

6. The use of a fast response airspeed sensor in the control system reduces aircraft responses to horizontal gusts.

7. The effective use of an angle of attack sensor located at the nose of the aircraft requires either compensation or a sufficient number of other control loops to minimize corruption of the measurement by the pitching motion of the aircraft.

8. The closed loop systems obtained in this study tend to have marginal speed stability. This characteristic might be corrected by minor changes in the control system gains.

9. The use of test gust signals of rectangular nature in the design process has resulted in closed loop systems having reasonable responses to sinusoidal gusts over a broad frequency range.

10. The inclusion of penalties on the feedback gains in the performance index of an optimization routine prevents large gains and excessively high frequency, lightly damped closed loop dynamics.

Langley Research Center,
National Aeronautics and Space Administration,
Hampton, Va., May 20, 1974.

APPENDIX A

AIRCRAFT SIMULATION MODEL

A mathematical model of the externally blown flap STOL aircraft was developed along conventional lines with some variance in the treatment of the transport lag between the wing and the tail. The longitudinal dynamics of the aircraft relative to the wind axes coordinate system are represented by a system of differential equations:

$$\left.\begin{aligned} mV\dot{\Gamma} &= L - mg\cos\Gamma \text{ (lift equation)} \\ m\dot{V} &= -D - mg\sin\Gamma \text{ (drag equation)} \\ mk_y^2\bar{c}^2\ddot{\Theta} &= M \text{ (pitching equation)} \end{aligned}\right\} \quad \text{(A1)}$$

The flight path angle, Γ, may be replaced by the equivalent expression, $\Theta - A_I$. In addition, each variable may be partitioned into two parts: a nominal variable corresponding to a normal flight trajectory and a relative variable being the variation of the original variable about its nominal value, for example, $\Theta = \Theta_o + \Delta\Theta = \Theta_o + \theta$. The aerodynamic forces may also be partitioned into portions contributed by the wing and by the tail, for example $L = L_w + L_t$. The incorporation of these items in equation (1) yields an alternate form for the aircraft dynamical equations.

$$\begin{aligned} m(V_o + v)(\dot{\Gamma}_o + \dot{\theta} - \dot{\alpha}_I) &= L_w + L_t - mg\cos(\Gamma_o + \theta - \alpha_I) \\ m(\dot{V}_o + \dot{v}) &= -D_w - D_t - mg\sin(\Gamma_o + \theta - \alpha_I) \\ mk_y^2\bar{c}^2(\ddot{\Theta}_o + \ddot{\theta}) &= M_w + M_t \end{aligned} \quad \text{(A2)}$$

The lift, drag, and moment produced by the wing (L_w, D_w, M_w) are functions of the angle of attack of the wing, the relative stream velocity at the wing, and the control surface deflections. The angle of attack is composed of the inertial angle of attack, α_I, caused by the motion of the aircraft through space, and contributions induced by gusts. The relative stream velocity at the wing is composed of the inertial velocity, V, and contributions induced by gusts. The lift produced by the wings may be expressed, in general, as

$$L_w = L_{w_o} + \bar{q}_w(V, V_V, V_H)SC_{L_w}(V, \alpha_I, V_V, V_H, \delta s, \delta f) \quad \text{(A3)}$$

Expansion of this expression by Taylor series and discarding terms above the first order results in the following linear expression for the lift of the wing:

$$L_w = L_{w_o} + \frac{1}{2}\rho V_o^2 S\left[\left(2C_{L_{w_o}} + C_{L_1}\right)u + C_{L_{\alpha_w}}\alpha_I + C_{L_{u_{V_w}}}u_V + C_{L_{u_{H_w}}}u_H + C_{L_{\delta s_w}}\delta s + C_{L_{\delta f_w}}\delta f\right] \tag{A4}$$

where

$$u = \frac{v}{V_o} = \frac{\Delta V}{V_o},\quad u_H = \frac{V_H}{V_o},\quad u_V = \frac{V_V}{V_o}$$

Similar linearized expressions can be derived for the drag and moment of the wing.

The lift, drag, and moment produced by the tail (L_t, D_t, M_t) are functions of the relative stream velocity and direction at the tail and the elevator deflection. The angle of attack of the horizontal tail is composed of the angle of attack of the wing, the downwash angle including gust effects, and the pitch rate of the aircraft. The relative stream velocity at the tail is composed of the inertial velocity of the aircraft and gust contributions. The effect of downwash variations reach the tail at a time ($\tau = \ell_t \bar{c}/V_o$) after the variations are caused at the wing. Also, the stream velocity variations at the tail due to the gusts occur at a time, τ, after the gusts effect the wing. The lift produced by the tail may be expressed, in general, as

$$L_t(t) = \bar{q}_t\left(V(t), V_V(t-\tau), V_H(t-\tau)\right) S C_{L_t}\left(\alpha_I(t), \epsilon(t), \dot{\Theta}(t), \delta e(t)\right) \tag{A5}$$

Expansion of this expression via Taylor series and discarding terms above the first order results in the following linear expression for the lift of the tail:

$$L_t = L_{t_o} + \frac{1}{2}\rho V_o^2 S\left[2C_{L_{t_o}}\left(u + u_t\right) + C_{L_{\alpha_t}}\left(\alpha_I - \epsilon\right) + C_{L_{\dot{\Theta}}}\dot{\Theta} + C_{L_{\delta e}}\delta e\right] \tag{A6}$$

where

$$u_t(t) = \frac{\partial u_t}{\partial u_H} u_H(t-\tau) + \frac{\partial u_t}{\partial u_V} u_V(t-\tau) \tag{A7}$$

The variable u_t is the portion of the stream velocity at the tail due to the gusts. Similar linearized expressions can be derived for the drag and moment of the tail (D_t and M_t).

The downwash angle is a function of the angle of attack of the wing, the gust velocities, the aircraft velocity, the spoiler deflection, and the flap deflection.

$$\epsilon(t) = \frac{\partial \epsilon}{\partial \alpha} \alpha_I(t - \tau) + \frac{\partial \epsilon}{\partial u} u(t - \tau) + \frac{\partial \epsilon}{\partial u_V} u_V(t - \tau) + \frac{\partial \epsilon}{\partial u_H} u_H(t - \tau)$$
$$+ \frac{\partial \epsilon}{\partial \delta s} \delta s(t - \tau) + \frac{\partial \epsilon}{\partial \delta f} \delta f(t - \tau) \tag{A8}$$

The linearized expressions for the lift, drag, and moment components (eqs. (A4) and (A6)) are substituted into the aircraft dynamic equations (eq. (A2)). Small angle approximations are made for the trigonometric functions. For the steady flight condition the following simplifying relations are utilized:

$$\left.\begin{aligned} \dot{\Gamma}_o &= 0 \\ \dot{V}_o &= 0 \\ \ddot{\Theta}_o &= 0 \\ L_o &= L_{w_o} + L_{t_o} = mg \cos \Gamma_o \\ D_o &= D_{w_o} + D_{t_o} = -mg \sin \Gamma_o \\ M_o &= M_{w_o} + M_{t_o} = 0 \end{aligned}\right\} \tag{A9}$$

Second order terms are dropped and the resulting linearized equations may be written as

$$-\dot{\alpha}_I = \frac{g}{V_o}\left[\Theta - \alpha_I\right] \sin \Gamma_o - \dot{\Theta} + \frac{1}{2} \frac{\rho}{m} V_o S \Big\{ C_{L_{\alpha_w}} \alpha_I + C_{L_{\dot{\Theta}}} \dot{\Theta}$$
$$+ \left[C_{L_{u_w}} + 2C_{L_o}\right] u + C_{L_{u_{V_w}}} u_V + C_{L_{u_{H_w}}} u_H + C_{L_{\delta f_w}} \delta f$$
$$+ C_{L_{\delta e}} \delta e + C_{L_{\delta s_w}} \delta s + 2C_{L_{t_o}} u_t - C_{L_{\alpha_t}} (\epsilon - \alpha_I) \Big\} \tag{A10a}$$

$$\ddot{\Theta} = \frac{1}{2} \frac{\rho V_o^2 S}{m k_y^2 \bar{c}} \Big\{ C_{m_{\alpha_w}} \alpha_I + C_{m_{\dot{\Theta}}} \dot{\Theta} + C_{m_{u_w}} u + C_{m_{u_{V_w}}} u_V + C_{m_{u_{H_w}}} u_H$$
$$+ C_{m_{\delta f_w}} \delta f + C_{m_{\delta e}} \delta e + C_{m_{\delta s_w}} \delta s + 2C_{m_t} u_t - C_{m_{\alpha_t}} (\epsilon - \alpha_I) \Big\} \tag{A10b}$$

$$\dot{u} = -\frac{1}{2}\frac{\rho}{m} V_o S \Big\{ C_{D_{\alpha_w}} \alpha_I + C_{D_{\dot{\theta}}} \dot{\theta} + \Big[C_{D_{u_w}} + 2C_{D_o} \Big] u + C_{D_{u_{V_w}}} u_V + C_{D_{u_{H_w}}} u_H$$

$$+ C_{D_{\delta f_w}} \delta f + C_{D_{\delta e}} \delta e + C_{D_{\delta s_w}} \delta s + 2C_{D_t} u_t - C_{D_{\alpha_t}} (\epsilon - \alpha_I) \Big\} - \frac{g}{V_o} \Big[\theta - \alpha_I \Big] \cos \Gamma_o \qquad \text{(A10c)}$$

The transport lags in equations (A7) and (A8) are treated differently from the usual procedure (see ref. 4). The lags are approximated by first order lags whose time constants are equal to the time of delay of the transport lags. The relations used to approximate ϵ and u_t are

$$\left.\begin{aligned} \frac{\bar{c}\ell_t}{V_o} \dot{\epsilon} &= \left\{ \frac{\partial \epsilon}{\partial \alpha} \alpha_I + \frac{\partial \epsilon}{\partial u_V} u_V + \frac{\partial \epsilon}{\partial u_H} u_H + \frac{\partial \epsilon}{\partial u} u + \frac{\partial \epsilon}{\partial \delta f} \delta f + \frac{\partial \epsilon}{\partial \delta s} \delta s \right\} - \epsilon \\ \frac{\bar{c}\ell_t}{V_o} \dot{u}_t &= \left\{ \frac{\partial u_t}{\partial u_V} u_V + \frac{\partial u_t}{\partial u_H} u_H \right\} - u_t \end{aligned}\right\} \qquad \text{(A11)}$$

APPENDIX B.– AIRCRAFT PARAMETERS

$\bar{c}$	= 3.203 m (10.51 ft)
S_w	= 74.45 m^2 (801.36 ft^2)
S_t	= 23.69 m^2 (255.0 ft^2)
l_t	= 3.2
h_t	= 1.6
m	= 25 022 kg (1715 slugs)
k_y^2	= 1.31
ρ	= 1.225 kg/m^3 (0.002378 $slug/ft^3$)
g	= 9.805 m/s^2 (32.17 ft/s^2)
δf_o	= 60^o
α_o	= 10^o
C_{μ_o}	= 1.87
δs_o	= 15^o
ϵ_o	= 13.89^o
δe_o	= -25^o
i_{t_o}	= 5.16^o
C_{L_w}	= 4.7633
C_{D_w}	= 0.3231
C_{m_w}	= -0.5160
C_{L_t}	= 0.4826
C_{D_t}	= -0.0326
C_{m_t}	= 0.5160
C_L	= 4.2807
C_D	= 0.2905
Γ_o	= -3.88^o
Θ_o	= 6.12^o
V_o	= 35.41 m/s (116.17 ft/s)

$C_{L_{\alpha_w}}$	= 5.7 rad^{-1}
$C_{D_{\alpha_w}}$	= 4.0 rad^{-1}
$C_{m_{\alpha_w}}$	= 1.7 rad^{-1}
$C_{L_{u_w}}$	= -3.50
$C_{D_{u_w}}$	= 1.00
$C_{m_{u_w}}$	= 1.13
$C_{L_{\delta f_w}}$	= 2.8 rad^{-1}
$C_{D_{\delta f_w}}$	= 3.5 rad^{-1}
$C_{m_{\delta f_w}}$	= -0.6 rad^{-1}
$C_{L_{\delta s_w}}$	= -2.89 rad^{-1}
$C_{D_{\delta s_w}}$	= -0.408 rad^{-1}
$C_{m_{\delta s}}$	= 1.581 rad^{-1}
$\frac{\partial \epsilon}{\partial \alpha}$	= 0.5590
$\frac{\partial \epsilon}{\partial u}$	= -0.3097 rad
$\frac{\partial \epsilon}{\partial \delta f}$	= 0.2746
$\frac{\partial \epsilon}{\partial \delta s}$	= -0.2834
$C_{L_{\alpha_t}}$	= 1.6146 rad^{-1}
$C_{D_{\alpha_t}}$	= 0.5185 rad^{-1}
$C_{m_{\alpha_t}}$	= -5.3700 rad^{-1}
$C_{L_{\dot{\Theta}}}$	= 0.4166 $(rad/sec)^{-1}$
$C_{D_{\dot{\Theta}}}$	= 0.1014 $(rad/sec)^{-1}$
$C_{m_{\dot{\Theta}}}$	= -1.3252 $(rad/sec)^{-1}$
$C_{L_{\delta e}}$	= 0.3062 rad^{-1}

APPENDIX B – Concluded

$C_{D_{\delta e}} = 0.0687 \text{ rad}^{-1}$

$C_{m_{\delta e}} = -0.9783 \text{ rad}^{-1}$

$C_{L_{u_{H_w}}} = 5.6050$

$C_{D_{u_{H_w}}} = 1.6942$

$C_{m_{u_{H_w}}} = -0.0175$

$C_{L_{u_{V_w}}} = 6.4174$

$C_{D_{u_{V_w}}} = -0.6501$

$C_{m_{u_{V_w}}} = 1.7027$

$\frac{\partial u_t}{\partial u_H} = 0.9977$

$\frac{\partial u_t}{\partial u_H} = 0.0677$

$\frac{\partial \epsilon}{\partial u_H} = -0.0098$

$\frac{\partial \epsilon}{\partial u_V} = -0.4425$

$t_e = 0.2 \text{ sec}$

$t_s = 0.2 \text{ sec}$

$t_f = 0.5 \text{ sec}$

APPENDIX C. – GAINS FOR VARIOUS CONTROL CONFIGURATIONS

Elevator Only Controller

$$\delta e_c = 0.1979\, a_n - 0.5115\, \dot{\Theta} - 0.0163\, \Theta + 1.2642\, u_A - 0.1878\, a_X$$

Spoiler Only Controller

$$\delta s_c = 1.5012\, a_n + 0.0220\, \dot{\Theta} - 0.2949\, \Theta + 0.6678\, u_A - 0.2343\, a_X$$

Flap Only Controller

$$\delta f_c = -0.0208\, a_n - 0.1035\, \dot{\Theta} - 0.56980\, \Theta - 0.8494\, u_A - 0.4984\, a_X$$

Elevator and Spoiler Controller

$$\delta e_c = 0.2391\, a_n - 0.0374\, \dot{\Theta} - 0.2849\, \Theta + 1.2540\, u_A + 0.3396\, a_X$$

$$\delta s_c = 0.7237\, a_n - 0.1142\, \dot{\Theta} + 0.2702\, \Theta + 0.5574\, u_A + 0.2592\, a_X$$

Elevator and Flap Controller

$$\delta e_c = -0.0491\, a_n - 0.0738\, \dot{\Theta} - 0.1001\, \Theta + 1.0275\, u_A + 0.0387\, a_X$$

$$\delta f_c = -0.1492\, a_n + 0.2446\, \dot{\Theta} - 0.8521\, \Theta + 0.4756\, u_A - 0.2899\, a_X$$

Spoiler and Flap Controller

$$\delta s_c = 0.7125\, a_n - 0.5137\, \dot{\Theta} + 0.5018\, \Theta - 0.0033\, u_A + 0.2706\, a_X$$

$$\delta f_c = 0.0553\, a_n - 0.2910\, \dot{\Theta} - 0.4811\, \Theta - 0.8547\, u_A - 0.4367\, a_X$$

Elevator, Spoiler, and Flap Controller

$$\delta e_c = 0.1949\, a_n + 0.2488\, \dot{\Theta} + 0.2135\, \Theta + 1.0216\, u_A - 0.2143\, a_X$$

$$\delta s_c = 0.6300\, a_n - 0.0989\, \dot{\Theta} + 0.2478\, \Theta + 0.3660\, u_A - 0.3990\, a_X$$

$$\delta f_c = -0.0251\, a_n + 0.2386\, \dot{\Theta} - 0.5350\, \Theta - 0.4027\, u_A - 0.0889\, a_X$$

APPENDIX D. – GAINS FOR VARIOUS SENSOR CONFIGURATIONS

Pitch Angle and Rate Only

$$\delta f_c = -0.8698\,\dot{\Theta} - 1.0033\,\Theta$$

$$\delta s_c = 0.7633\,\dot{\Theta} + 7408\,\Theta$$

$$\delta e_c = 1.7368\,\dot{\Theta} + 0.7324\,\Theta$$

With Normal Acceleration

$$\delta f_c = -0.2938\,a_n - 0.8821\,\dot{\Theta} - 1.0025\,\Theta$$

$$\delta s_c = 0.9888\,a_n - 0.3343\,\dot{\Theta} + 0.2485\,\Theta$$

$$\delta e_c = 0.8505\,a_n - 1.3370\,\dot{\Theta} - 0.1589\,\Theta$$

With Airspeed at C.G.

$$\delta f_c = -0.0340\,\dot{\Theta} - 0.6664\,\Theta - 0.4253\,u_A$$

$$\delta s_c = 0.5283\,\dot{\Theta} + 0.3308\,\Theta + 0.3893\,u_A$$

$$\delta e_c = -0.4929\,\dot{\Theta} + 0.1900\,\Theta + 1.0931\,u_A$$

With Axial Acceleration

$$\delta f_c = -0.4759\,\dot{\Theta} - 0.9072\,\Theta + 0.4755\,a_X$$

$$\delta s_c = 0.7183\,\dot{\Theta} + 0.6706\,\Theta + 0.0258\,a_X$$

$$\delta e_c = 1.0721\,\dot{\Theta} + 0.3726\,\Theta - 1.8043\,a_X$$

APPENDIX D – Concluded

With Airspeed at Nose

$$\delta f_c = -0.4153\,\dot{\Theta} - 0.5166\,\Theta - 0.4282\,u_F$$

$$\delta s_c = 0.5793\,\dot{\Theta} + 0.1827\,\Theta + 0.2908\,u_F$$

$$\delta e_c = -0.0866\,\dot{\Theta} - 0.0250\,\Theta + 1.0320\,u_F$$

With Angle of Attack at Nose

$$\delta f_c = -0.8277\,\dot{\Theta} - 1.0057\,\Theta + 0.3754\,\alpha_F$$

$$\delta s_c = 0.6282\,\dot{\Theta} + 0.5092\,\Theta + 0.2117\,\alpha_F$$

$$\delta e_c = 1.3419\,\dot{\Theta} + 1.0476\,\Theta - 0.6551\,\alpha_F$$

With Airspeed at Nose and Normal Acceleration

$$\delta f_c = -0.2575\,a_n - 0.2421\,\dot{\Theta} - 0.3619\,\Theta - 0.3550\,u_F$$

$$\delta s_c = 0.8365\,a_n - 0.0501\,\dot{\Theta} + 0.2024\,\Theta + 0.1678\,u_F$$

$$\delta e_c = -0.0652\,a_n + 0.2805\,\dot{\Theta} - 0.1670\,\Theta + 1.0908\,u_F$$

With Airspeed and Angle of Attack at Nose

$$\delta f_c = -0.4075\,\dot{\Theta} - 0.4012\,\Theta - 0.5519\,u_F - 0.2200\,\alpha_F$$

$$\delta s_c = 0.6000\,\dot{\Theta} + 0.1426\,\Theta + 0.3553\,u_F + 0.3093\,\alpha_F$$

$$\delta e_c = 0.0029\,\dot{\Theta} - 0.1102\,\Theta + 1.0436\,u_F + 0.0226\,\alpha_F$$

REFERENCES

1. Lasdon, L. S.; Mitter, S. K.; and Waren, A. D.: The Conjugate Gradient Method for Optimal Control Problems. IEEE Trans. Automat. Contr., vol. AC-12, no. 2, Apr. 1967.

2. Parlett, Lysle P.; Greer, H. Douglas; Henderson, Robert L.; and Carter, C. Robert: Wind-Tunnel Investigation of an External-Flow Jet-Flap Transport Configuration Having Full-Span Triple-Slotted Flaps. NASA TN D-6391, 1971.

3. Freeman, Delma C., Jr.; Parlett, Lysle P.; and Henderson, Robert L.: Wind-Tunnel Investigation of a Jet Transport Airplane Configuration With an External-Flow Jet Flap and Inboard Pod-Mounted Engines. NASA TN D-7004, 1970.

4. Phillips, William H.; and Kraft, Christopher C., Jr.: Theoretical Study of Some Methods for Increasing the Smoothness of Flight Through Rough Air. NACA TN 2416, 1951.

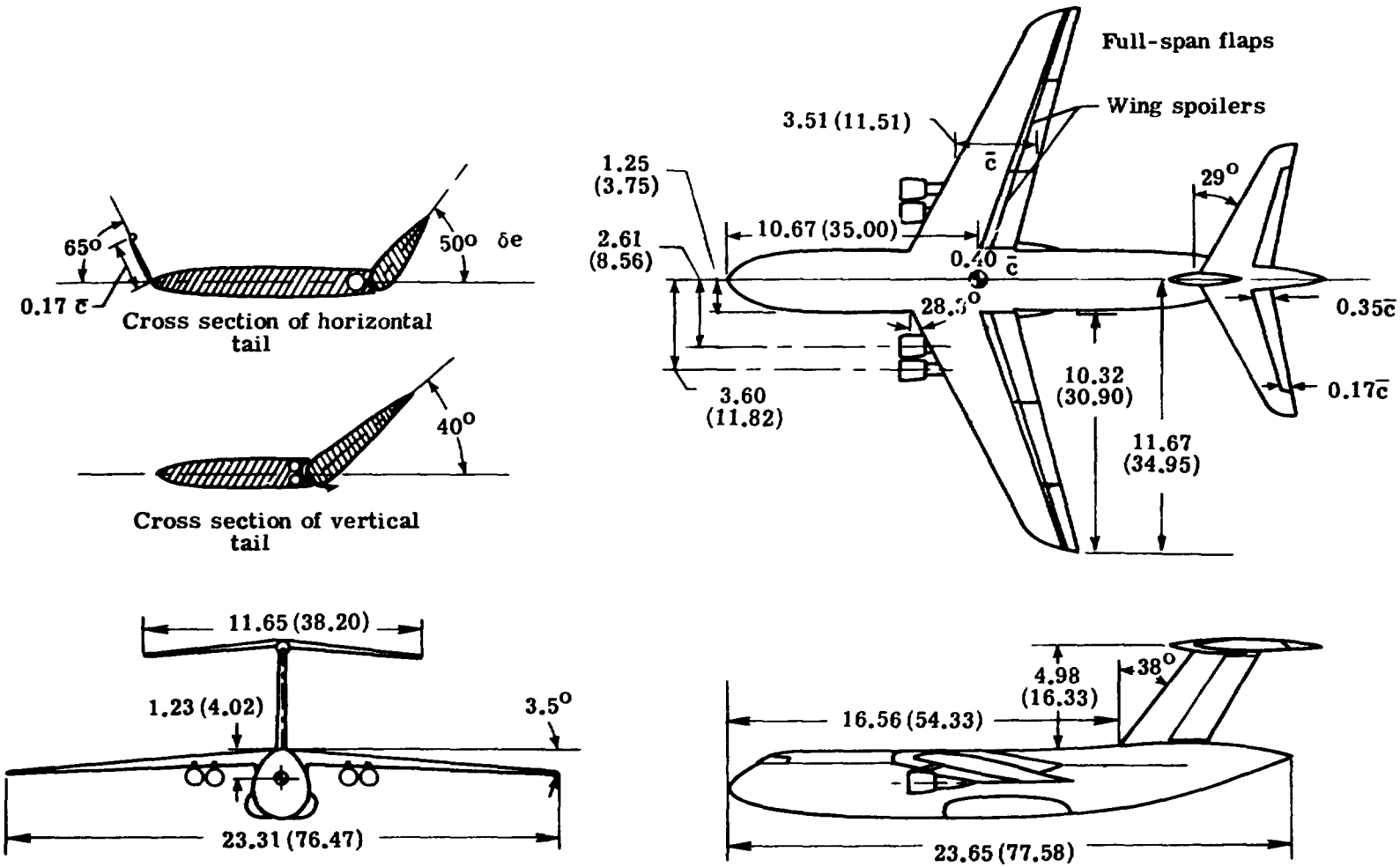

Figure 1.- Three-view drawing of simulated airplane. All linear dimensions are in meters (feet).

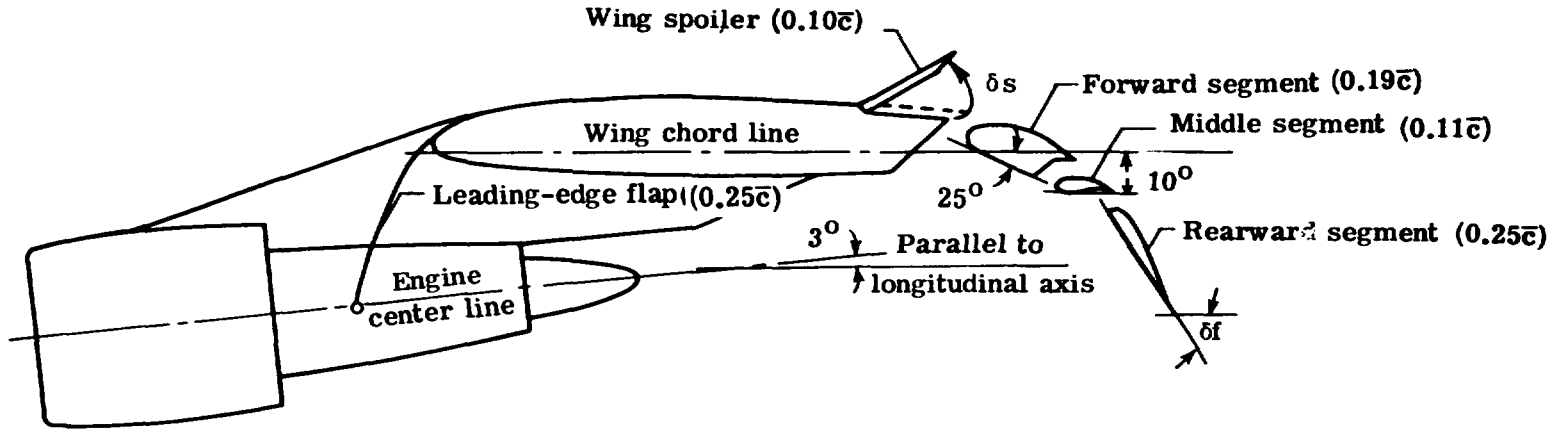

Figure 2.- Flap assembly and engine pylon detail.

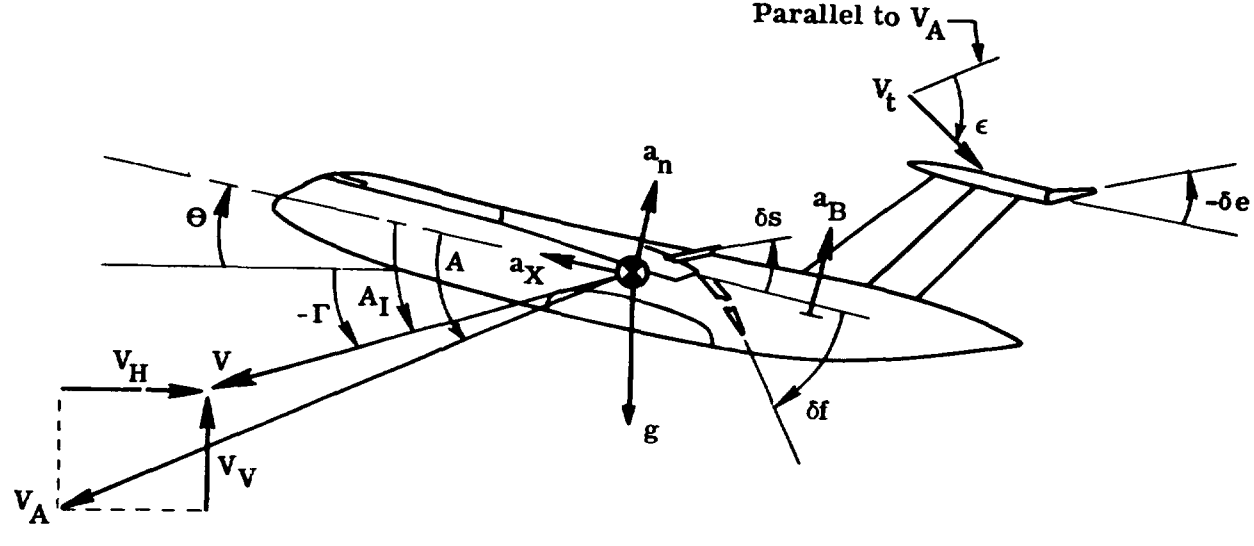

Figure 3.- Simulation variables.

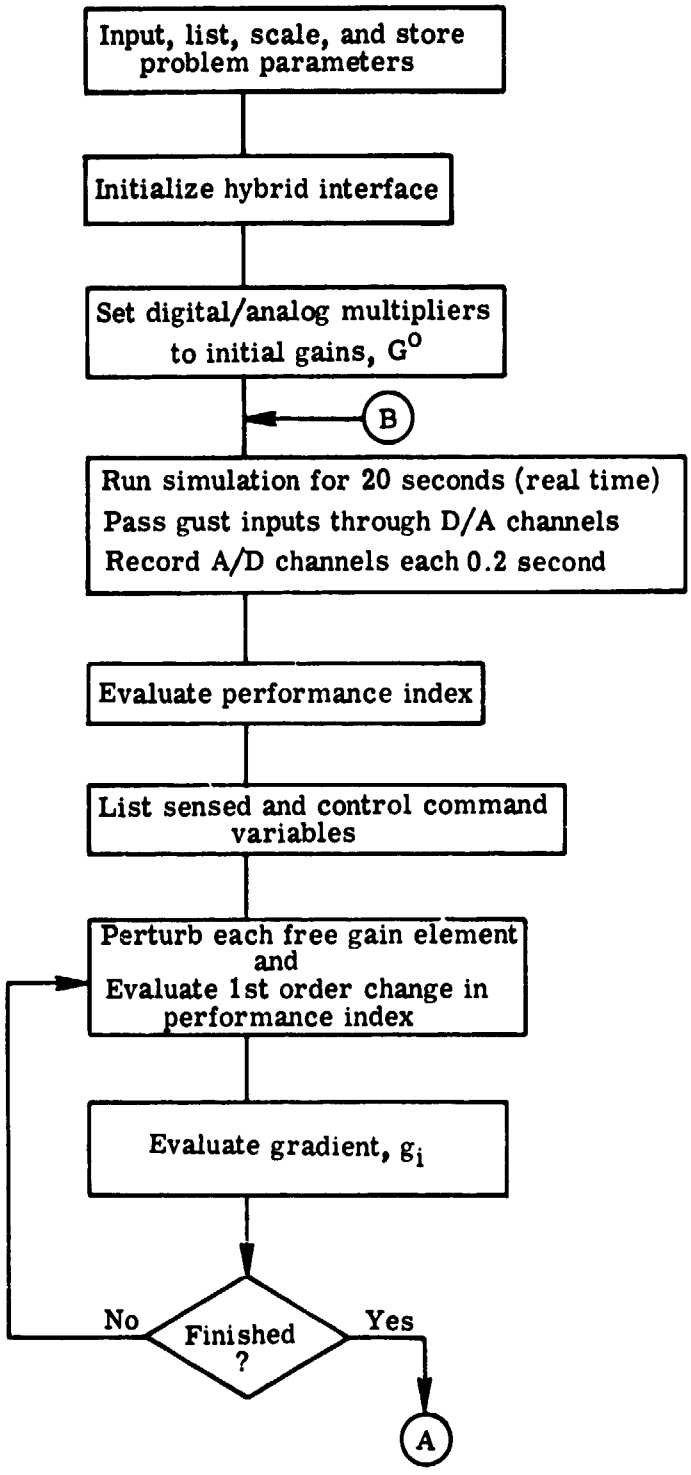

Figure 4.- Conjugate gradient algorithm logic flow chart.

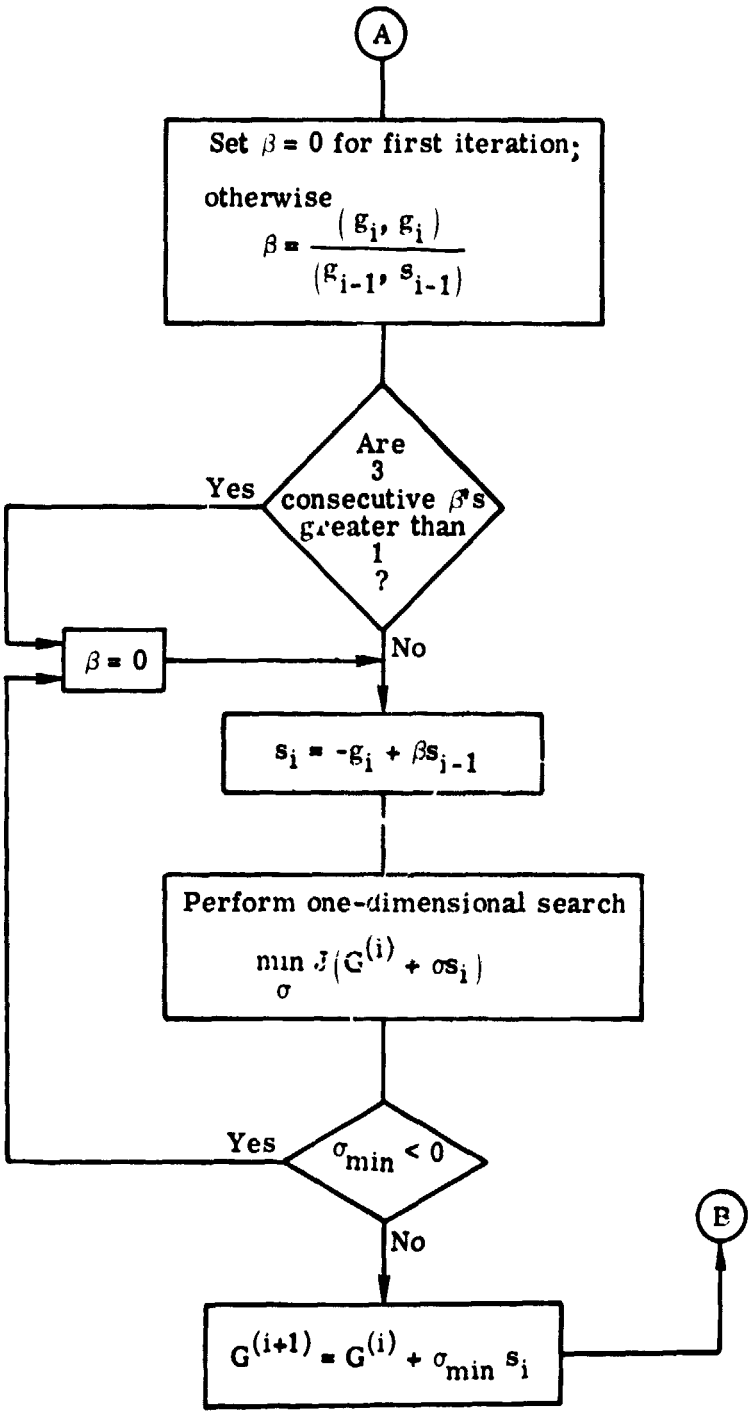

Figure 4.- Concluded.

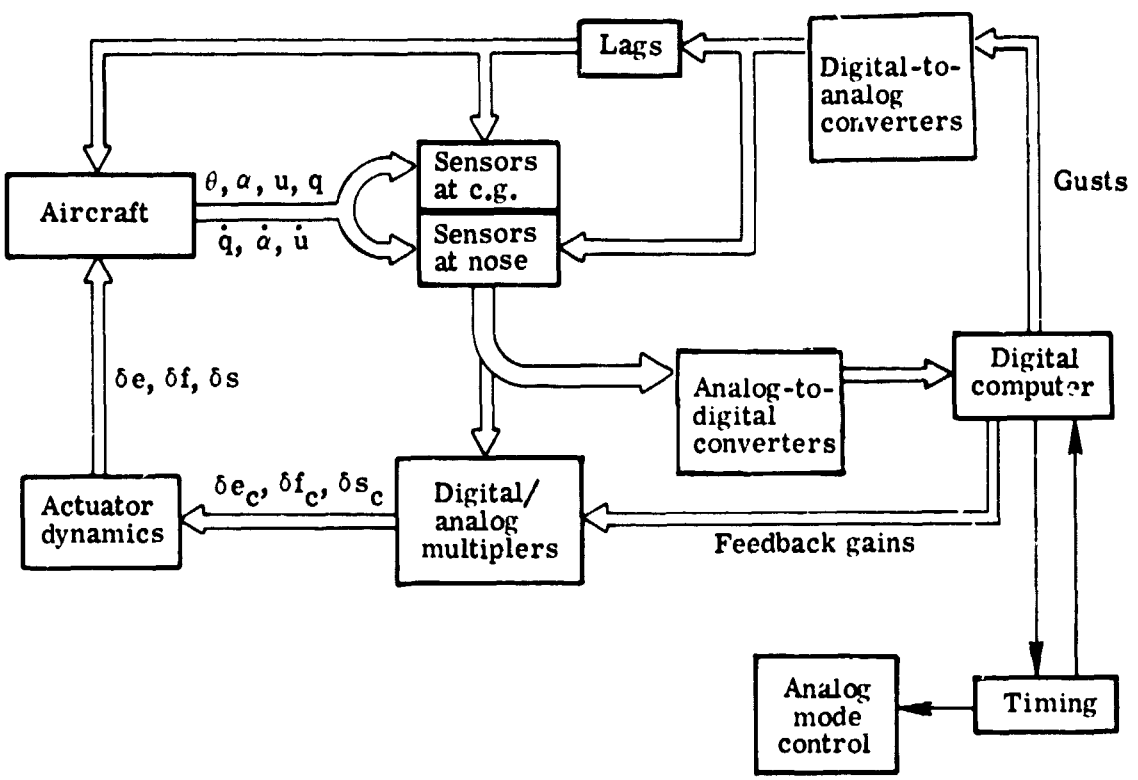

Figure 5.- Hybrid computer setup.

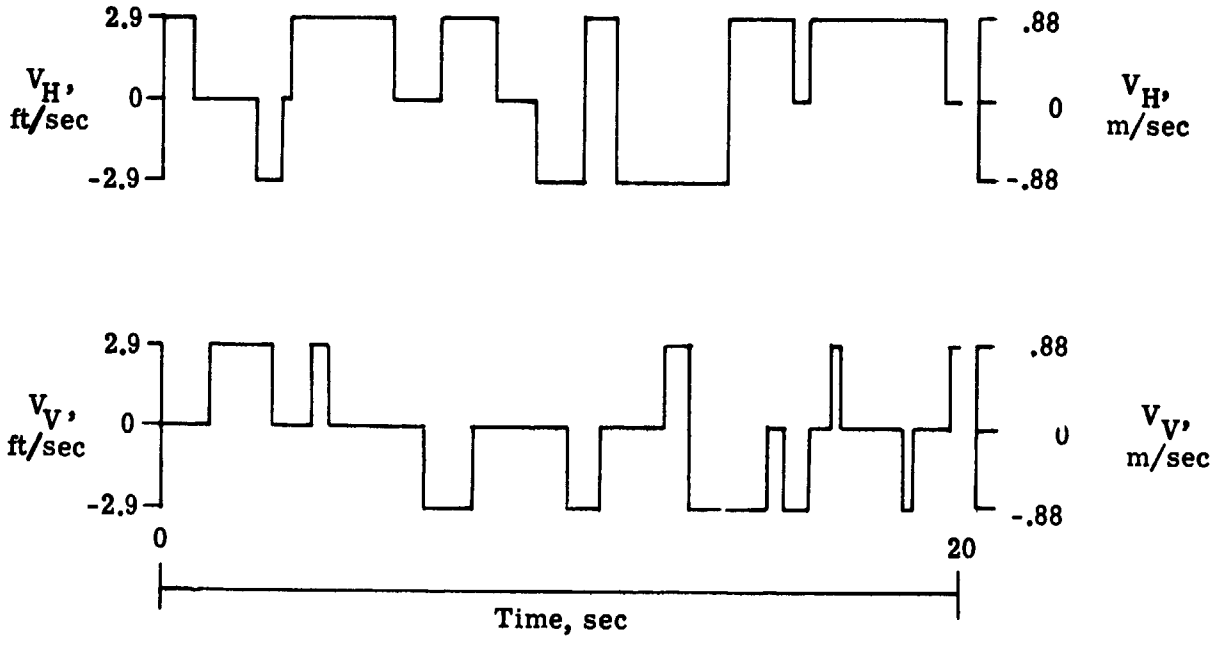

Figure 6.- Test gusts.

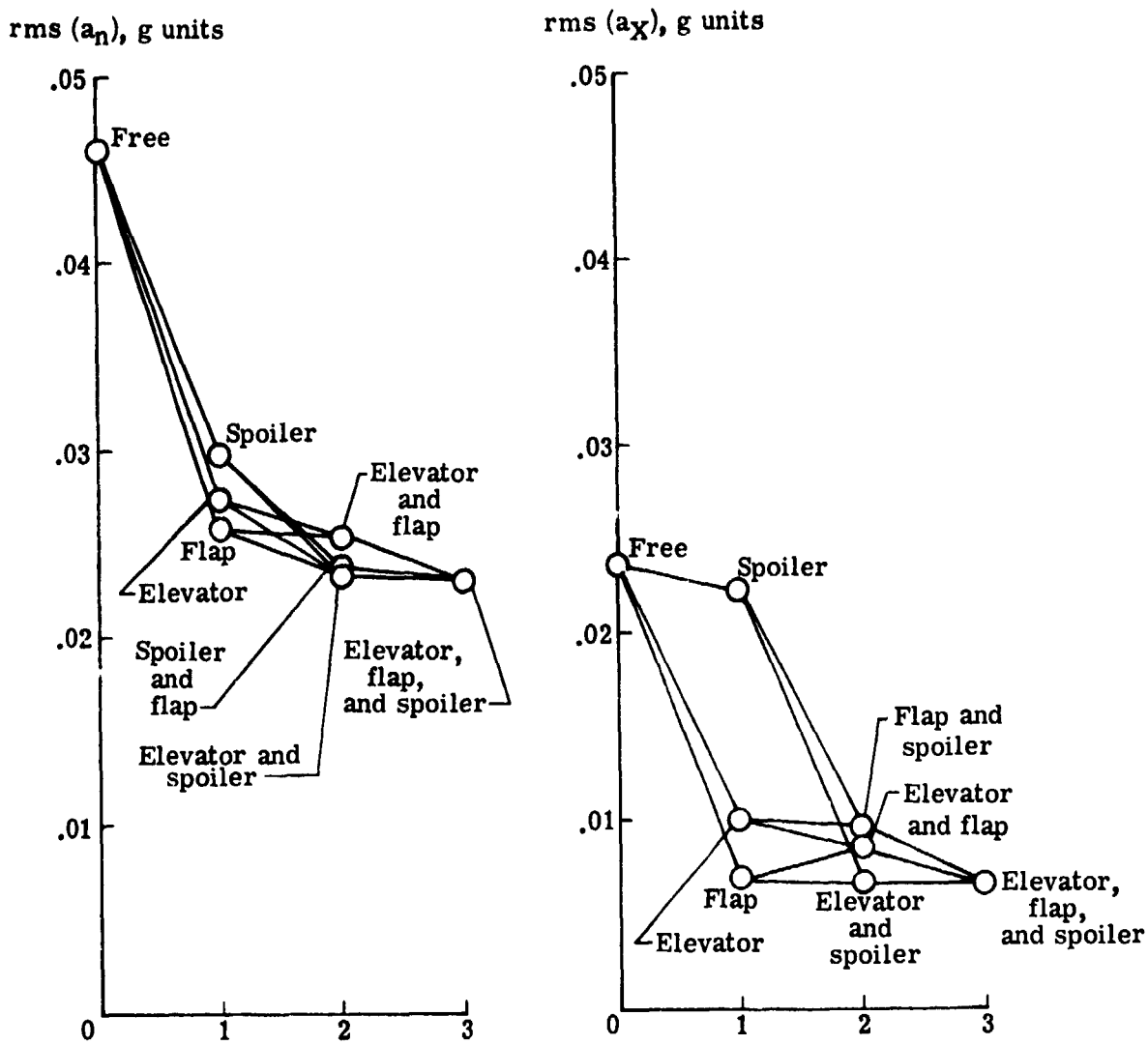

(a) Normal acceleration.

(b) Axial acceleration.

Figure 7.- Observed variable magnitudes for different control configurations.

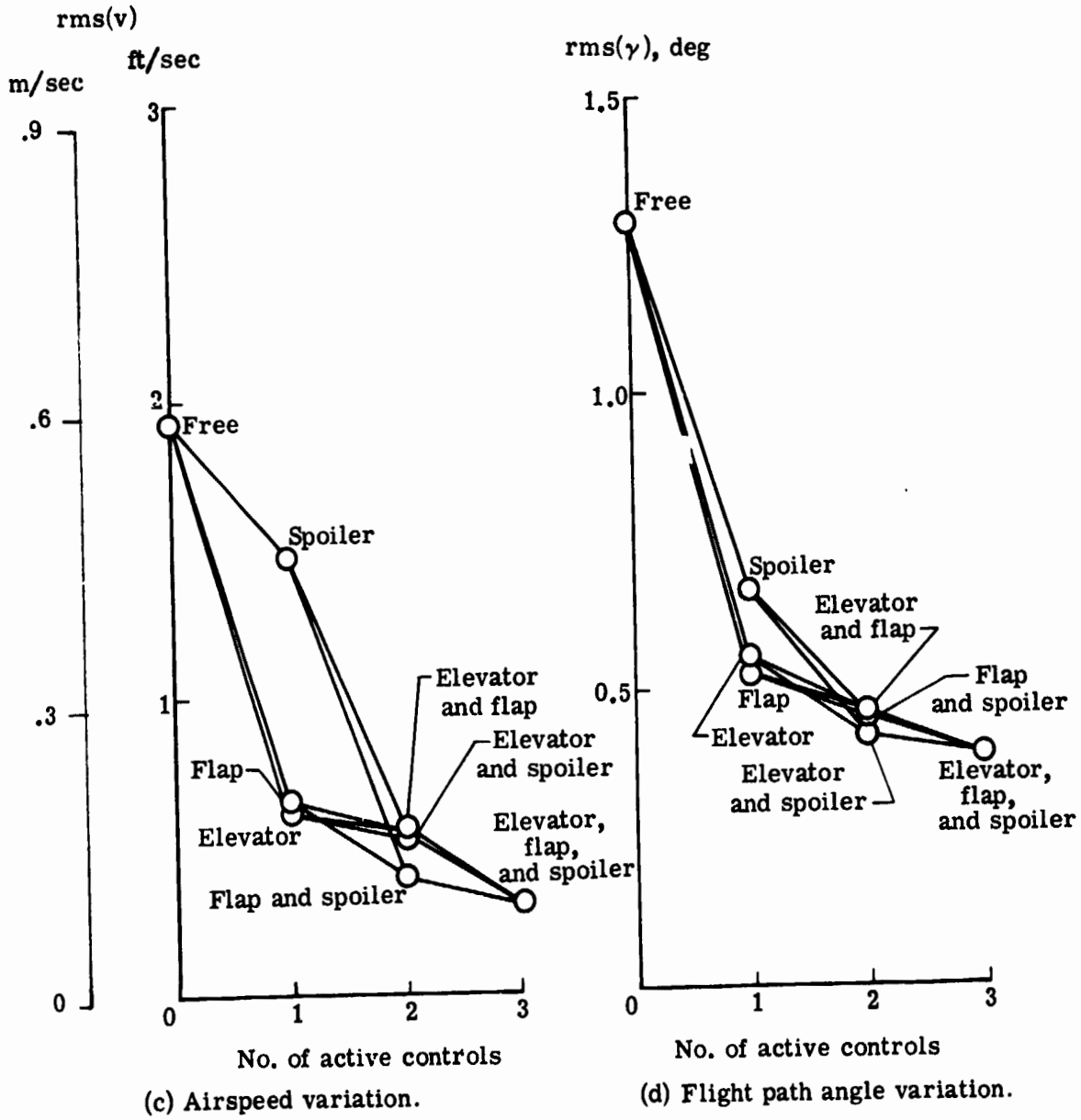

(c) Airspeed variation.

(d) Flight path angle variation.

Figure 7.- Continued.

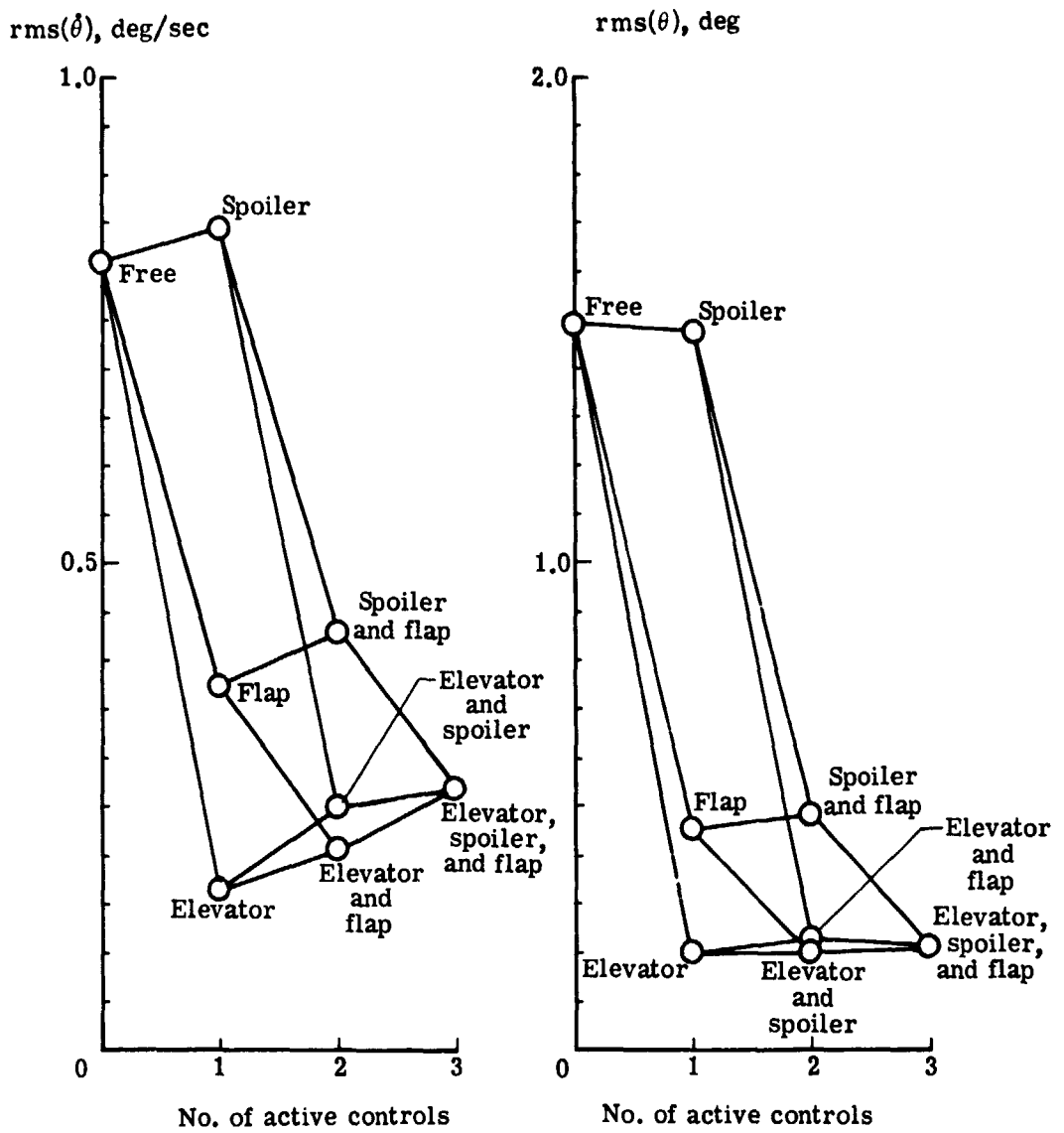

(e) Pitch rate.

(f) Pitch angle variation.

Figure 7.- Concluded.

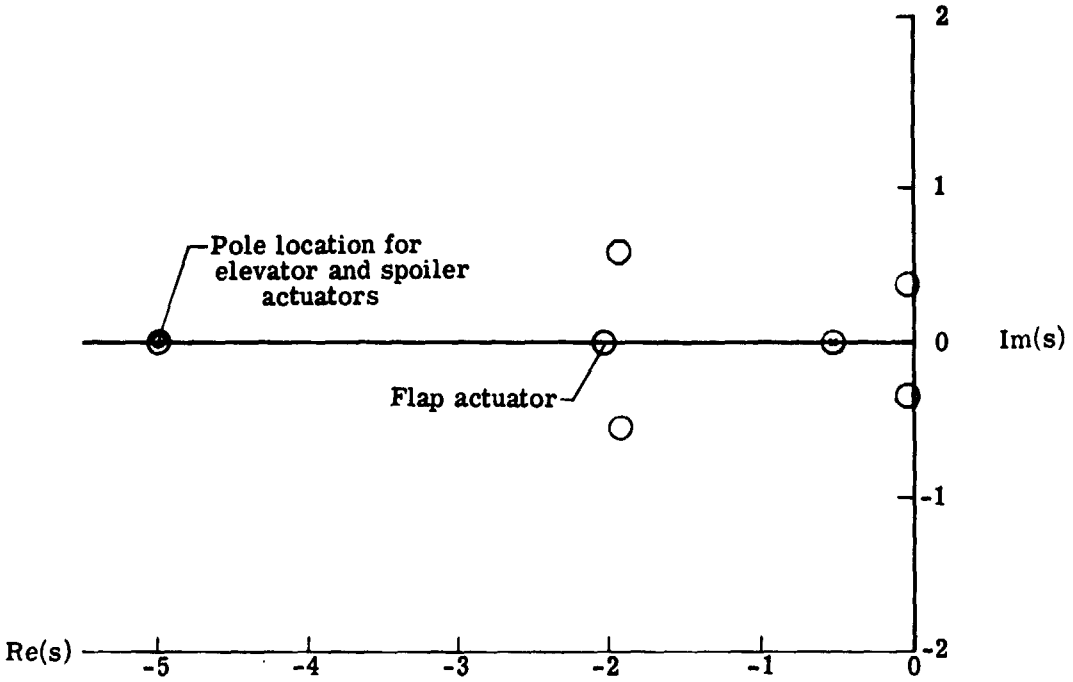

(a) Locked controls.

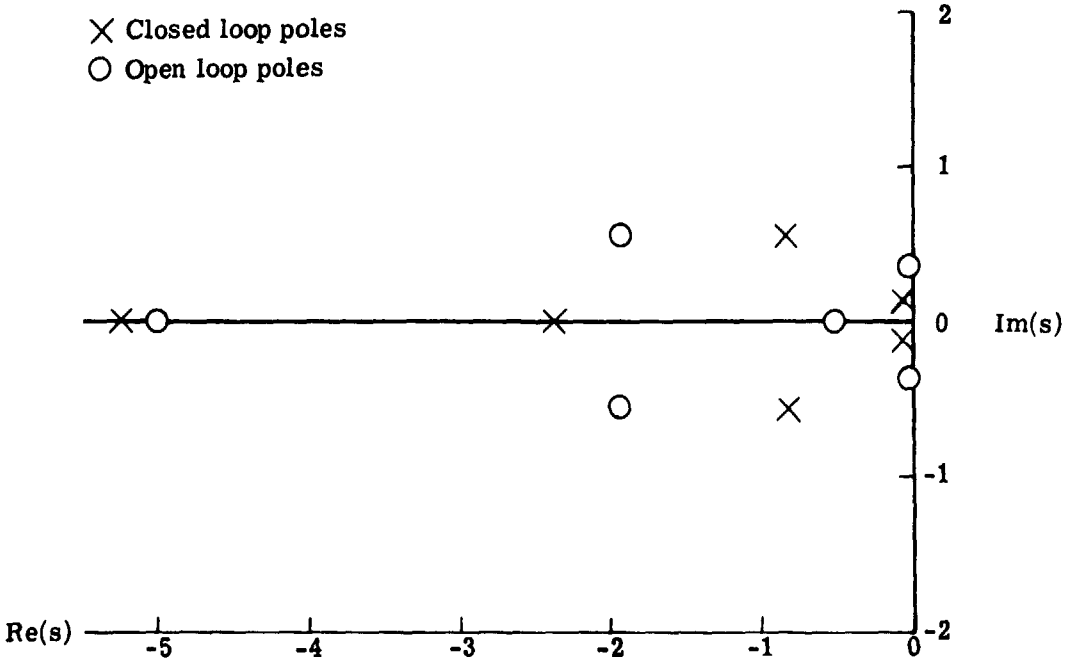

(b) Elevator only controller.

Figure 8.- Pole locations for various control combinations.

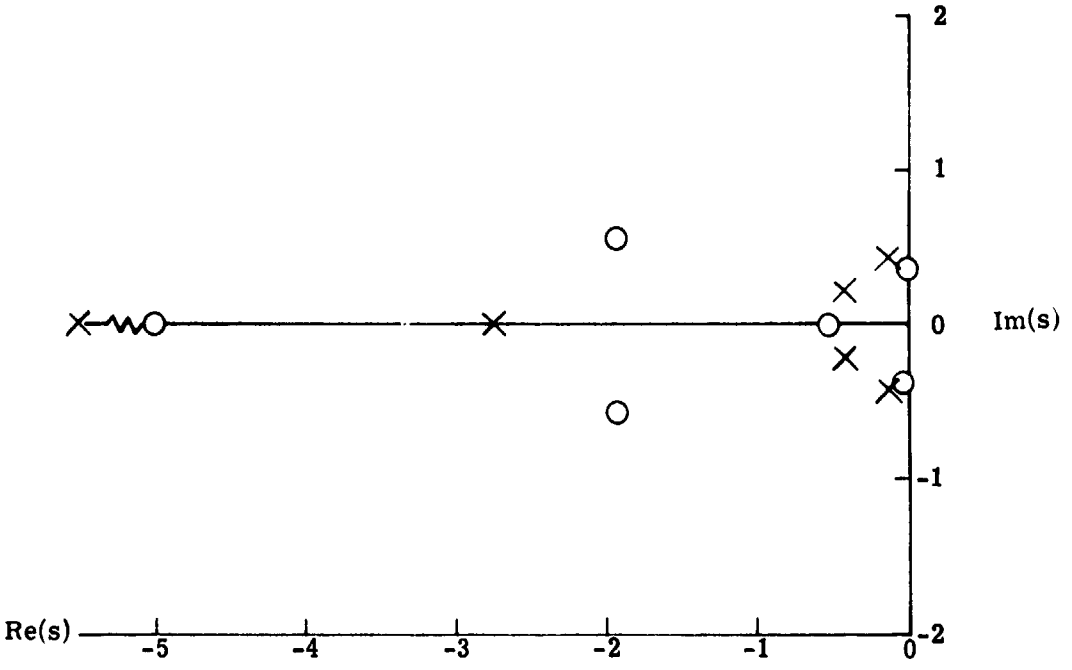

(c) Spoiler only controller.

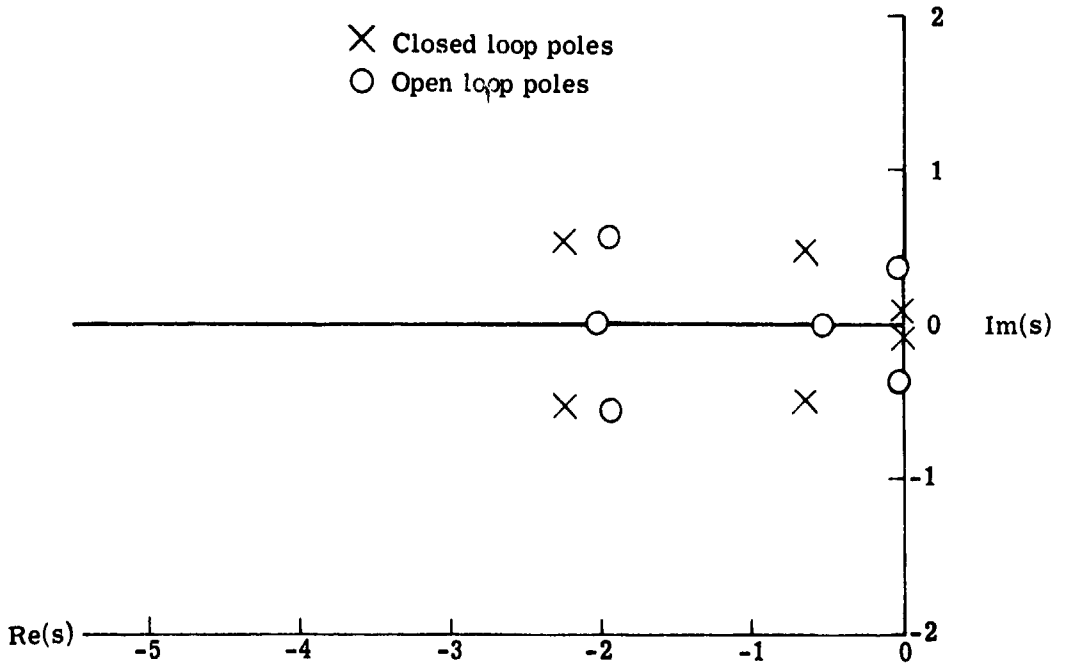

(d) Flap only controller.

Figure 8.- Continued.

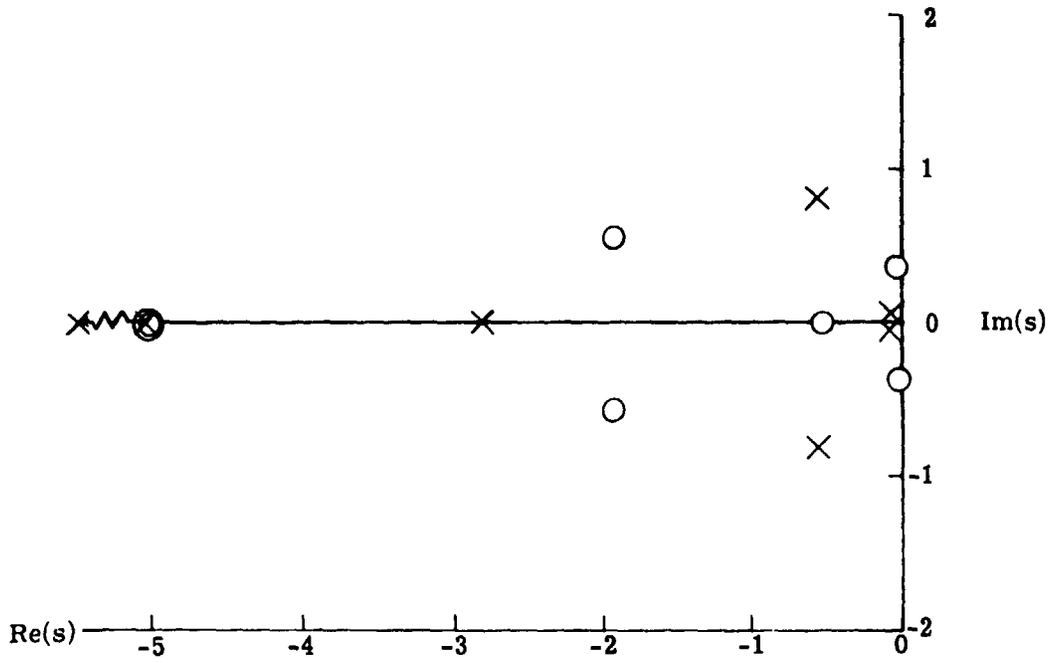

(e) Elevator and spoiler controller.

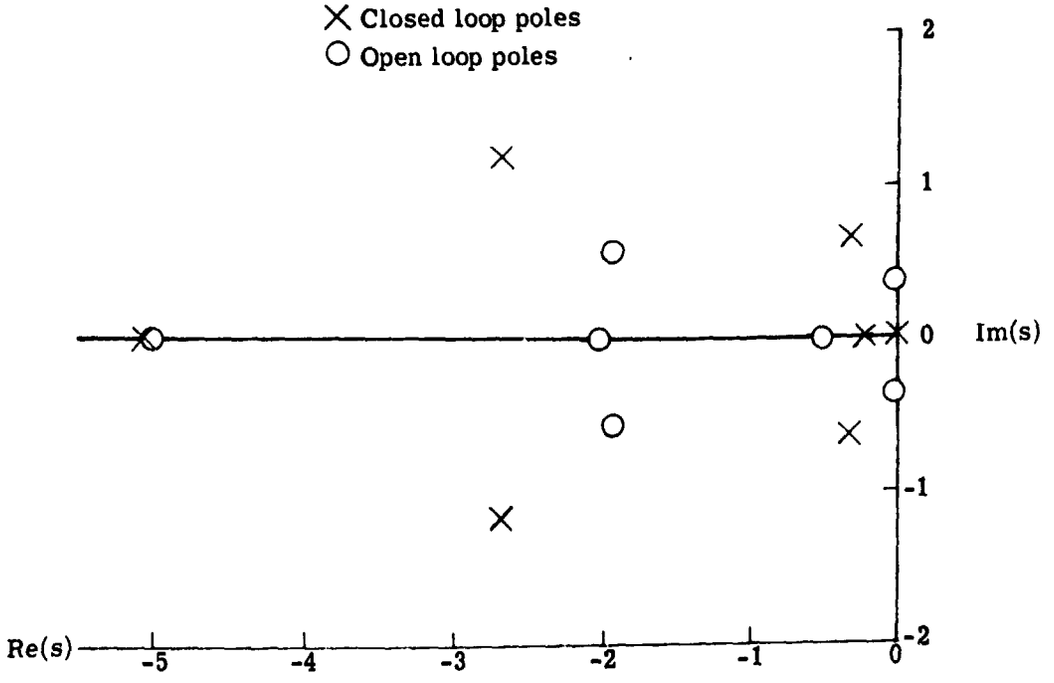

(f) Elevator and flap controller.

Figure 8.- Continued.

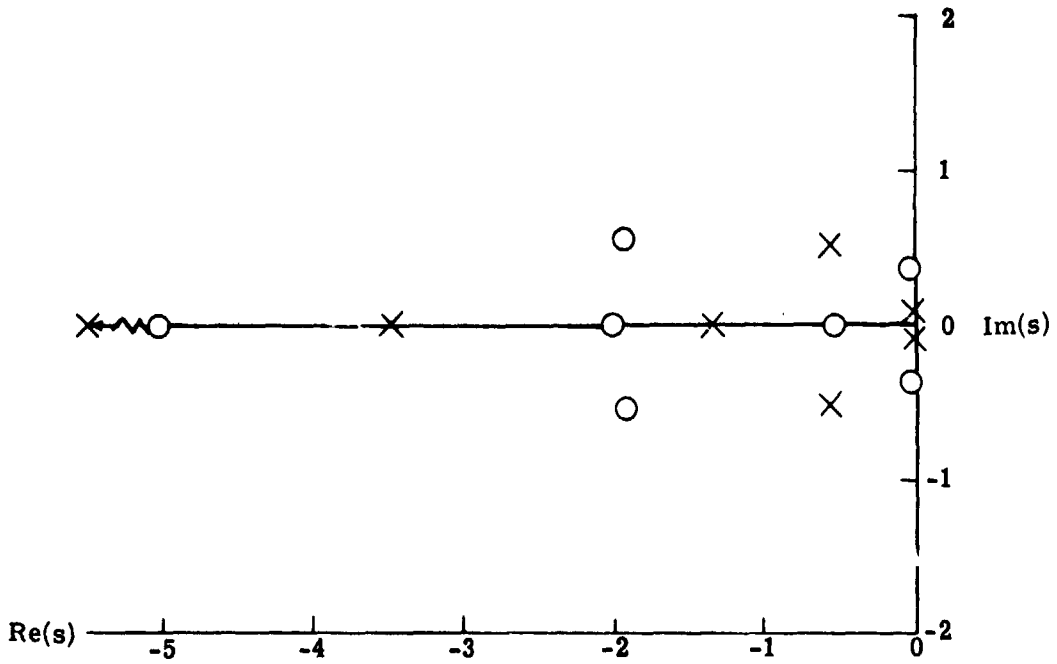

(g) Flap and spoiler controller.

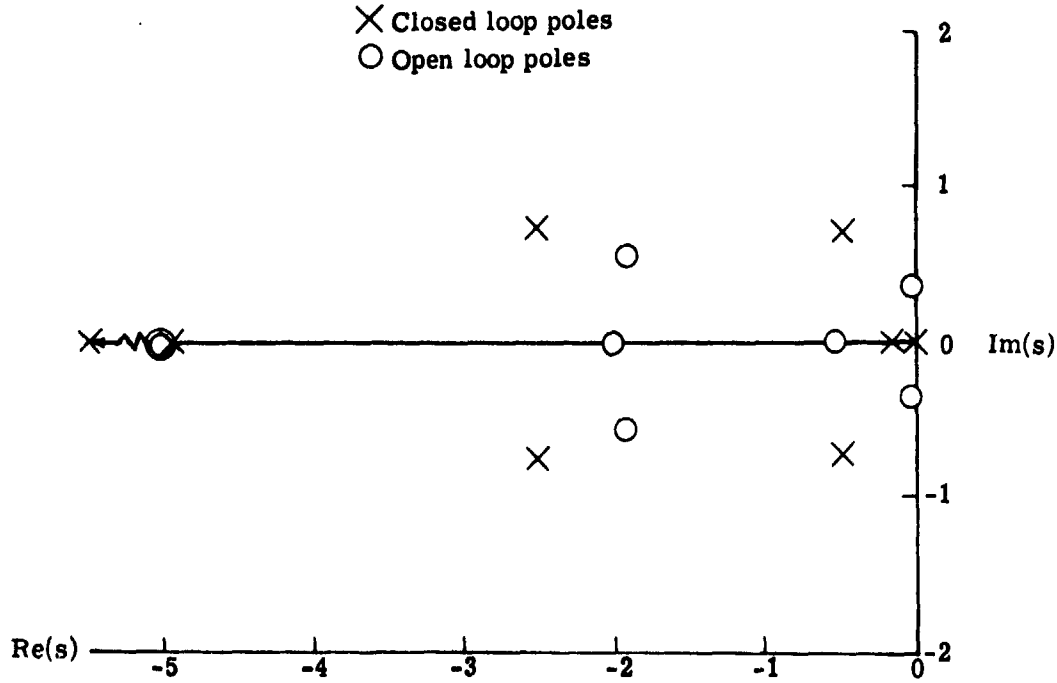

(h) Flap, spoiler, and elevator controller.

Figure 8.- Concluded.

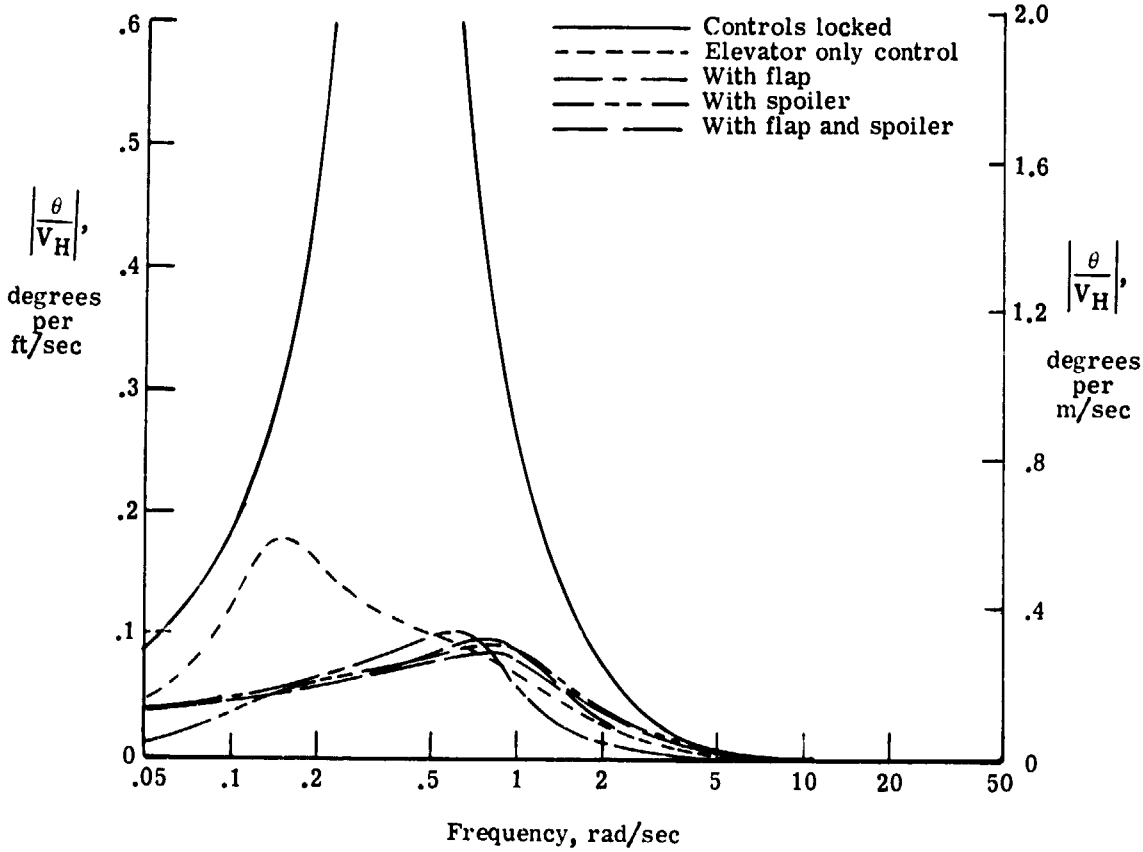

(a) Pitch angle response to horizontal gust.

Figure 9.- Frequency responses to unit amplitude sinusoidal gusts for various control configurations.

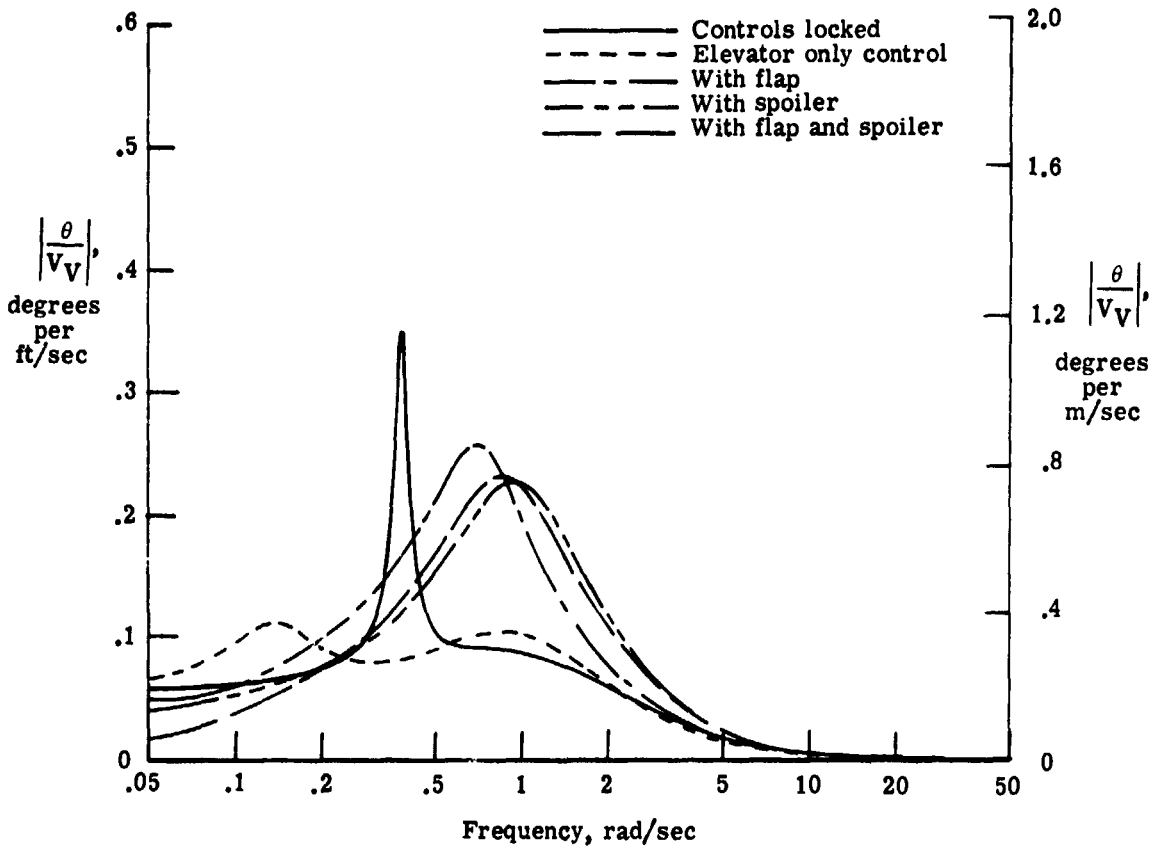

(b) Pitch angle response to vertical gust.

Figure 9.- Continued.

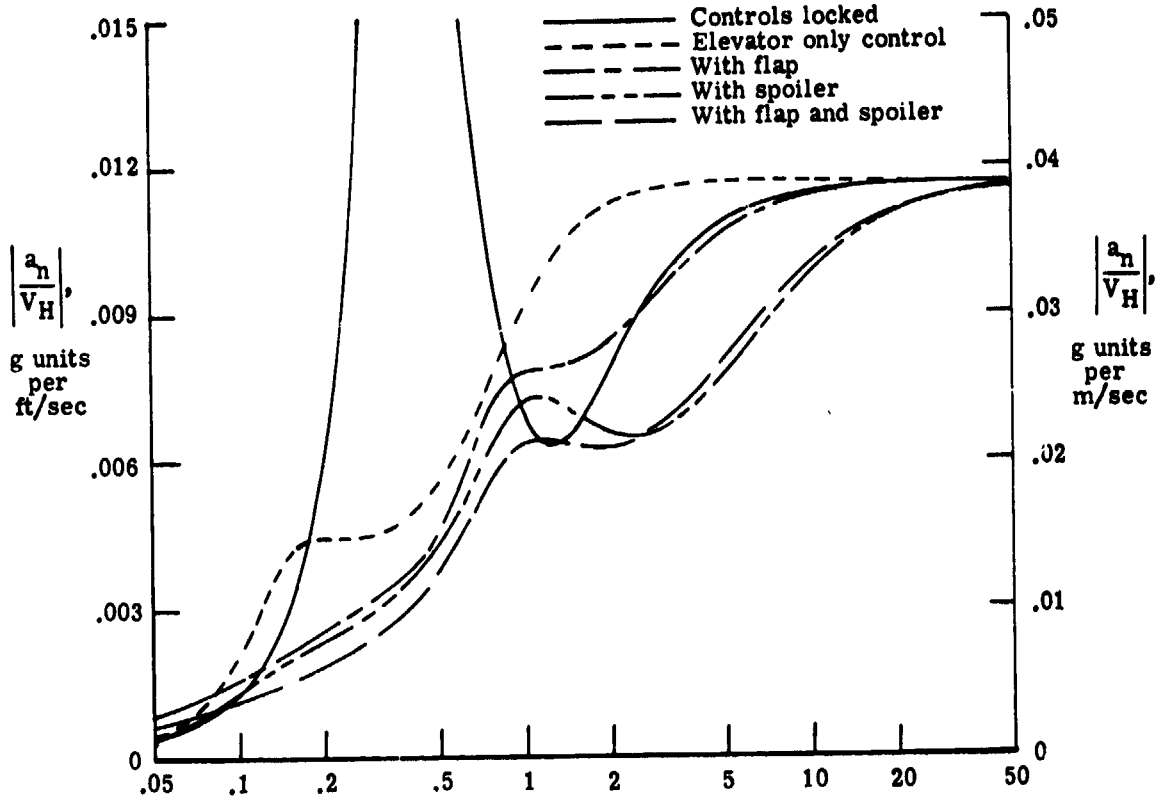

(c) Normal acceleration response to horizontal gust.

Figure 9.- Continued.

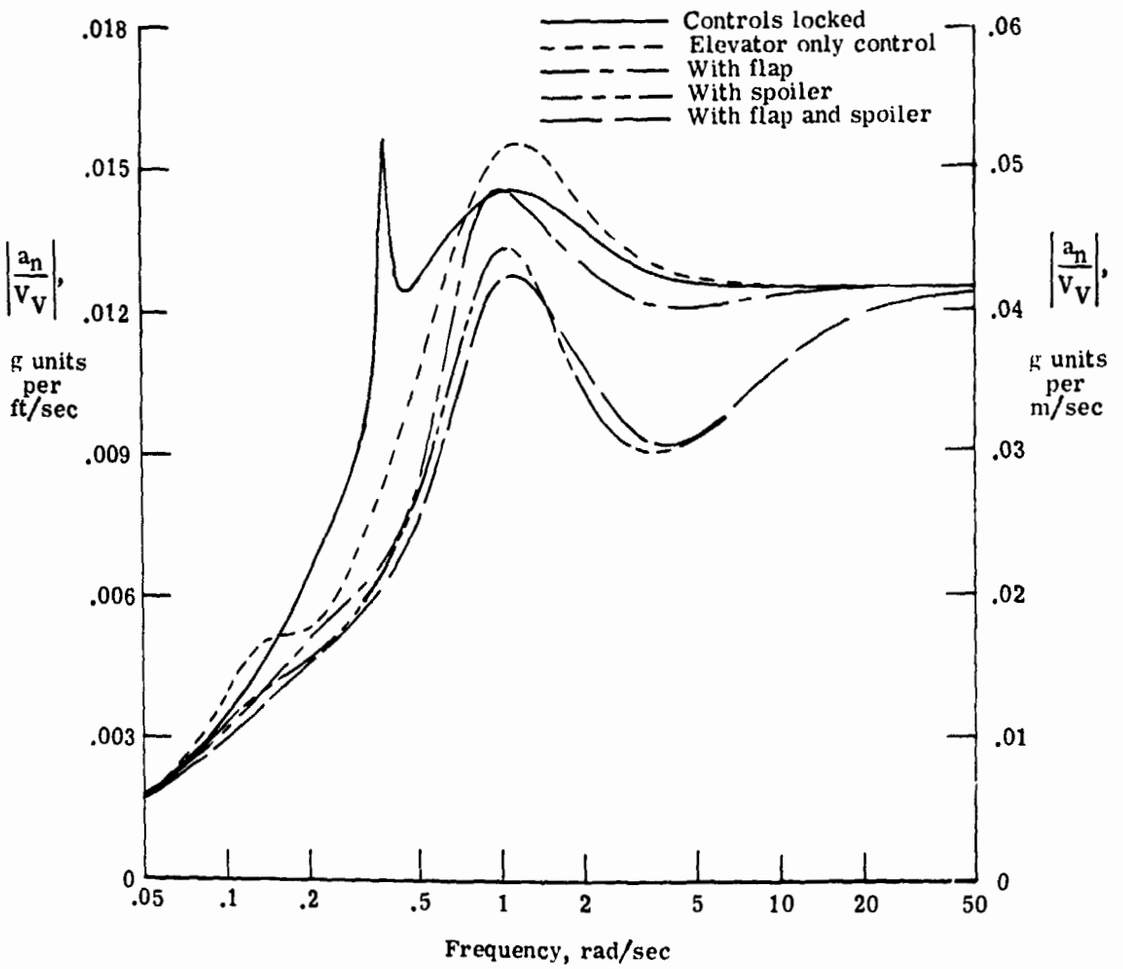

(d) Normal acceleration response to vertical gust.

Figure 9.- Continued.

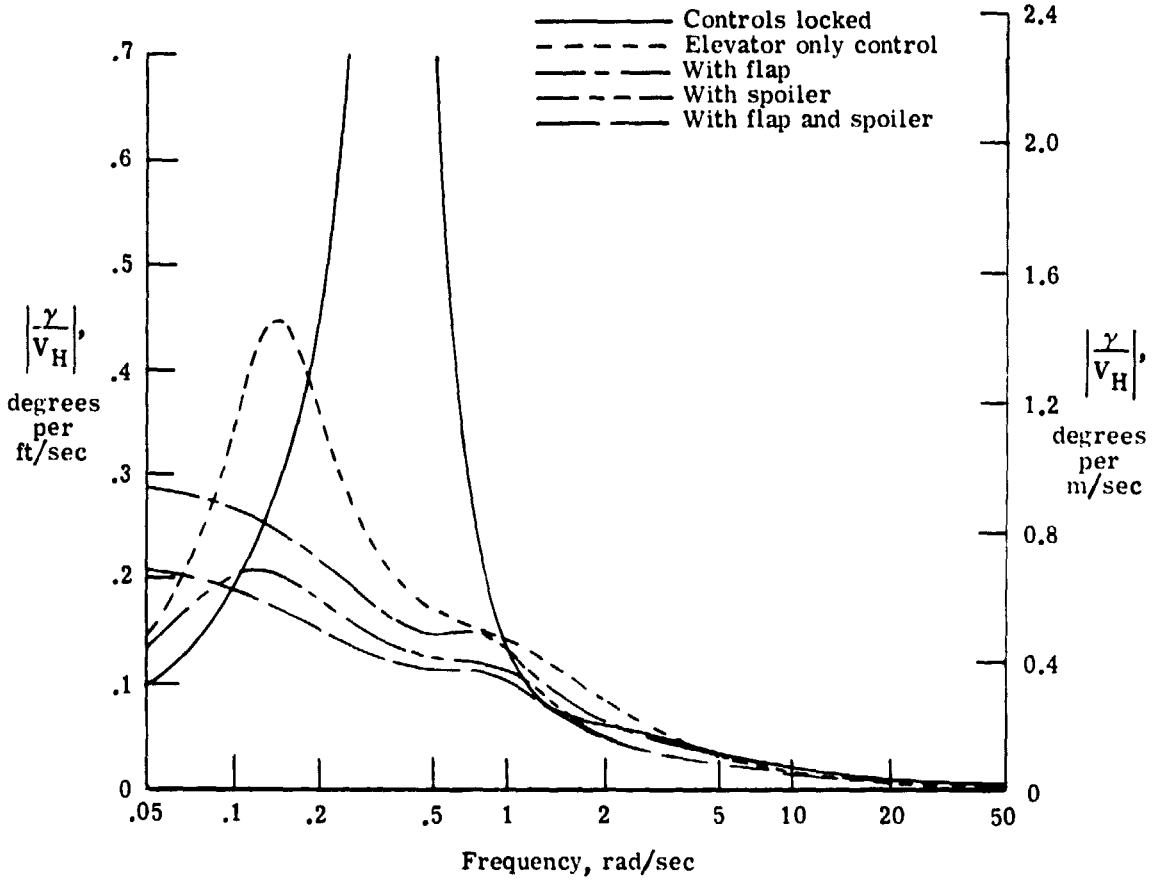

(e) Flight path angle response to horizontal gust.

Figure 9.- Continued.

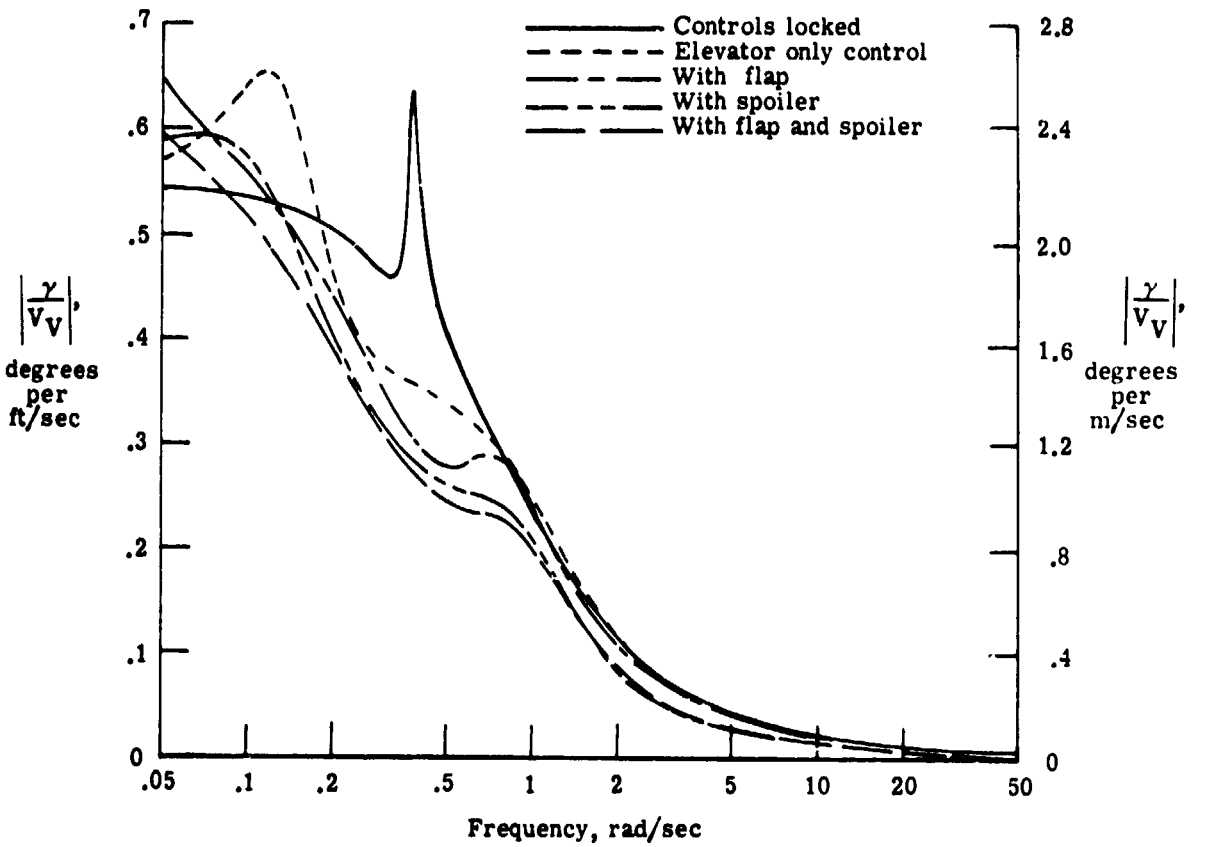

(f) Flight path angle response to vertical gust.

Figure 9.- Continued.

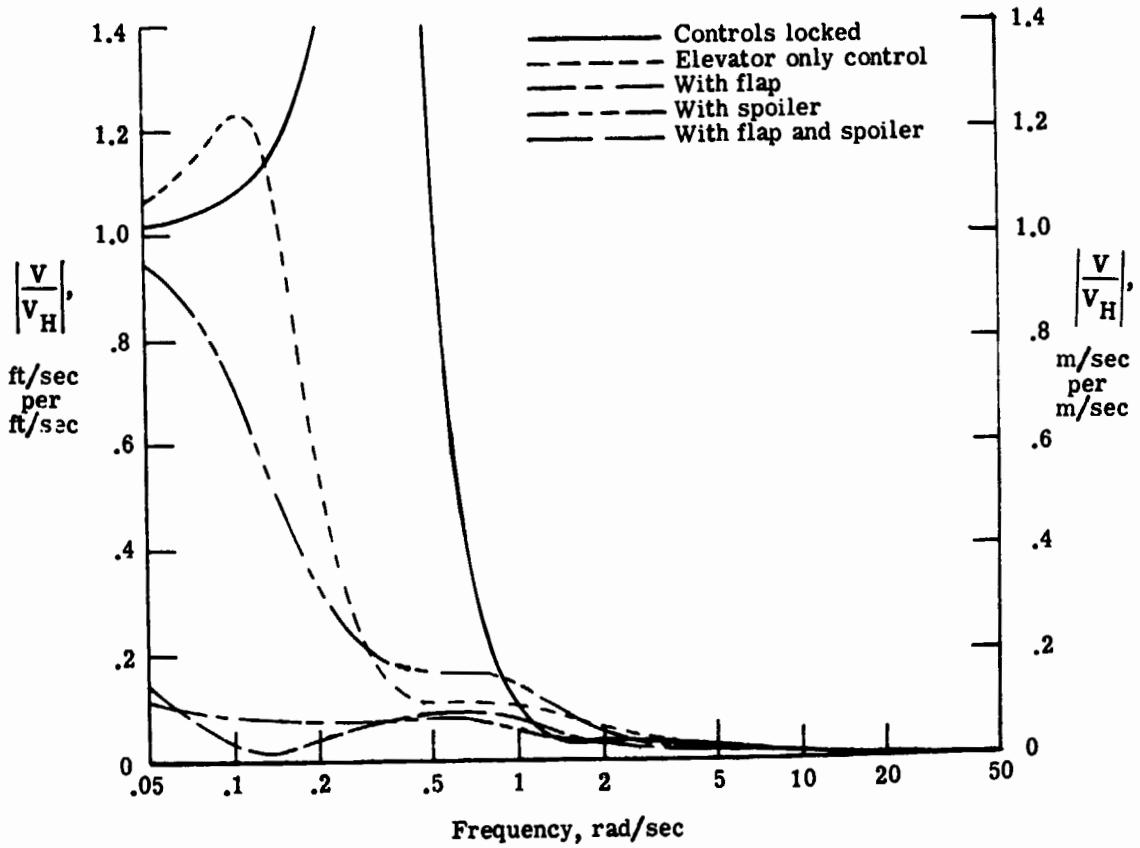

(g) Speed response to horizontal gust.

Figure 9.- Continued.

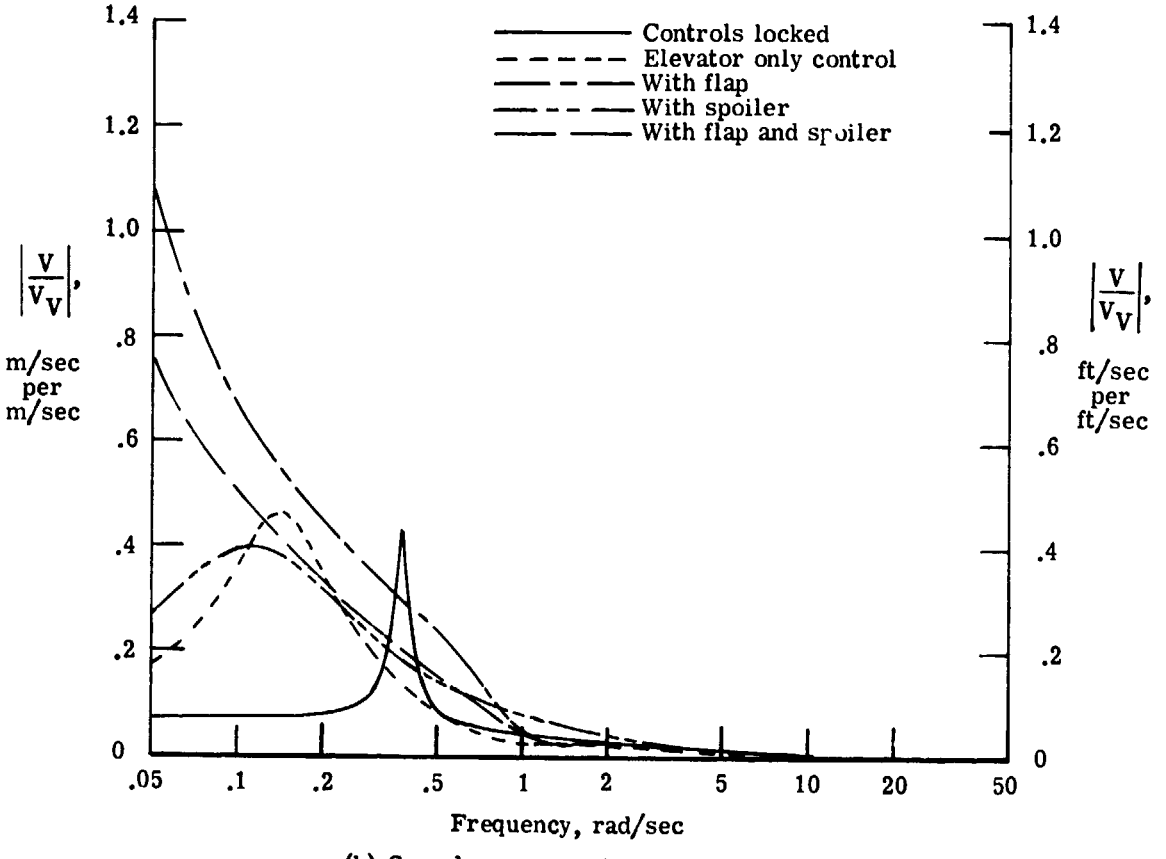

(h) Speed response to vertical gust.

Figure 9.- Concluded.

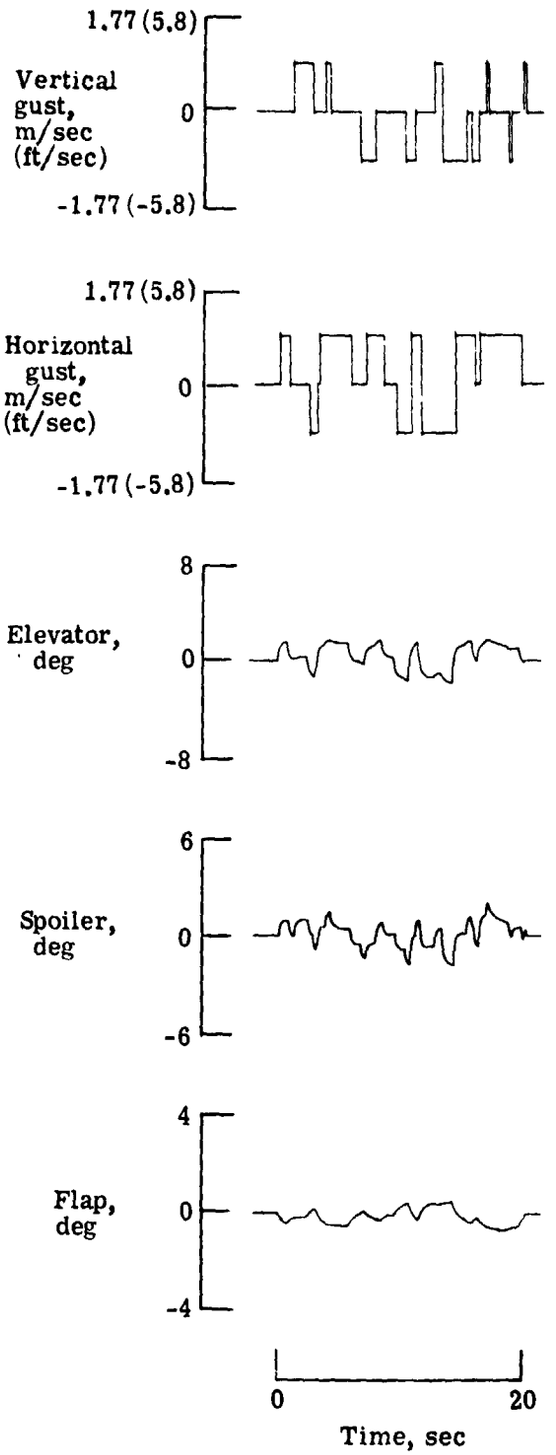

Figure 10.- Test gusts and control deflections.

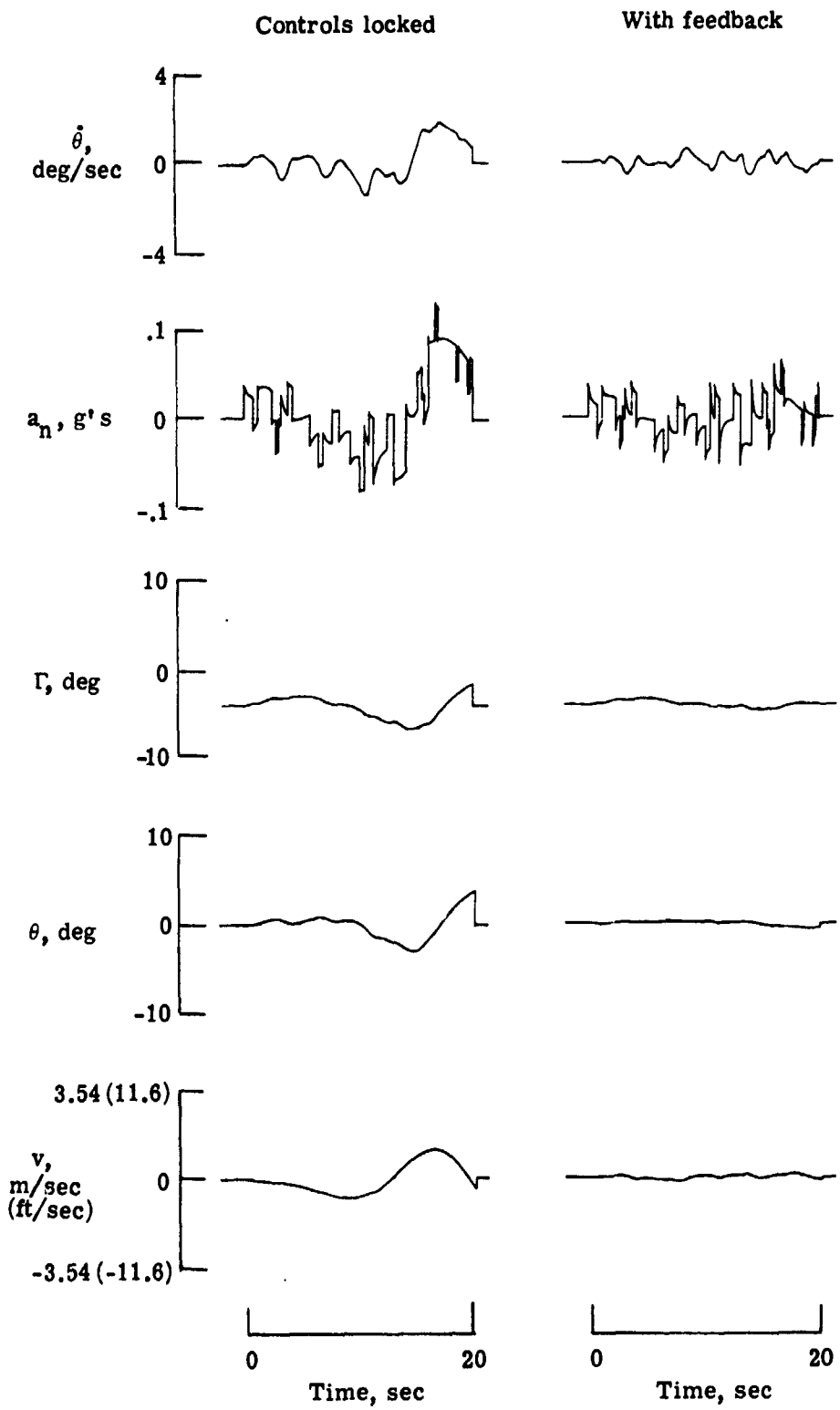

Figure 11.- Feedback system effectiveness.

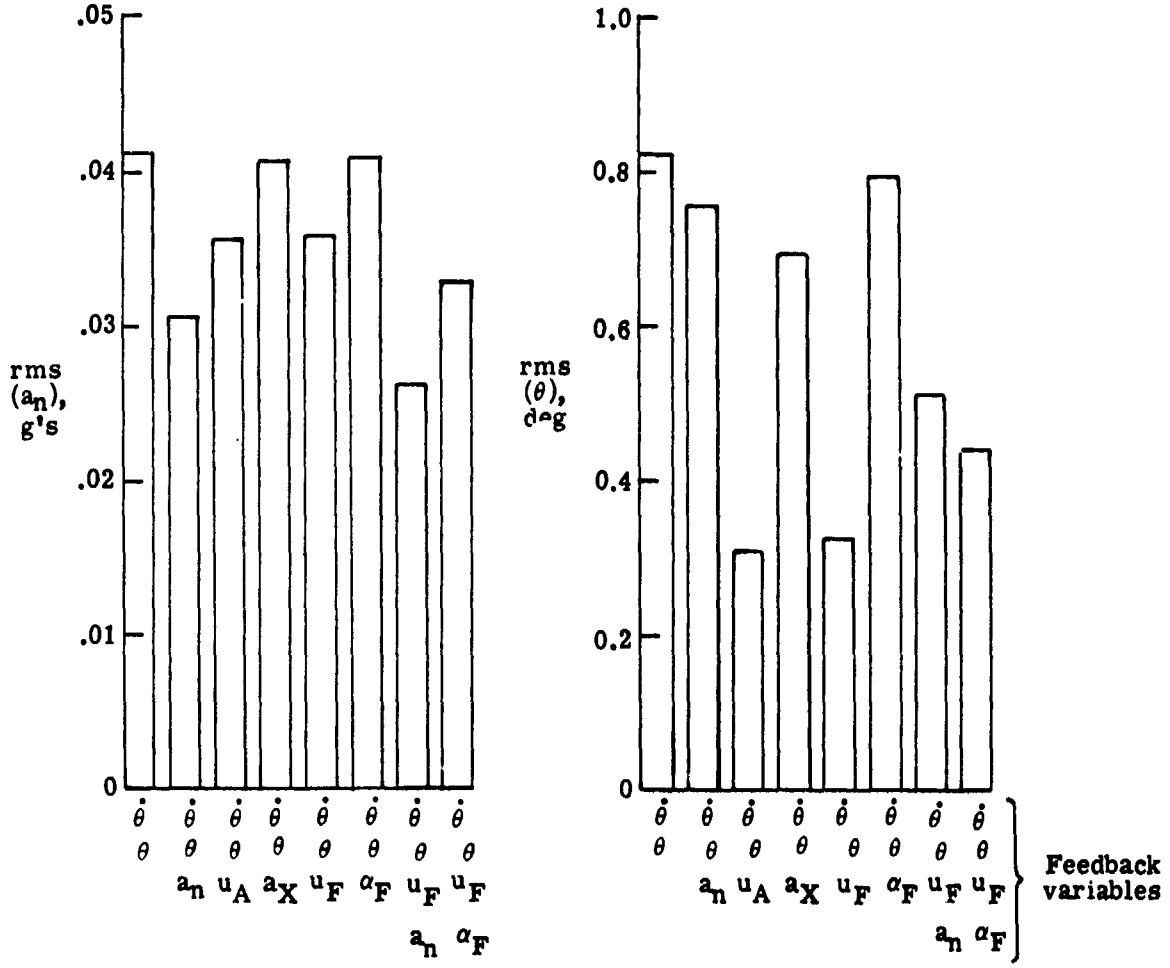

(a) Normal acceleration.

(b) Pitch angle.

Figure 12.- Addition of sensors to pitch angle and rate feedback control system.

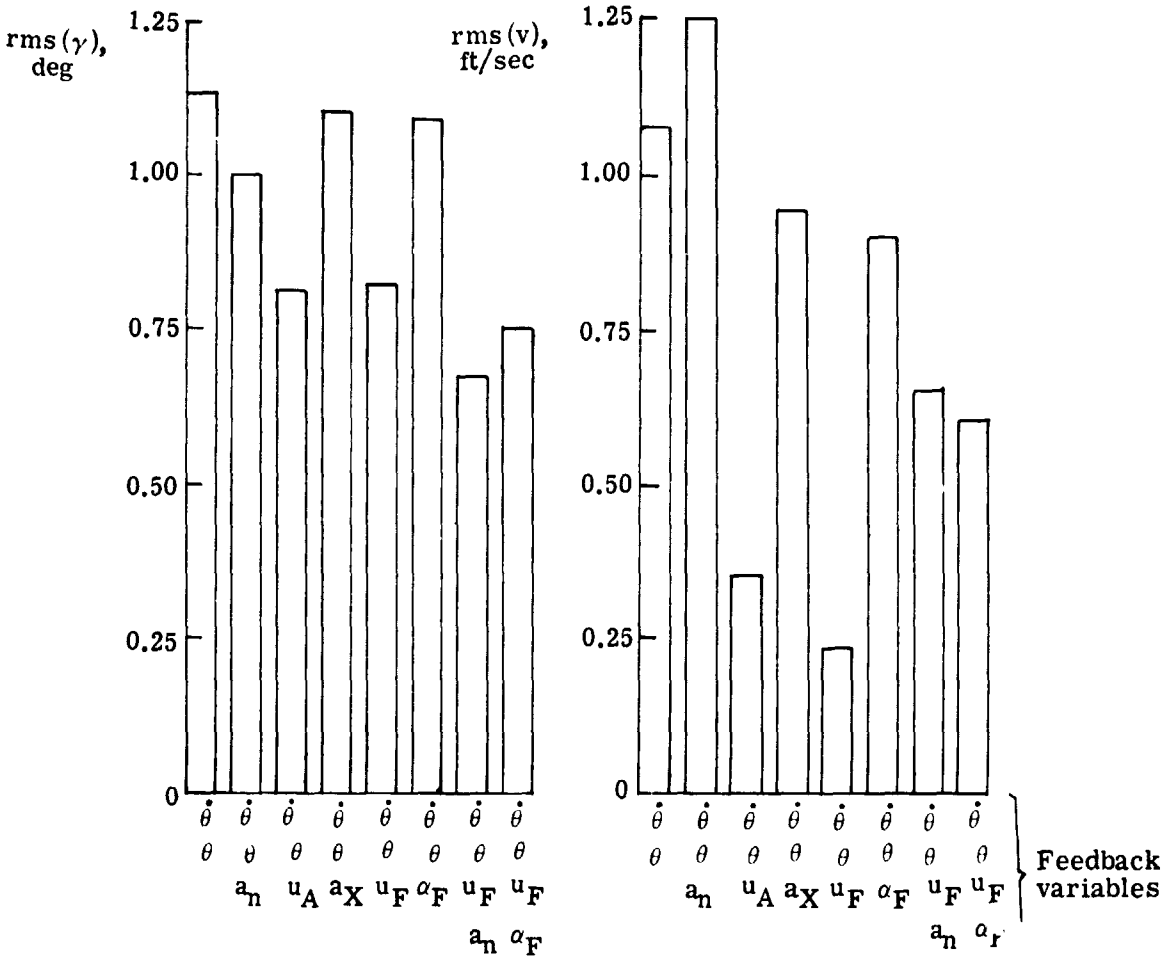

(c) Flight path angle.

(d) Speed.

Figure 12.- Concluded.

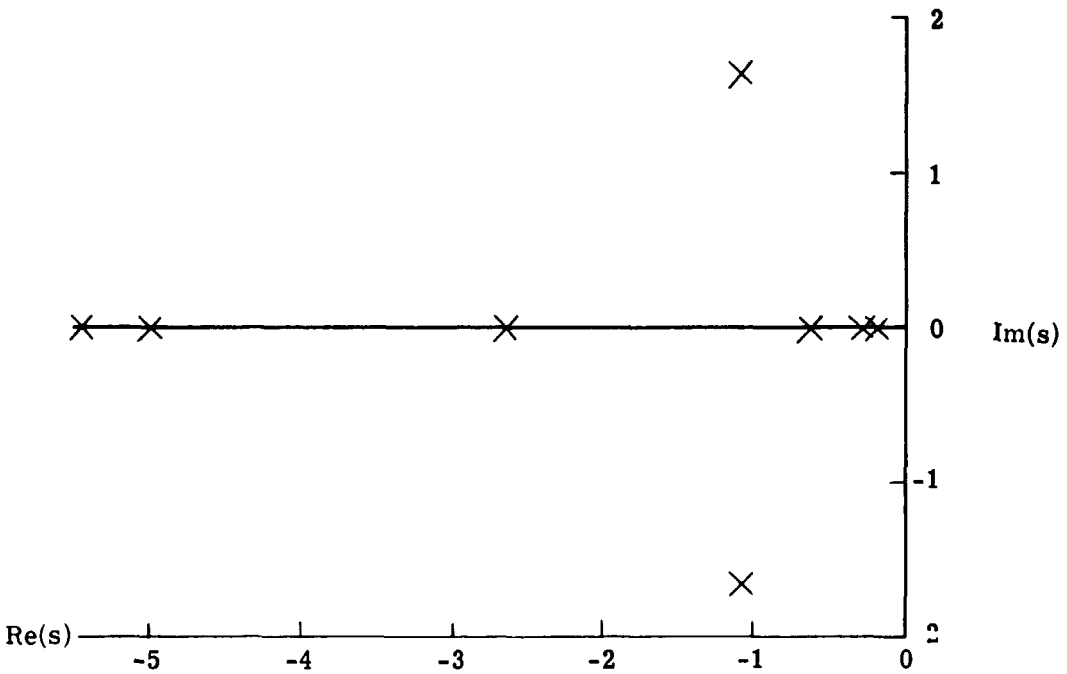

(a) Pitch angle and pitch rate only.

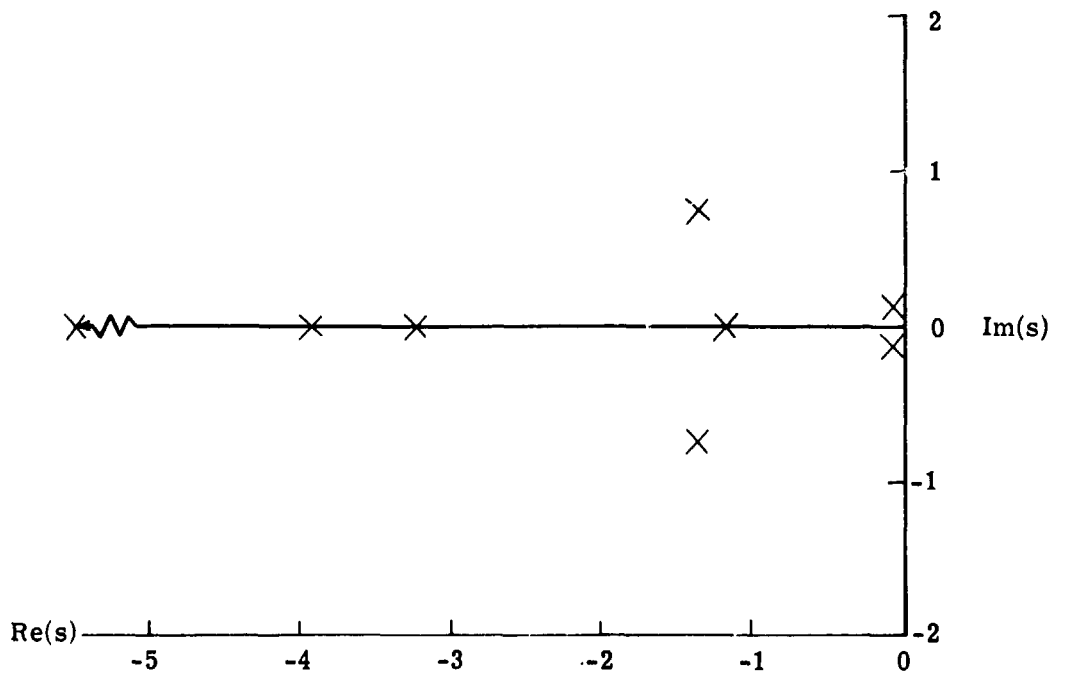

(b) Pitch angle, pitch rate, and normal acceleration.

Figure 13.- Pole locations for various sensor configurations.

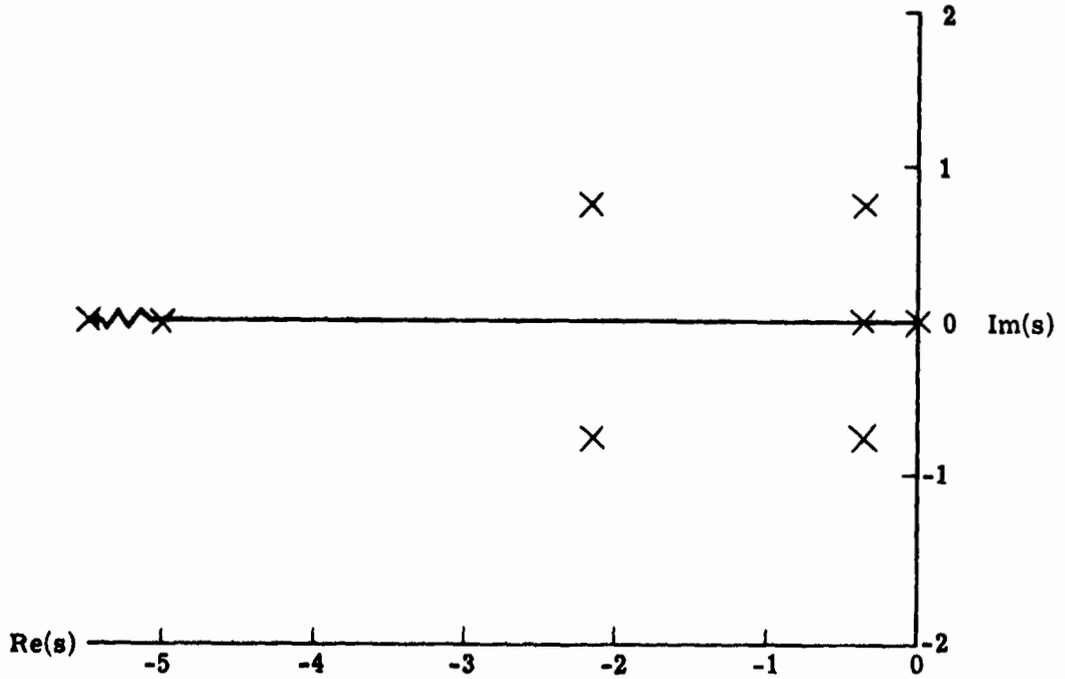

(c) Pitch angle, pitch rate, and airspeed at center of gravity.

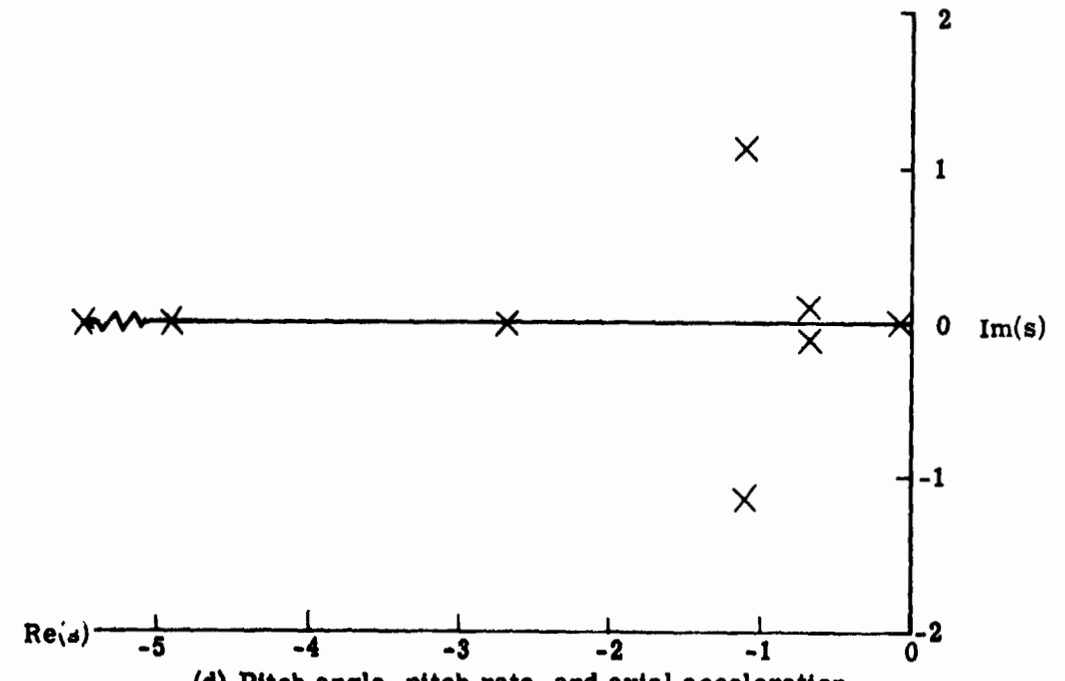

(d) Pitch angle, pitch rate, and axial acceleration.

Figure 13.- Continued.

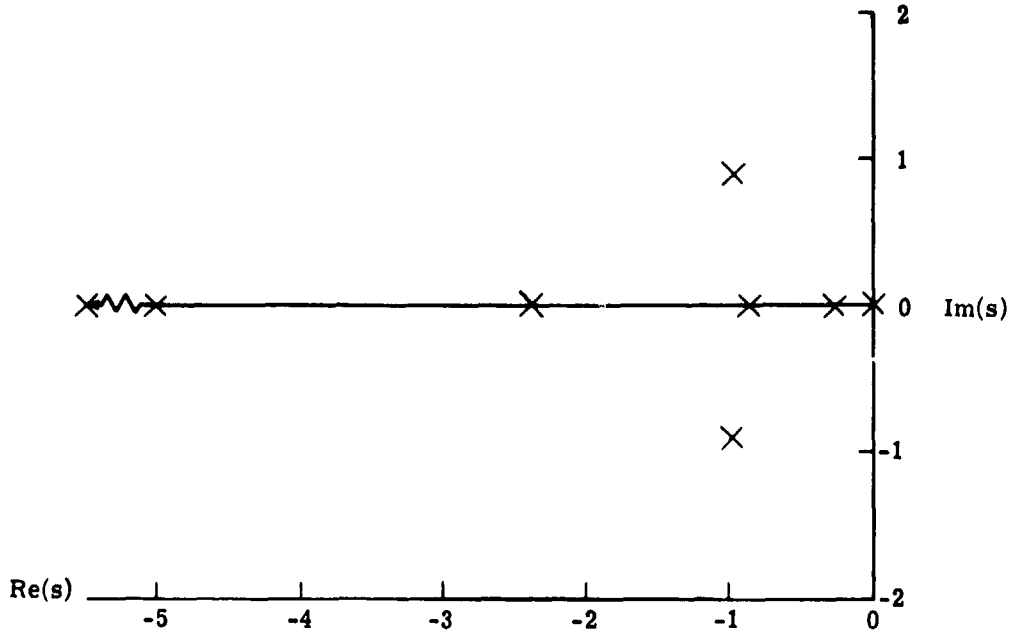

(e) Pitch angle, pitch rate, and airspeed at nose.

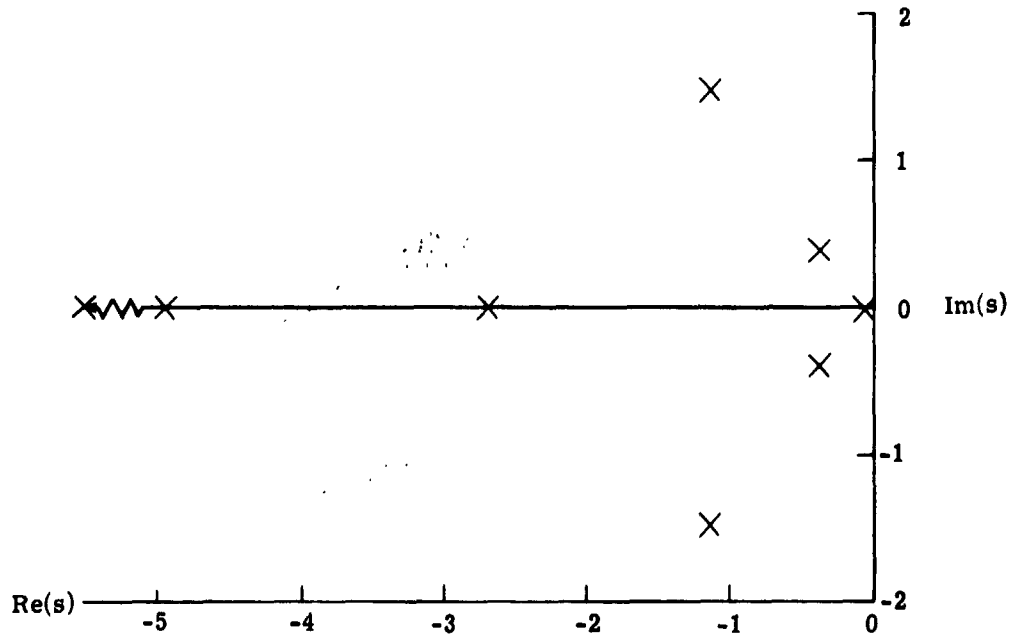

(f) Pitch angle, pitch rate, and angle of attack at nose.

Figure 13.- Continued.

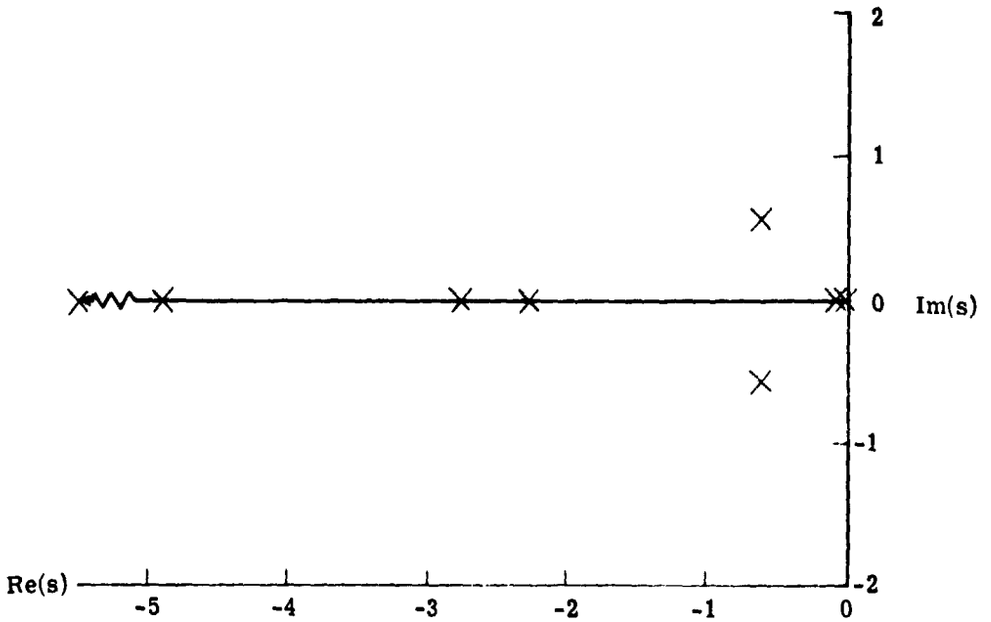

(g) Pitch angle, pitch rate, airspeed at nose, and normal acceleration.

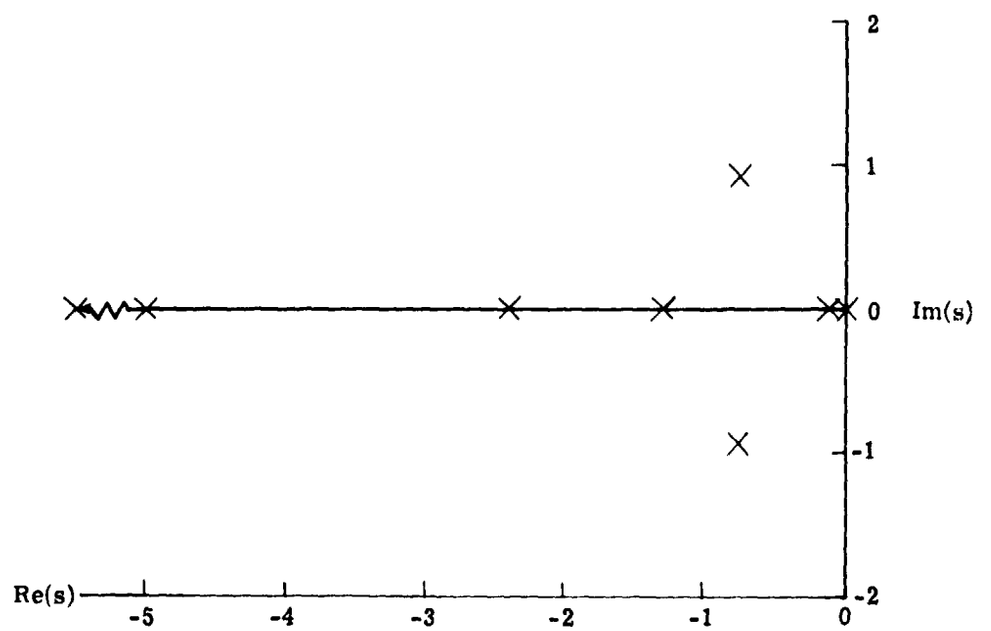

(h) Pitch angle, pitch rate, airspeed at nose, and angle of attack at nose.

Figure 13.- Concluded.

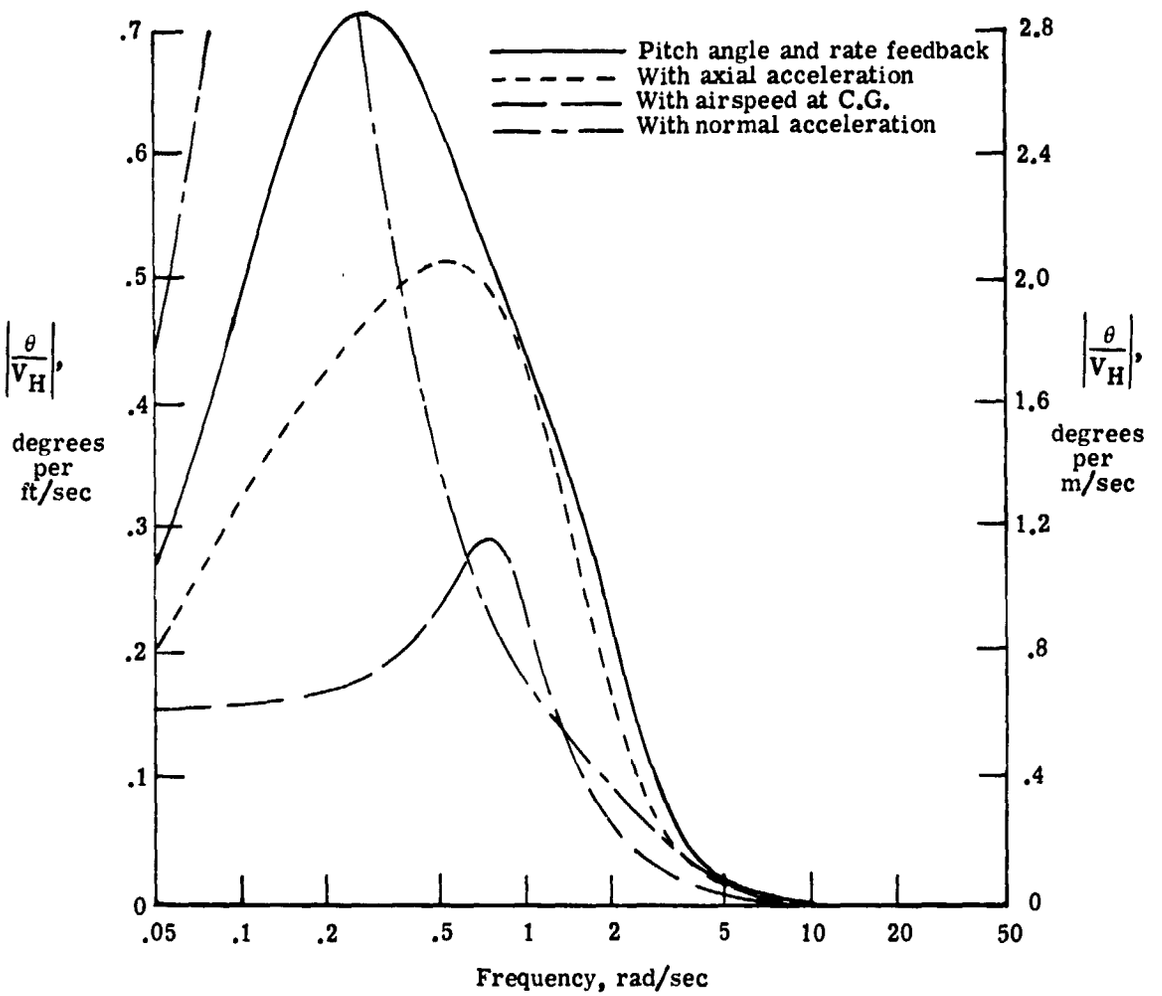

(a) Pitch angle response to horizontal gust.

Figure 14.- Frequency responses to unit amplitude sinusoidal gusts for various sensor configurations.

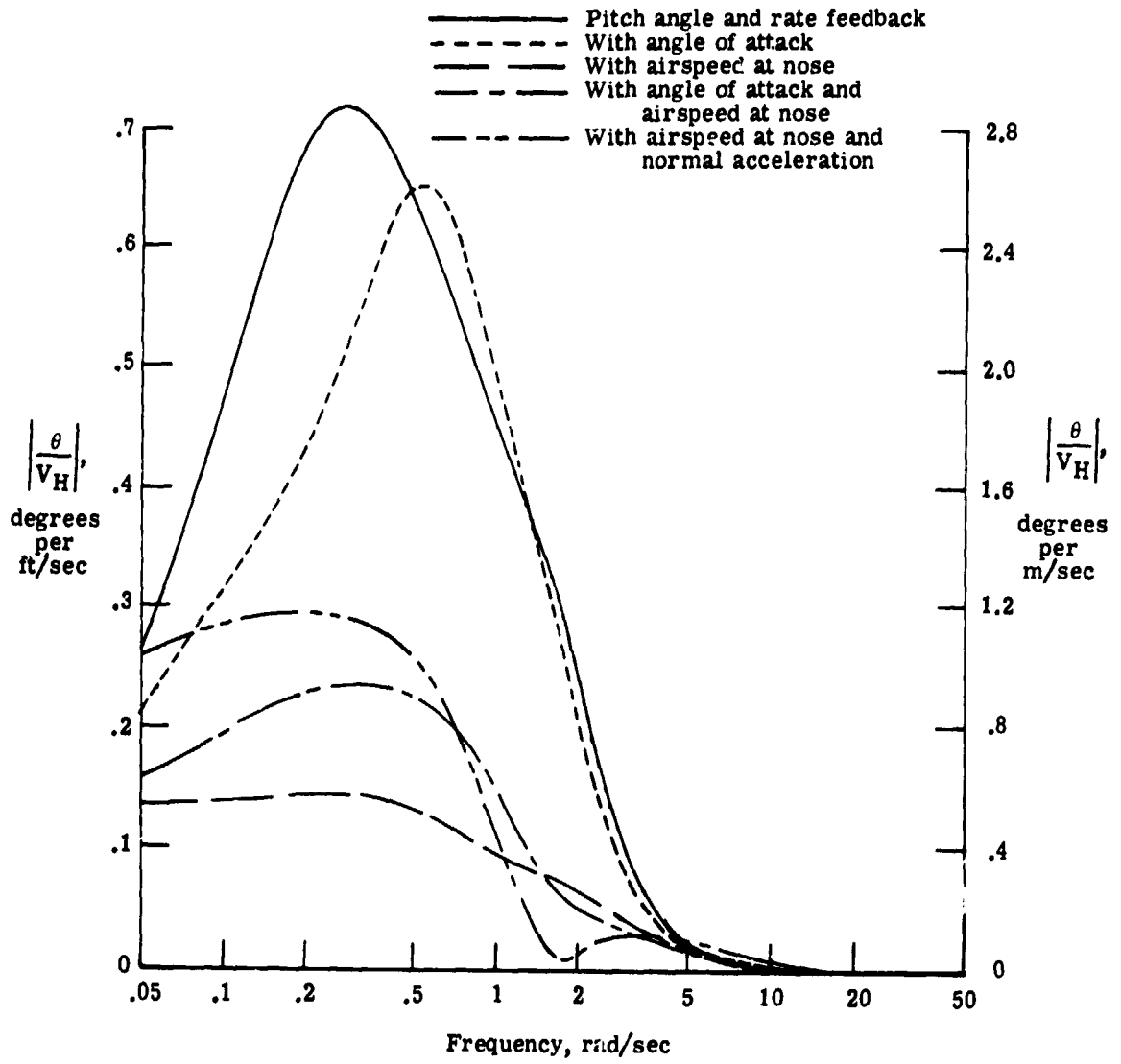

(a) Pitch angle response to horizontal gust – Concluded.

Figure 14.- Continued.

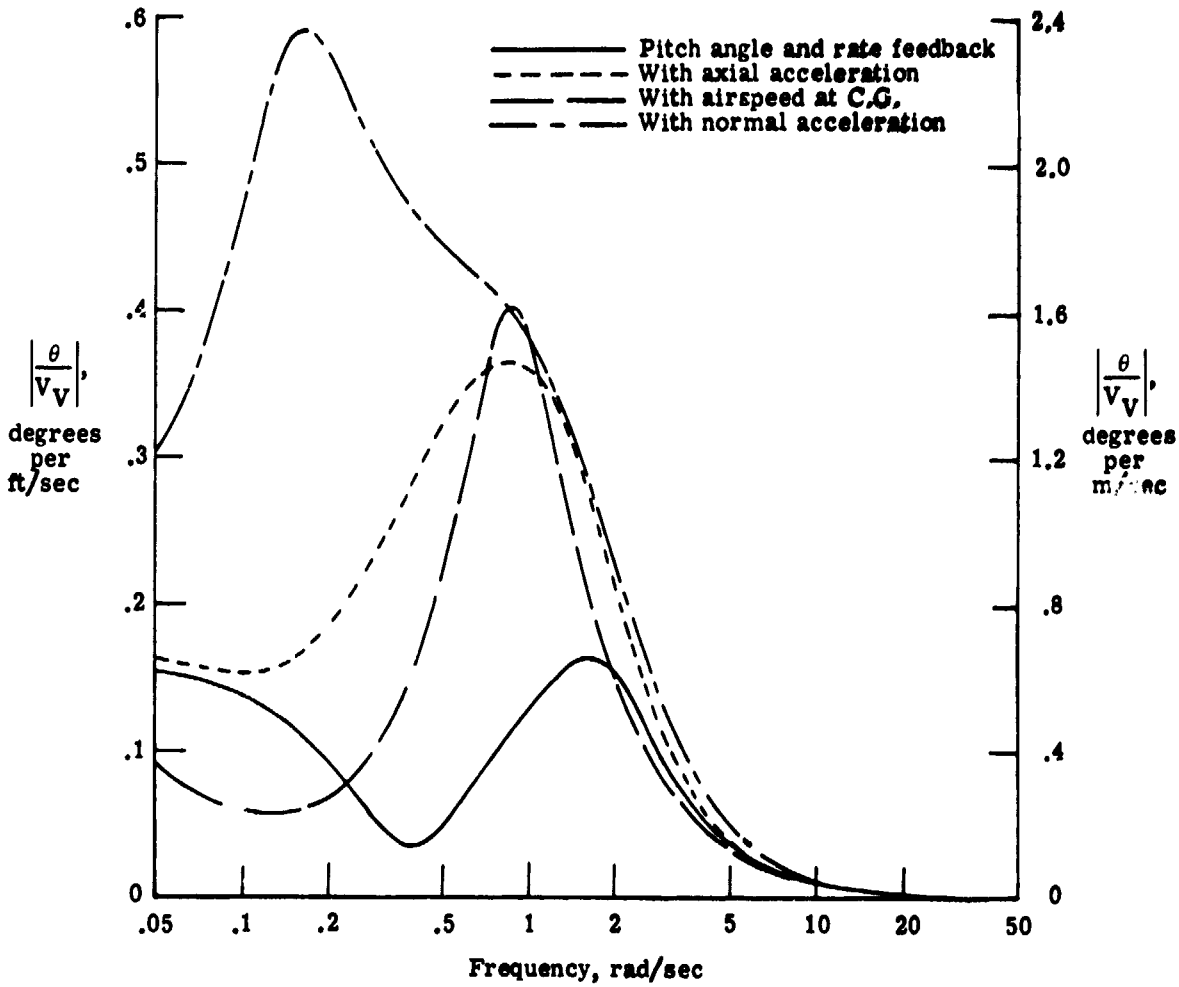

(b) Pitch angle response to vertical gust.

Figure 14.- Continued.

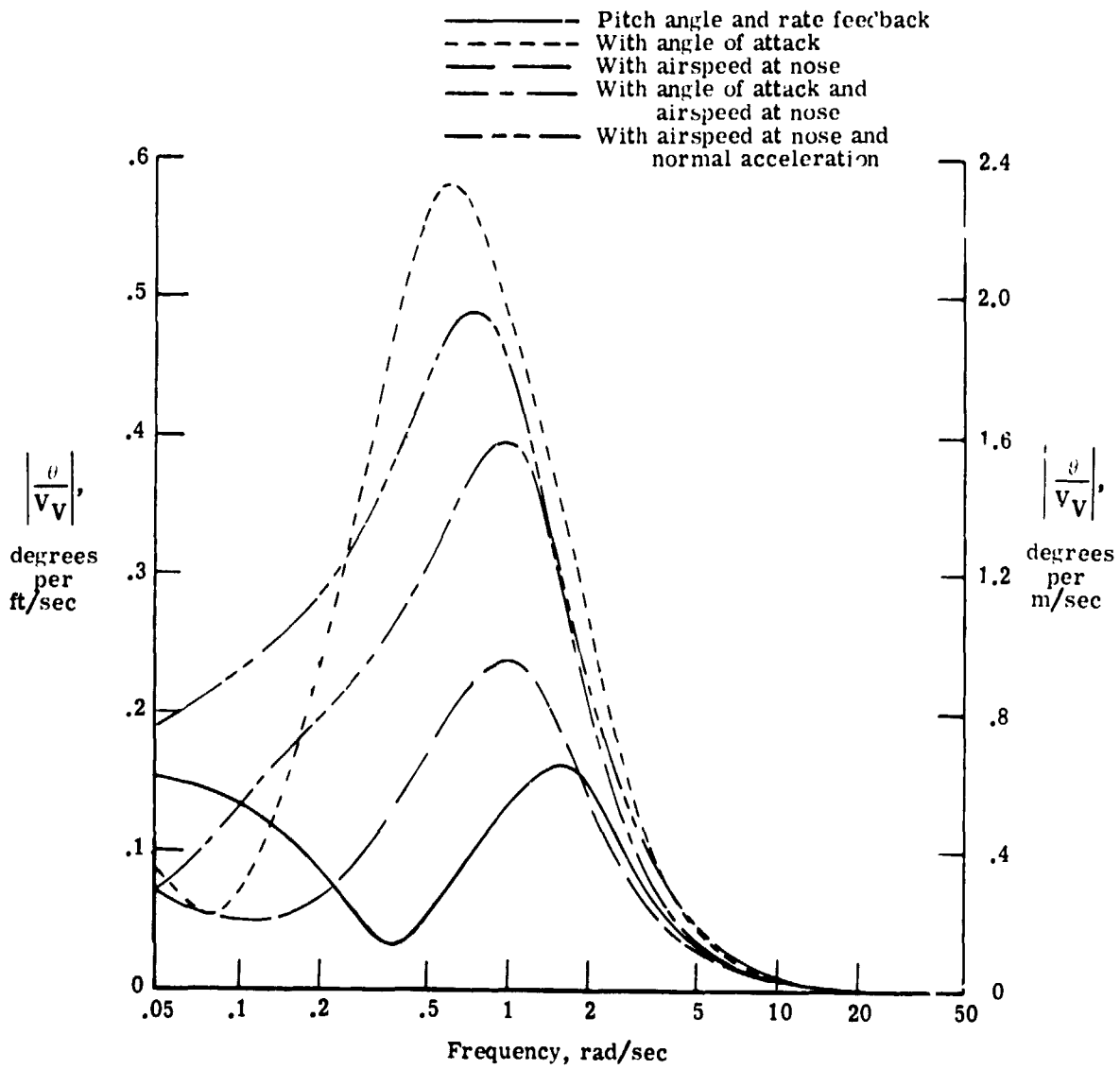

(b) Pitch angle response to vertical gust – Concluded.

Figure 14.- Continued.

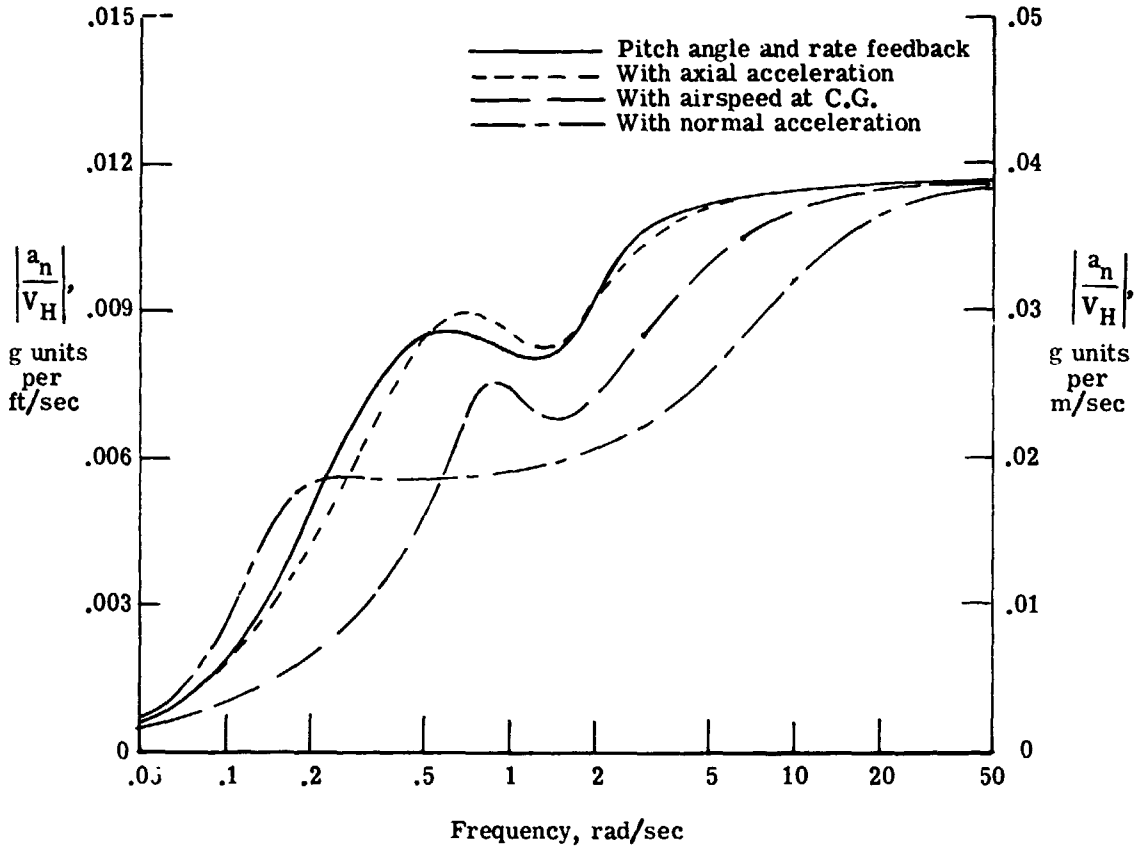

(c) Normal acceleration response to horizontal gust.

Figure 14.- Continued.

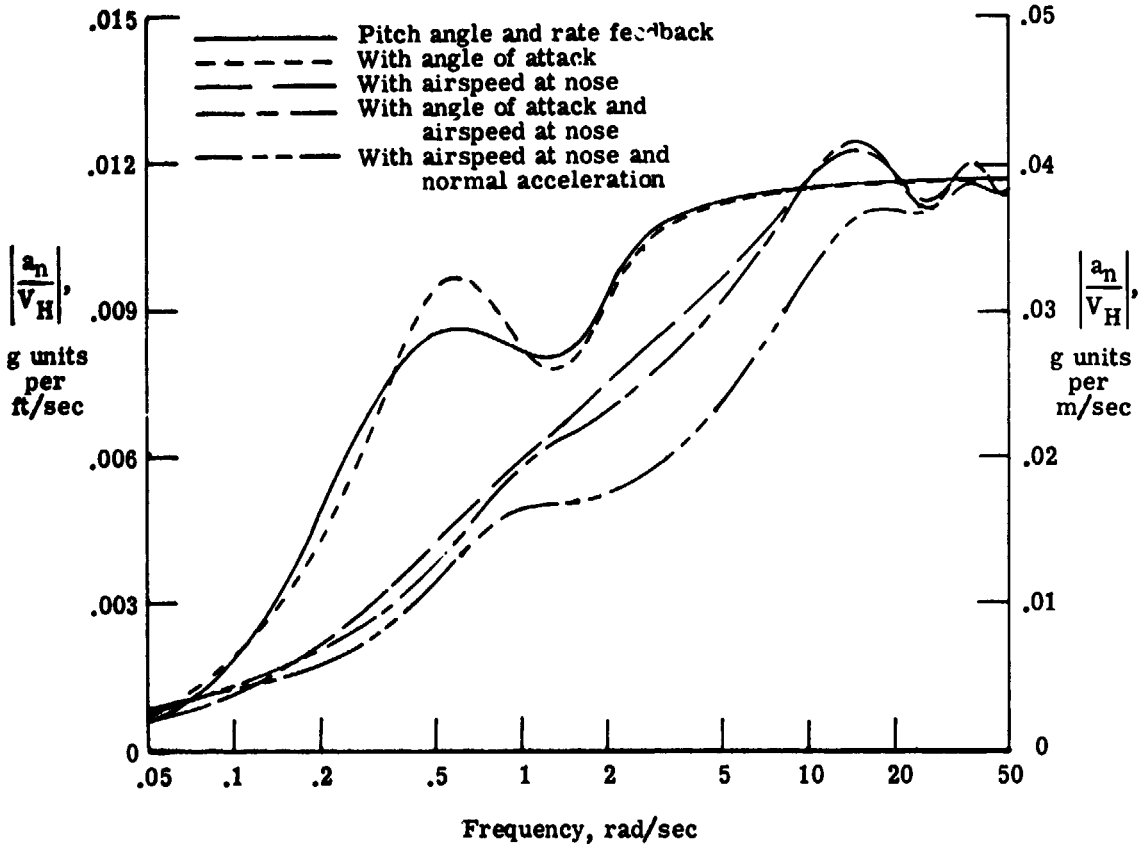

(c) Normal acceleration response to horizontal gust – Concluded.

Figure 14.- Continued.

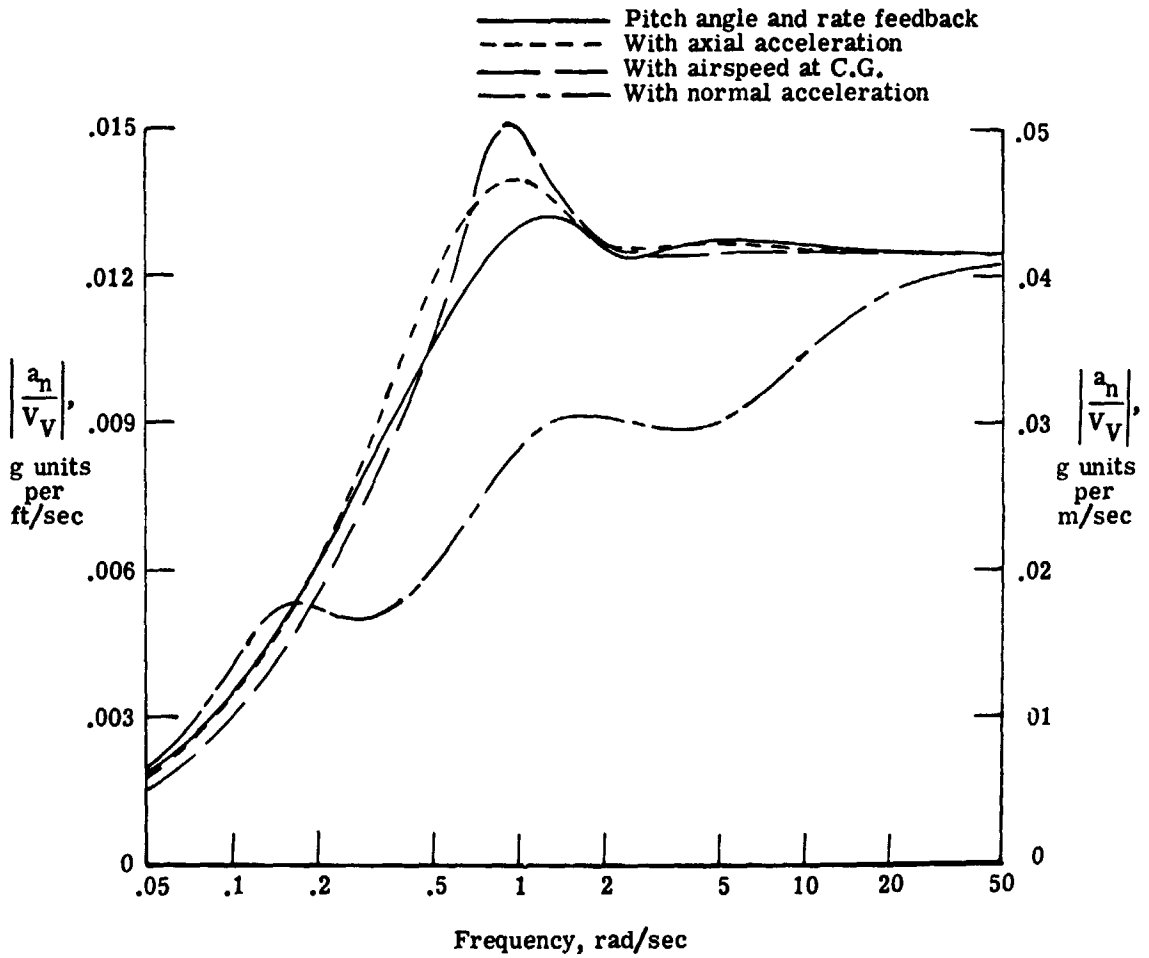

(d) Normal acceleration response to vertical gust.

Figure 14.- Continued.

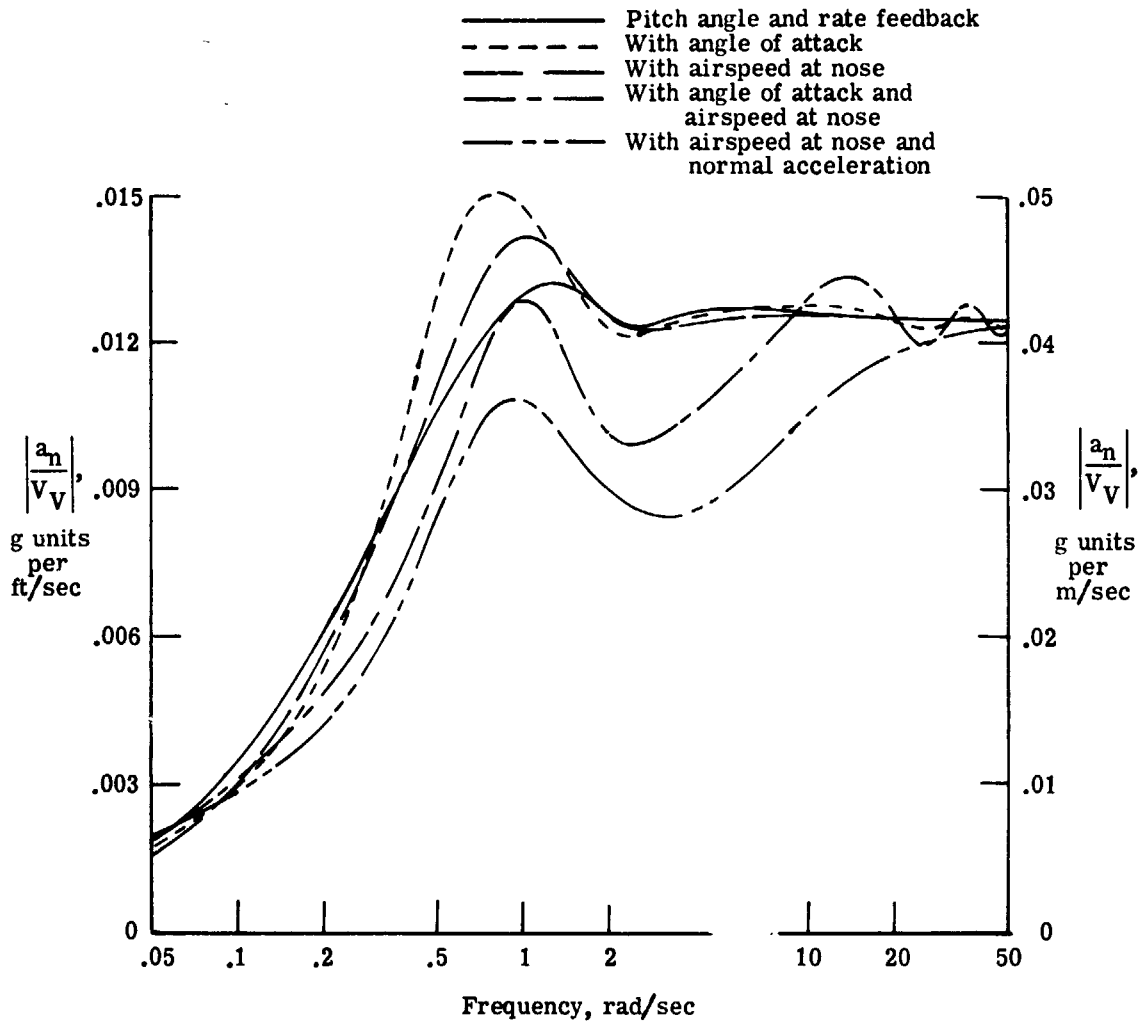

(d) Normal acceleration response to vertical gust – Concluded.

Figure 14.- Continued.

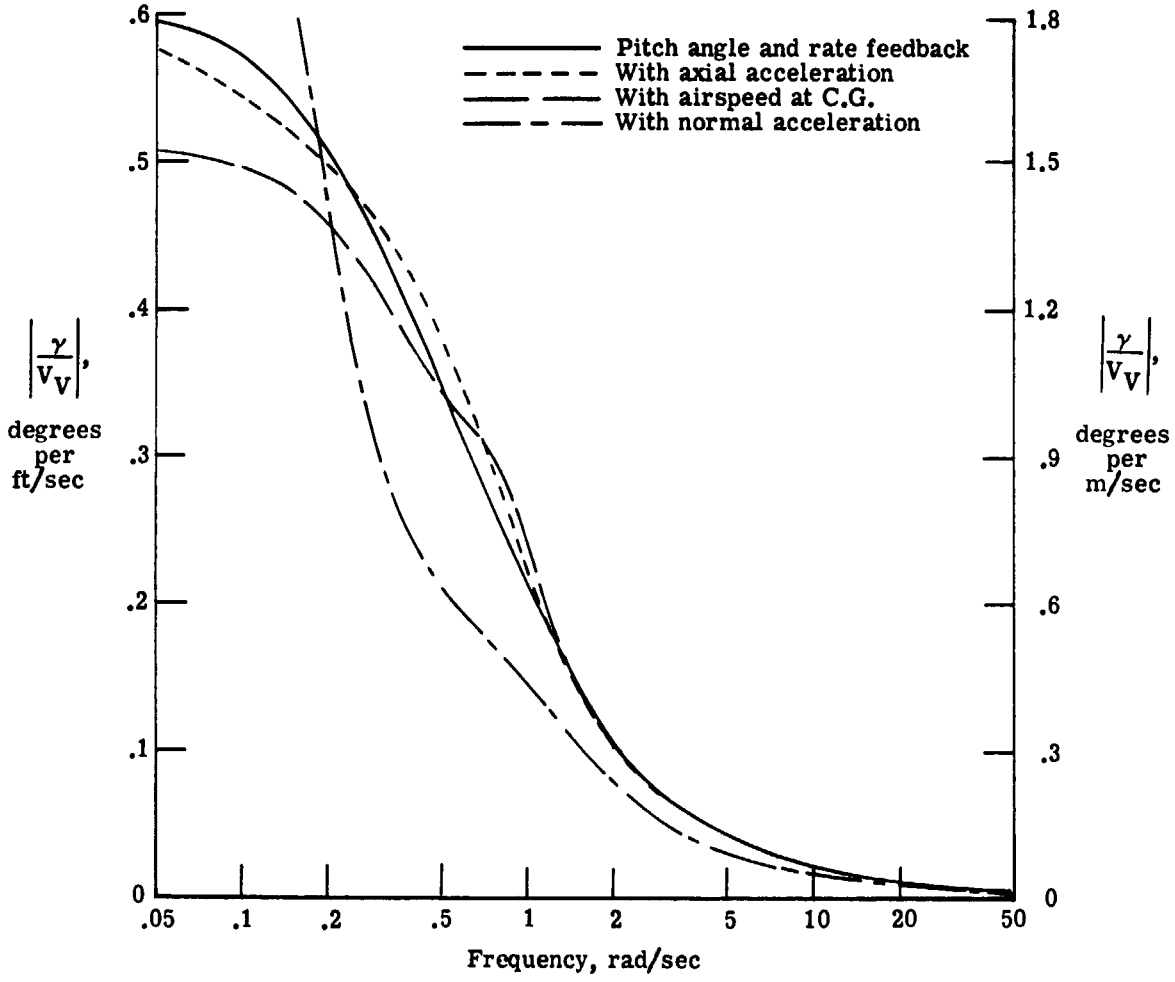

(e) Flight path angle response to vertical gust.

Figure 14.- Continued.

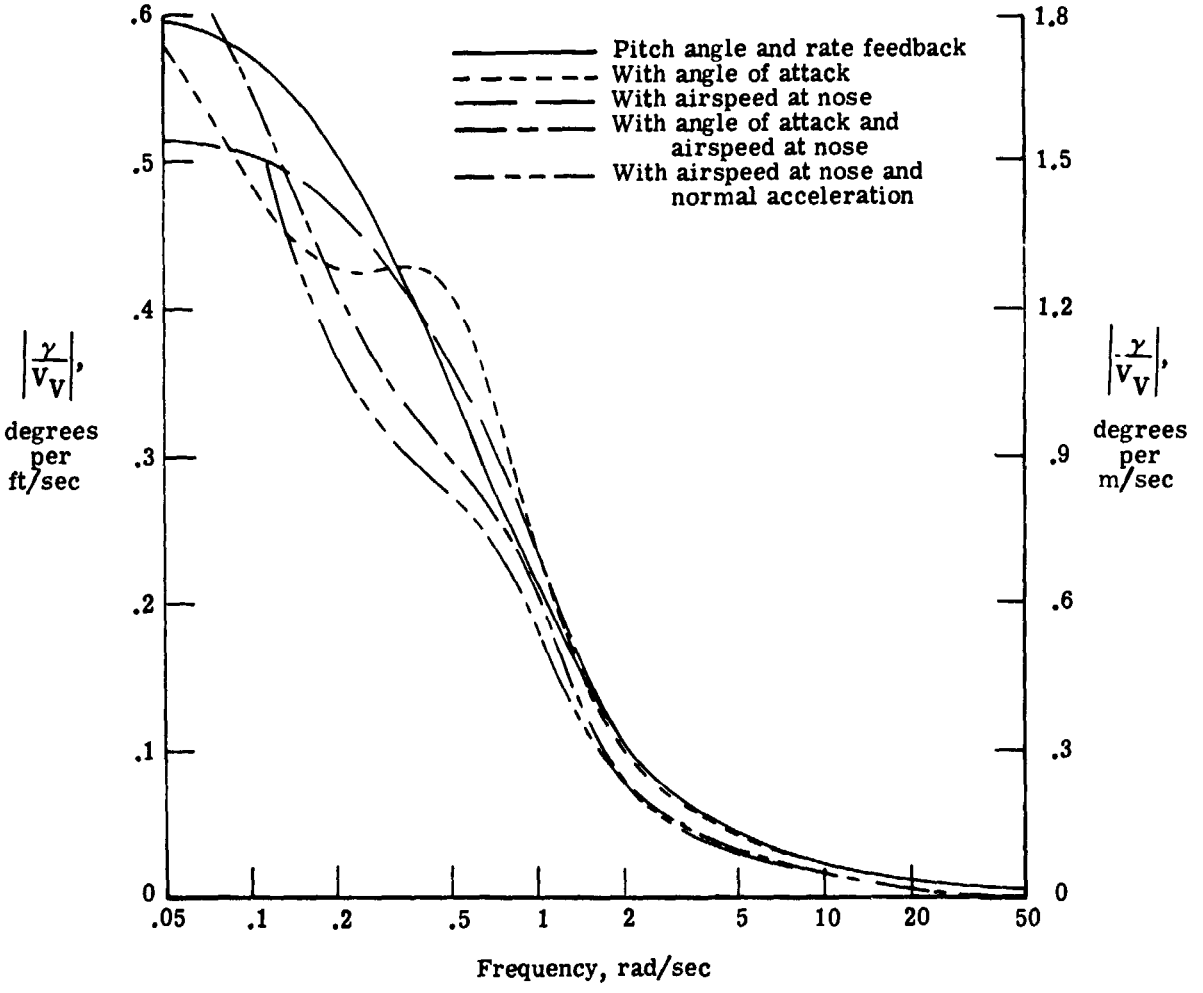

(e) Flight path angle response to vertical gust – Concluded.

Figure 14.- Continued.

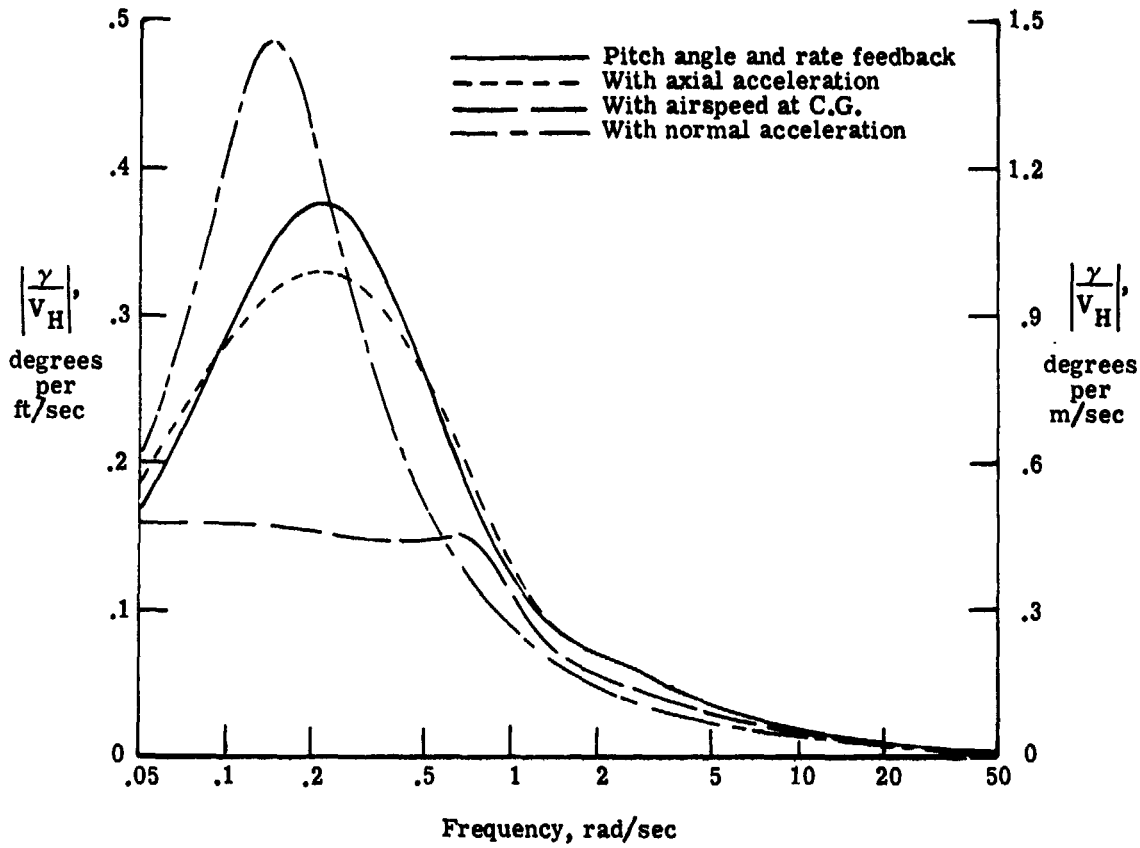

(f) Flight path angle response to horizontal gust.

Figure 14.- Continued.

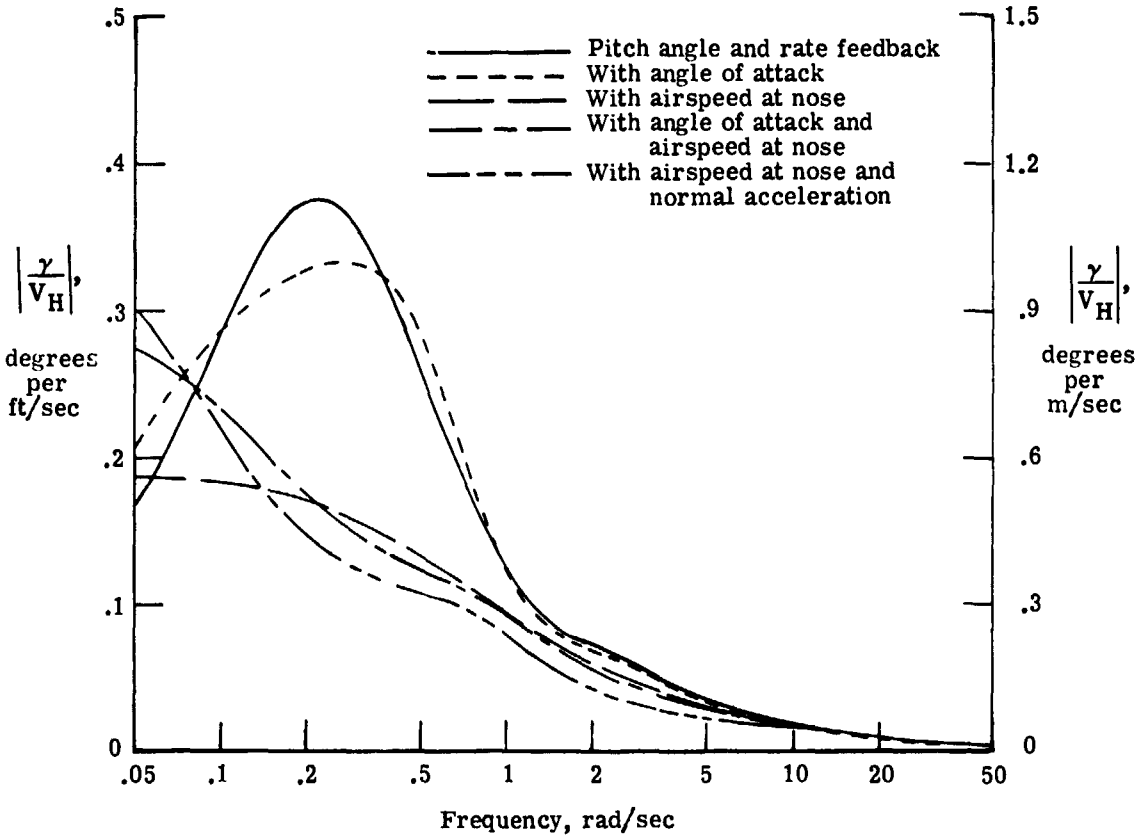

(f) Flight path angle response to horizontal gust – Concluded.

Figure 14.- Continued.

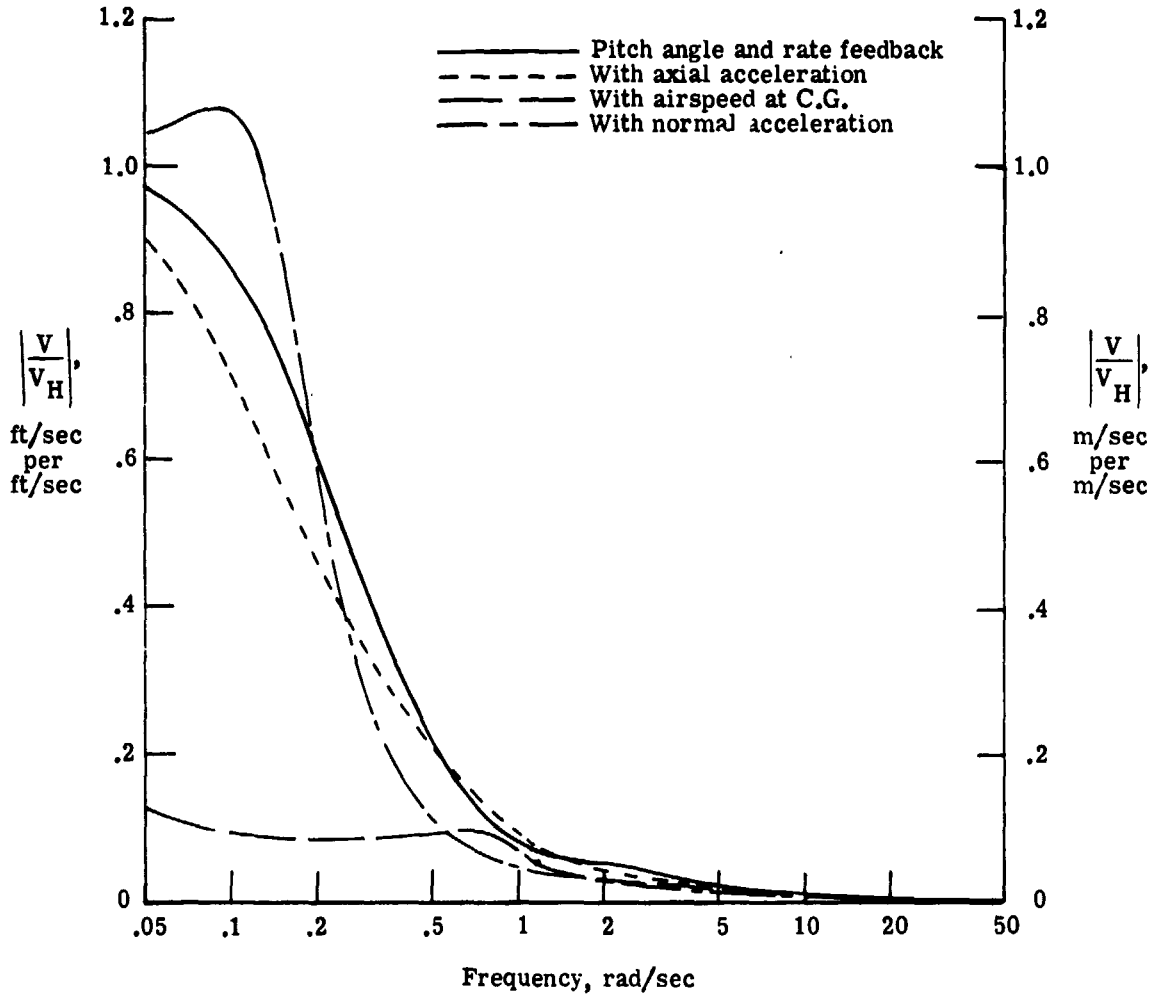

(g) Speed response to horizontal gust.

Figure 14.- Continued.

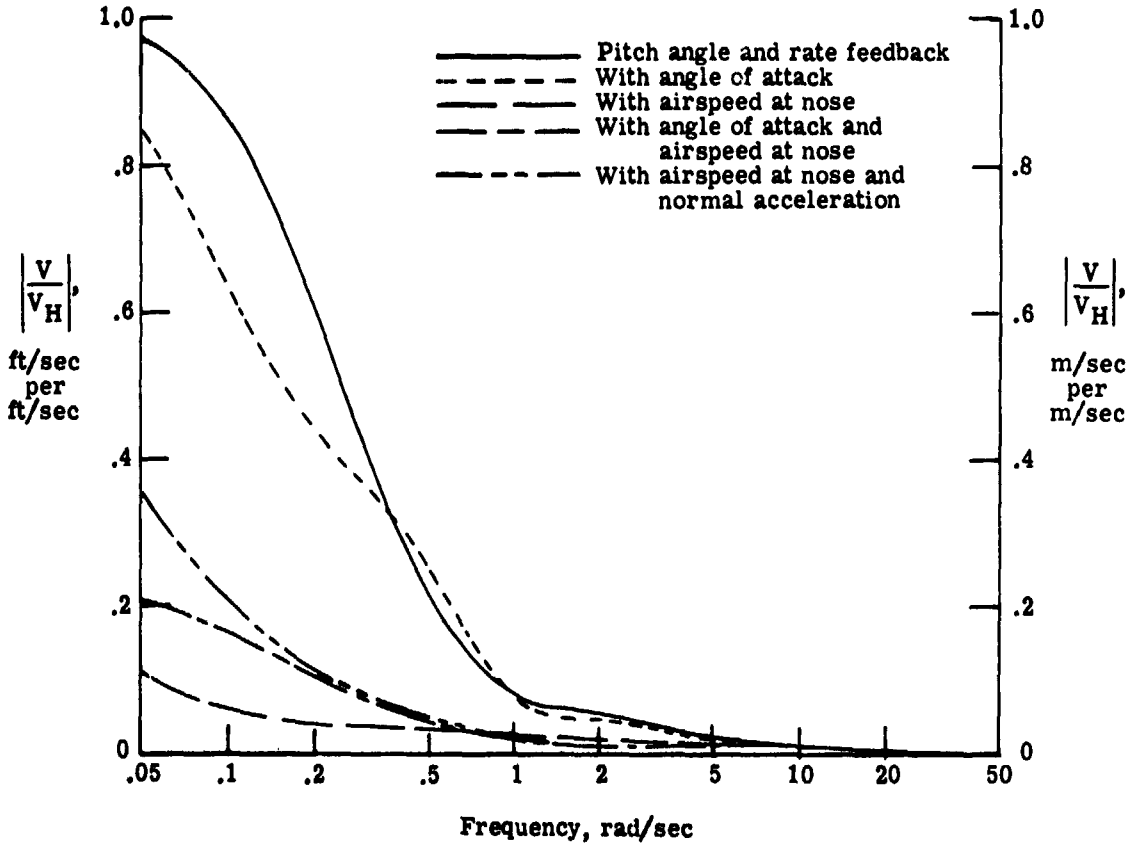

(g) Speed response to horizontal gust – Concluded.

Figure 14.- Continued.

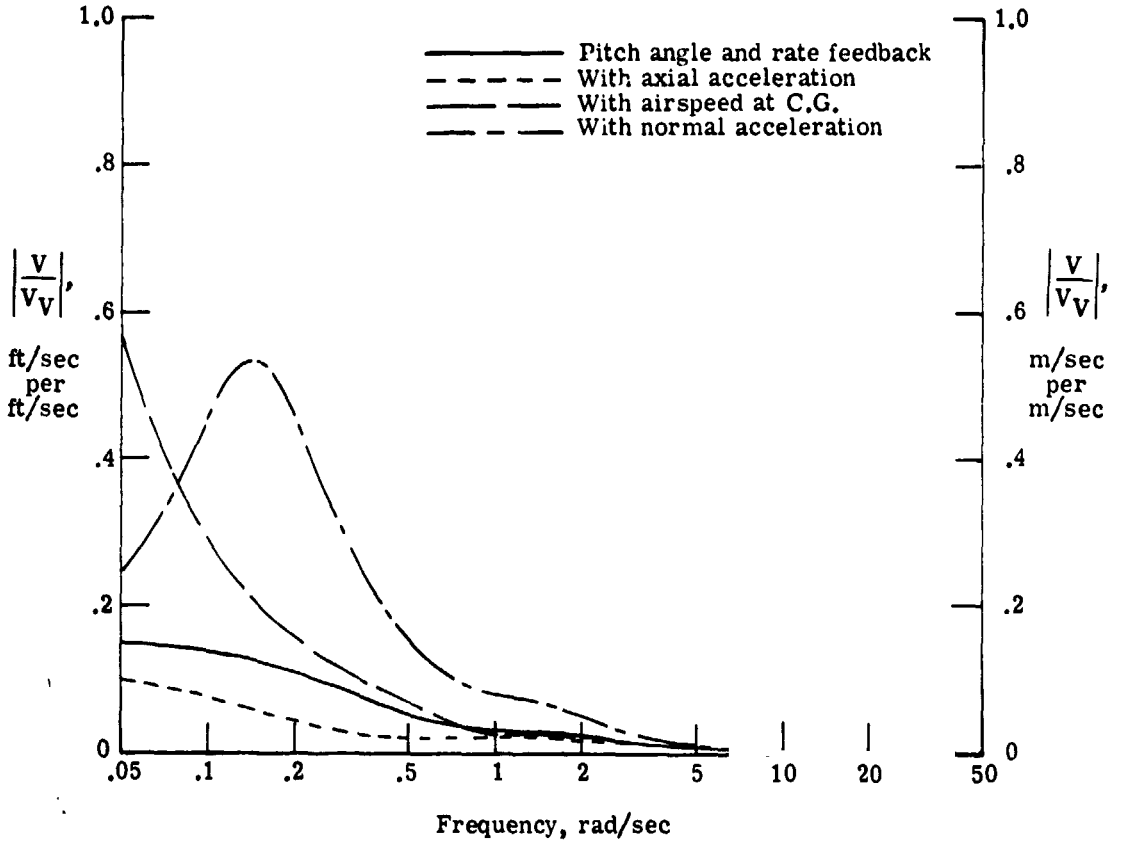

(h) Speed response to vertical gust.

Figure 14.- Continued.

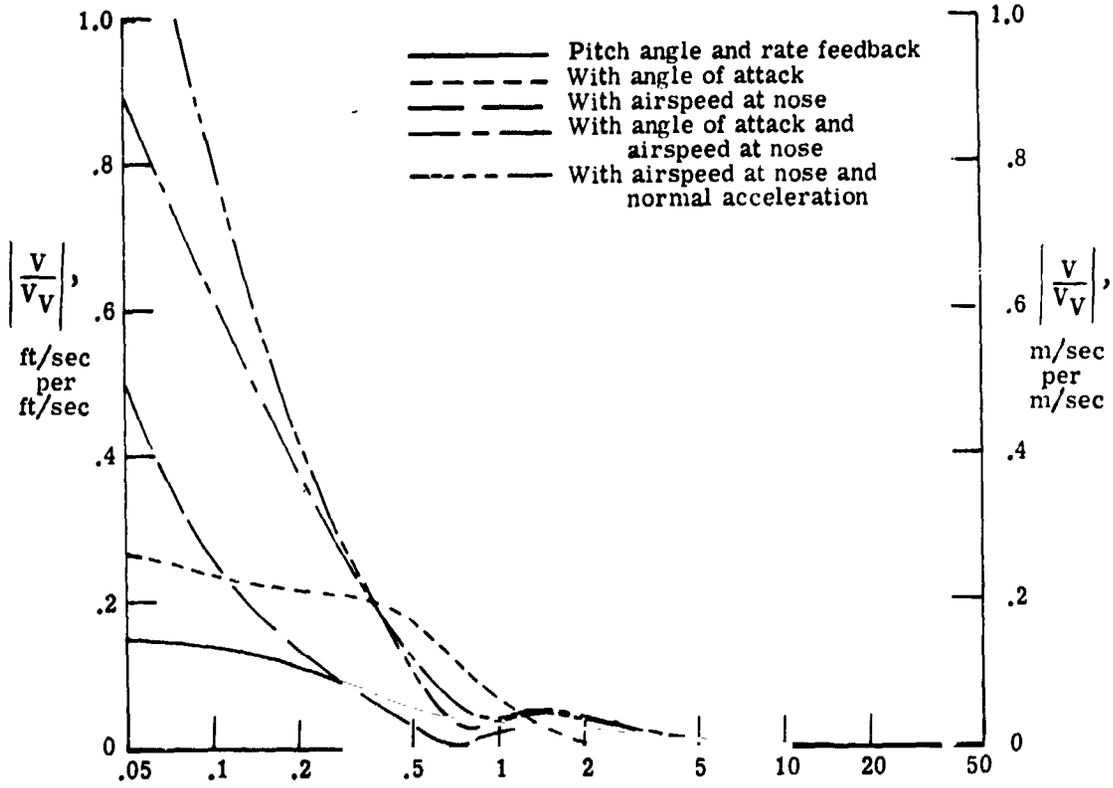

(h) Speed response to vertical gust – Concluded.

Figure 14.- Concluded.

NASA-Langley, 1974 L-9250